A STRESS-STRAIN MODEL FOR THE UNDRAINED RESPONSE OF OIL SAND

by

KA FAI HENRY CHEUNG
B.Sc., University of Manchester, 1983

A THESIS SUBMITTED IN PARTIAL FULFILMENT OF
THE REQUIREMENTS FOR THE DEGREE OF
MASTER OF APPLIED SCIENCE

in

FACULTY OF GRADUATE STUDIES
Department of Civil Engineering

We accept this thesis as conforming
to the required standard

THE UNIVERSITY OF BRITISH COLUMBIA
April 1985

In presenting this thesis in partial fulfilment of the requirements for an advanced degree at THE UNIVERSITY OF BRITISH COLUMBIA, I agree that the Library shall make it freely available for reference and study. I further agree that permission for extensive copying of this thesis for scholarly purposes may be granted by the Head of my Department or by his or her representative. It is understood that copying or publication of this thesis for financial gain shall not be allowed without my written permission.

Department of Civil Engineering

THE UNIVERSITY OF BRITISH COLUMBIA
2075 Wesbrook Place
Vancouver, B.C.
CANADA, V6T 1W5

Date: April, 1985

ABSTRACT

An efficient undrained model for the deformations analyses of oil sand masses upon undrained loading is presented in this thesis.

An analysis which couples the soil skeleton and pore fluids is used. The soil skeleton is modelled as a non-linear elastic-plastic isotropic material. In undrained conditions, the constitutive relationships for the pore fluids are formulated based on the ideal gas laws. The coupling between the soil skeleton and the pore fluids is based upon volume compatibility.

The undrained model was verified with the experimental results and one dimensional expansion of soil sand cores. Comparisons between computed and measured responses are in good agreement and suggest that this model may prove useful as a tool in evaluating undrained response of oil sand.

The response of a wellbore in oil sand upon unloading was analysed using the developed model. Such analyses are important in the rational design of oil recovery systems in oil sand.

TABLE OF CONTENTS

LIST OF TABLES

LIST OF FIGURES

LIST OF FIGURES - Continued

LIST OF SYMBOLS

The following is a list of the commonly used symbols in this thesis. Multiple use of several symbols is unavoidable because of the complexity of the formulations. The symbol will be defined immediately in the text where the use of symbols differs from those listed below.

SYMBOL	MEANING
β	compressibility
Δ	change
σ	stress
ϵ	strain
ν	Poisson's ratio
ϕ	friction angle
α	temperature solubility constants
σ_r	radial stress
σ_θ	tangential stress
σ_z	vertical stress
B	bulk modulus
e	void ratio
E	Young's modulus
G	shear modulus
H	Henry's constant
k	permeability
K_a	apparent bulk fluid modulus

K_f	bulk fluid modulus
n	porosity
P	pressure
q	flow rate
r	radius (variable)
R	radius (constant)
R_c	radius of plastic zone
r_w	radius of wellbore
S	saturation
T	temperature
u	pore fluid pressure
V	volume

Subscripts

1	final
a	air
f	pore fluid
g	gas
i	initial (internal in Chapter 6)
o	oil (outer in Chapter 6)
S	soil skeleton
v	volumetric
w	water
cb	combined
dg	dissolved gas
fg	free gas
Tg	total gas

Superscripts

e	elastic
f	final
i	initial
p	plastic

ACKNOWLEDGEMENTS

I am greatly indebted to my supervisor, Professor P.M. Byrne, for his guidance, encouragement and enthusiastic interest throughout this research. I would also like to thank Professor Y.P. Vaid for reviewing the manuscript and making valuable suggestions. My colleagues, U. Atukorala, F. Salgado, J. She, H. Vaziri and especially, C. Lum, shared a common active interest in soil mechanics. I thank them all for their helpful discussions and constructive criticisms.

Appreciation is extended to Ms. S.N. Krunic for typing the manuscript and her patience during the preparation of this thesis.

Support and assistance provided by the Natural Science and Engineering Research Council of Canada is acknowledged with deep appreciation.

A special thanks is extended to my family and Priscilla, for their constant support and encouragement.

1.1 INTRODUCTION

Many schemes for oil recovery require open excavations, tunnels or wellbore in oil sand. As a result, an accurate and efficient analysis of stresses and deformations around these openings is becoming increasingly important. Mathematical models have been developed by Byrne et al (1980), Dusseault (1979), and Harris and Sobkowicz (1977) to investigate these problems. An efficient undrained model for analysing the stresses and deformations around open excavations, tunnels and wellbores in oil sand is presented in this thesis.

Oil sand is comprised of a dense sand skeleton with its pore spaces filled with bitumen, water and free or dissolved gas. The presence of bitumen reduces the effective permeability of oil sand, hence undrained conditions occur on rapid unloading. Gas evolves from pore fluids during unloading when the pore fluid pressure is below gas saturation pressure. Because gas exsolution takes some time to occur, two undrained conditions arise, (1) an immediate or short term condition in which there is no time for gas exsolution, and (2) a long term or equilibrium condition in which complete gas exsolution has occured. Both of these conditions are considered in this thesis. The rate of gas exsolution is not considered herein. The drained analysis with pore pressures under steady-state conditions is also addressed.

The sand skeleton is modelled as a non-linear elastic-plastic porous material. The fluids stress-strain relationships for undrained condition are formulated on the basis of ideal gas law. For the undrained condition, the pore pressure changes are computed from the constant of volume compatibility between the sand skeleton and the pore fluids. It is assumed that the pore fluid pressures are known in the drained analysis.

Validation of the stress strain model is made by comparing responses with theoretical solutions and observed data. The observed data are the experimental results in Sobkowicz's doctorate thesis.

The stresses and deformations around a wellbore in oil sand upon unloading is investigated using the new stress-strain model.

1.2 BEHAVIOUR OF OIL SAND

Oil sand is comprised of a dense, highly incompressible, uncemented, interlocked skeleton with pore spaces filled by water, bitumen, and dissolved or free gas. The interpenetrative structure leads to the low in-situ void ratio and high shear strength.

The response of oil sand is mainly governed by the rate of loading. Undrained conditions occur as a result of:

1) low effective permeability to pore fluids
2) large amount of dissolved gas in pore fluids
3) rapid unloading

The response of oil sand may be physically modelled by a set of springs shown in Figure 1.1. The oil sand is split into two load carrying components - soil skeleton and pore fluids. The soil skeleton compressibility, β_s, characterizes the deformation of soil skeleton, which results in a change in effective stress. The pore fluid compressibility, β_f, characterizes the deformation of pore fluids (because of free gas) which results in a change in pore pressure.

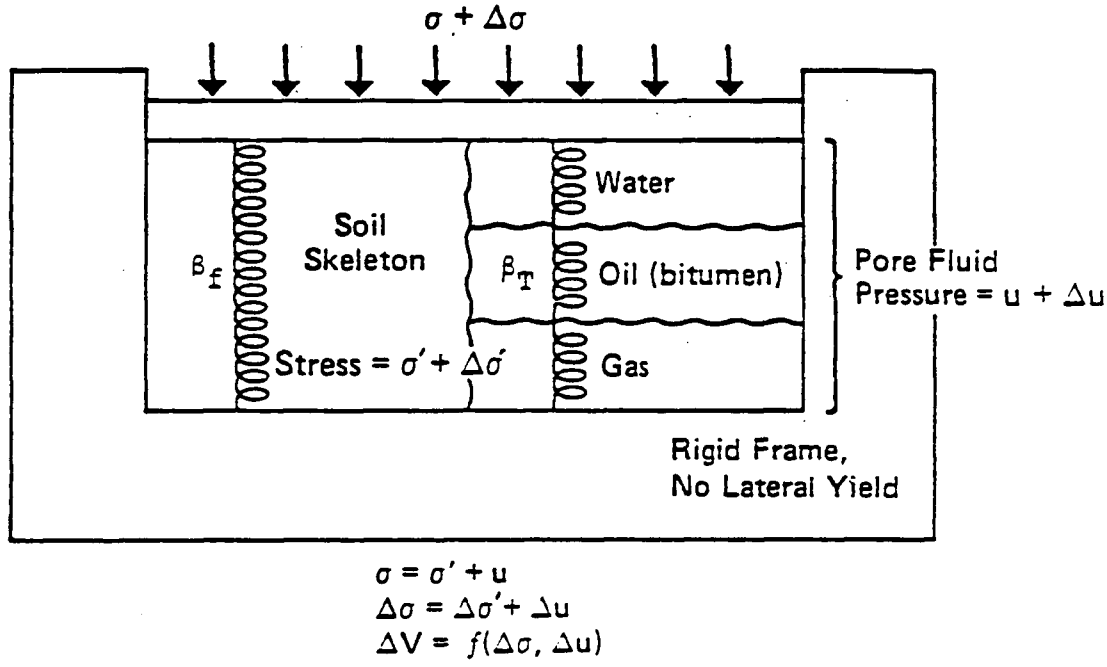

Fig.1.1 - Schematic spring analogy for oil sand

(After Dusseault , 1979)

Strain compatibility between the pore fluids and soil skeleton controls the relative magnitudes of the changes in pore pressures and effective stress which together equal the change in total stress. Stress changes (unloading) are shared between the sand skeleton and pore fluids according to their compressibilities. When the pore pressure is above the gas saturation pressure and the oil sand is 100% saturated, the stress changes will be accommodated by the pore fluids because their compressibilities are lower. Once the pore pressure drops below the gas saturation pressure, gas starts to evolve which increases the fluids' compressibilities. Therefore the sand skeleton becomes the less compressible phase and takes up the stresses rather than the pore fluids. When the effective stress drops to zero, the soil skeleton is very compressible relative to the pore fluids; hence any further decrease in total stress is entirely accommodated by the pore pressure.

The gas exsolution takes some time to occur, hence two undrained conditions (Sobkowicz, 1982) arise. The expressions 'short term' and 'long term' will be applied to these processes exclusively.

1) 'Short term' undrained in which there is no time for gas exsolution
2) 'Long term' undrained in which equilibrium state has been reached, i.e. completion of gas exsolution.

In the field, the unusal behaviour of oil sand manifests in a number of ways. They include:

1) Volumetric expansion of 5 to 15% occurred when core samples were left in an unconfined state, i.e. not retained by plastic core sleeves (Dusseault 1980; Byrne et al 1980).
2) Core samples spontaneously split longitudinally and perpendicularly to the core axis, effervescence was observed on several freshly recovered cores (Hardy and Hemstock 1963).
3) Retrogression of slopes in oil sand on rapid excavation.
4) Oil sand at the base of excavation subjects to softening and heaving, followed by settlement on reloading.

When the decrease in external stress occurs over a period of time, the evolved gas has time to drain off and effective stress does not go to zero which results in an undisturbed sand skeleton. Its high in-situ density and hence high shear strength is retained. Such situations can be seen on the exposures of oil sand deposits along the Valley of Athabasca River where erosion (unloading) by the river has occurred over thousands of years. These oil sand deposits are standing on steep stable slopes with slope angles in excess of 60° and heights up to 60 metres, exhibiting high strength (Harris and Sobkowicz 1977).

1.3 THE SCOPE

The purpose of this study is to present a stress-strain model (Vaziri, 1985) for the deformation analyses of oil sand masses, i.e. to explain the behaviour of oil sand as described in Section 1.2.

Modelling the undrained response of oil sand requires the pore fluids pressure to be numerically evaluated. For the undrained condition, pore fluid pressures are computed from the constraint of

volumetric compatibility between the sand skeleton and pore fluid phases.

Compressibilities of sand skeleton and pore fluids have to be evaluated in the new stress-strain model. A non-linear stress-strain relationship (Duncan et al 1970) is adopted for the sand skeleton. The compressiblities of pore fluids are formulated on ths basis of ideal gas laws.

The new stress-strain model is incorporated into finite element programmes (INCOIL, MHANS). For the validation of the stress-strain relationship, the computed results are compared with the theoretical solutions and observed data.

The validated programme was used to study the unloading response of stress and deformations around a deep wellbore in oil sand.

1.4 ORGANIZATION OF THE THESIS

This thesis consists of seven chapters. A review of previous work on undrained models for oil sand is given in Chapter 2. This chapter concentrates on the examinations of their capabilities and shortcomings.

A stress-strain model which was developed by Vaziri is presented in Chapter 3. Appropriate soil skeleton and pore fluids constitutive relationships are also recommended in this chapter.

Chapter 4 summarizes the finite element formulations used in the development of the programme.

Validation of the developed model by comparing predicted response with existing theoretical solutions, field and laboratory

observations is mentioned in Chapter 5. The response of a wellbore in oil sand upon unloading is investigated in Chapter 6 using the validated finite element programme.

A summary of work and major conclusions are presented in Chapter 7.

CHAPTER 2 : REVIEW OF PREVIOUS WORK

2.1 INTRODUCTION

Theoretical solutions for the undrained response of oil sand were not available until 1977 because of its unusual behaviour. Due to the increase in demand for construction in oil sand formation, such as open pit mining, tunnels and deep shafts, a considerable amount of research has been done on this topic since 1977.

These developed theoretical relations share the same basic approach of coupling the soil skeleton and pore fluids together. Pore pressure changes are computed from the constraint of volumetric compatibility between the soil skeleton and pore fluids. Harris and Sobkowicz's model is capable of evaluating pore pressure change upon a stress or/and temperature change. This model was then extended by Byrne et al and incorporated in a finite element programme. Dusseault's approach is restricted to one dimensional problems.

A careful examination of these theoretical models and their applications is made and several shortcomings are also reviewed.

2.2 MATHEMATICAL MODELS FOR OIL SAND

2.2.1 Harris and Sobkowicz (1977)

Harris and Sobkowicz presented a mathematical model to analyse the undrained response of oil sand subjected to changes of stress and/or temperature. This is the first analytical model developed to explain the behaviour of oil sand such as:

1) Movement and stability of slopes and tunnels formed in oil

sand.

2) Settlements or heave of structures placed in oil sand (e.g. hot oil tank).

3) Heave at the base of excavations in oil sand.

The model can be explained by the same spring analogy as shown in Figure 1.1.

The response of oil sand to changes in stresses or/and to changes in temperature may be computed by the following equations:

a) One-Dimensional Analysis

Δu can be obtained from a quadratic equation

$$L * \Delta u^2 + M * \Delta u + N = 0 \qquad 2.2$$

where

$$L = \beta_s$$

$$M = \beta_s(P_i - \Delta\sigma_1) + n_g + P_1 \frac{T_1}{T_a} (n_w H_w + n_o H_o)$$

$$N = P_i \left[n_g(1 - \frac{T_1}{T_i}) - \Delta\sigma_1\beta_s\right] - P_1 \Delta T \frac{T_1}{T_a} (n_w\beta_w + n_o\beta_o)$$

b) Two-Dimensional Analysis

from strain compatibility again

$$\Delta u = \frac{\Delta\sigma_3 + A_p\,(\Delta\sigma_1 - \Delta\sigma_3)}{1 + \frac{n\beta_f}{\beta_s}} \qquad 2.3$$

and

$$P\,\Delta u^2 + Q\,\Delta u + R = 0 \qquad 2.4$$

where

$$P = \beta_s$$

$$Q = \beta_s\,(P_i - X) + n_g + P_l\,\frac{T_l}{T_a}\,(n_w H_w + n_o H_o)$$

$$R = P_l\left[n_g\,(1 - \frac{T_l}{T_a}) - X\,\beta_s\right] - P_i\,\Delta T\,\frac{T_l}{T_a}\,(n_w\alpha_w + n_o\alpha_o)$$

$$X = \Delta\sigma_2 + A_p\,(\Delta\sigma_1 - \Delta\sigma_2)$$

and

$\frac{\Delta V}{V}$ = volumetric strain

β_s = soil skeleton compressibility

n = porosity of soil

n_o = porosity of oil

n_w = porosity of water

n_g = porosity of gas

$\Delta\sigma$ = change in total stress

P_i = initial pore fluid pressure

Δu = change in pore fluid pressure

$\Delta\sigma_1$ = change in major principal stress

$\Delta\sigma_3$ = change in minor principal stress

T_a = standard temperature (288 °K)

T_i = initial pore fluid temperature °K

T_1 = final pore fluid temperature °K

ΔT = change in temperature

α_w = temperature solubility constant for gas in water

α_o = temperature solubility constant for gas in oil

H_w = Pressure solubility constants for gas in water

H_o = Pressure solubility constants for gas in oil

A_p = soil skeleton dilatancy factor

Harris and Sobkowicz examined the response of oil sand during excavation and reloading of a square footing, and the behaviour of a tunnel excavation in the same material. Their results will allow an assessment of the applicability and shortcoming of the theory.

1) This solution incorporated a linear constitutive relationship for the soil. As oil sand behaves like an elastic-plastic material, there will be a plastic zone developed adjacent to the tunnel wall on unloading when the effective stresses are such that failure (Mohr Coulomb Criteria) occurs.
2) The extent of the plastic zone is only an approximation because redistribution of stresses has not been taken into

account during the formation of plastic zone.

3) An iterative procedure is required to obtain Δu

2.2.2 DUSSEAULT

Dusseault (1979) extended the one dimensional Skempton's B equation to analyse the behaviour of cohesionless materials with large amount of free or dissolved gas in pore fluids. He presented a more rigorous derivation for the compressibility of pore fluids, and coupled the compressibility with that of soil skeleton (e - σ' relationship) in Skempton's B equation.

This model shares the same basic idea as the previous one (Harris and Sobkowicz), which has two load carrying components - soil skeleton and pore fluids. The relative compressibilities of these components control the magnitude of changes in pore pressure and effective stress which together balance the change in total stress in an undrained state.

The traditional Skempton's B equation is

$$B = \frac{\Delta u}{\Delta \sigma} = \frac{1}{1 + n\frac{\beta_f}{\beta_s}} \qquad 2.5$$

β_f = compressibility of pore fluid (water)

β_s = compressibility of soil skeleton

The extended one is

$$\frac{\Delta u}{\Delta \sigma} = 1/[1 + f(u,\sigma)] \qquad 2.6$$

$$f(u,\sigma) = \frac{\sigma-u}{b}\left[e_o\beta_o + e_w\beta_w + \frac{a+b\ell n(\sigma-u)-e_o-e_w+H_o e_o+H_w e_w}{u}\right]$$

a, b = void ratio - effective stress relationship parameters

e_o, e_w, e_g = void ratios : oil, water, gas

H_o, H_w = Henry's constants : oil, water

β_o, β_w = compressibility : oil, water

u, σ = current values of pore pressure and total stress

Dusseault applied this model to investigate the response of an element of oil sand upon unloading. He examined a shallow case (15 m) and a deeper one (500 m). His results will allow an assessment of the applicability and shortcoming of the theory:

1) In order for the solution to be numerically stable, further reduction in total stress is assumed to be entirely taken by the pore pressure once effective stress drops to zero.
2) This solution incorporated a non-linear constitutive relationship for the soil.
3) Accurate e - σ' relationship or compressibility of oil sand is extremely difficult to obtain since they are very sensitive to sample disturbances. No undisturbed oil sand samples have been cored so far.

4) An iterative procedure is required to get Δu.

2.2.3. Byrne and Janzen

Byrne et al (INCOIL, 1983) developed an incremental analytical finite element method for predicting stresses and deformations in excavations and around tunnels in oil sand using a nonlinear elastic sand skeleton with shear dilation. An extension to Harris and Sobkowicz's model was used to evaluate the pore pressure change, Δu.

The finite element program, INCOIL, can handle both undrained and drained analyses. For the undrained condition, pore fluid pressures are computed from the constraint of volumetric compatibility between the sand skeleton and the pore fluids. For the fully drained condition, it is assumed that the pore fluid pressures are known.

The general framework of the finite element model for oil sand are as follows:

$$[K]\ (\delta) = (\Delta f) - (K_w)\ (\Delta u) \qquad 2.7$$

where

$$\Delta u = \frac{\frac{u_a T_1}{T_a} * \Delta T * (n_w \alpha_w + n_o \alpha_o) - u_o\left[n_g * (1 - \frac{T_1}{T_o}) - \Delta\varepsilon_v\right]}{\frac{u_a T_1}{T_a}(n_w H_w + n_o H_o) + n_g - \Delta\varepsilon_v} \qquad 2.8$$

Derivation of equation 2.7 is presented in Appendix A

The effective stress may be evaluated from

$$(\Delta\varepsilon) = [C]\ (\Delta\delta) \qquad 2.9$$

$$(\Delta\sigma') = [D']\ (\Delta\varepsilon) \qquad 2.10$$

where

$[C]$ = the matrix which depends on element geometry

$[D']$ = the matrix property matrix (affective stress)

$[\Delta\sigma']$ = the change in effective stress vector

$[\Delta\varepsilon]$ = the change in strain vector

$[K]$ = the element stiffness matrix

$(\Delta\delta)$ = the incremental element nodal deflections vector

(Δf) = the incremental element nodal forces vector

(K_w) = the pore pressure load vector

n_w, n_o, n_g = porosity : water, oil and gas phase

α_w, α_o = temperature solubility constant : water, oil

H_w, H_o = pressure solubility constant : water, oil

u_a = reference (atmospheric) pressure

T_a = reference temperature (288°K)

T_o = initial temperature (°K)

T_1 = final temperature (°K)

ΔT = change in temperature ($T_1 - T_o$) (°K)

u_o = initial absolute pore pressure

$\Delta\varepsilon_v$ = volumetric strain (compression positive)

They examined the response of cylindrical shaft in oil sand on reduction of support pressure and the response of an element of oil sand to one dimensional unloading. The latter case is to simulate core samples of oil sand left in an unconfined state. Their results will allow an assessment of the applicability and shortcoming of the theory:

1) The predicted expansion of the core on unloading is small compared with those measured in the field which is 5-15% when core samples of oil sand are left in an unconfined state.
2) An iterative procedure is required to obtain Δu.

CHAPTER 3 : STRESS-STRAIN MODEL

3.1 INTRODUCTION

It is noted that the mathematical models described in Chapter 2 have quite a few shortcomings. Therefore, a more sophisticated and efficient undrained model was developed (Naylor 1973, Vaziri 1985) and is incorporated in a finite element programme.

A total stress approach coupling the soil skeleton and pore fluids is used . Pore pressure changes are computed from the constraint of volume compatibility between the soil skeleton and pore fluids under undrained conditions.

Separate constitutive relationships for soil skeleton and pore fluids are required in the new undrained model. An incremental non-linear elastic and isotropic stress-strain model as described by Duncan et al is adopted for the soil skeleton. Depending on the component of the pore fluids, different formulations for the non-linear elastic and isotropic stress-strain relationships of pore fluid are derived.

3.2 DEVELOPMENT OF UNDRAINED MODEL

The effective stress concepts (Terzaghi) in conventional soil mechanics seem to be applicable to determine the shear strength of oil sand (Hardy and Hemstock). However, the pore pressures of fluids in the oil sand have to be numerically evaluated in the effective stress approach. Hence, a quantitative relationship between the magnitudes of stress release and pore pressure is required.

When a saturated soil mass is subjected to undrained loading,

stress change must be shared between the soil skeleton and pore fluid (Bishop and Eldin 1950). A theoretical expression for the relationship between total stress change and resulting pore fluid pressure change was derived by Skempton (1954) which is the Skempton's B equation.

Using the finite element method, Christian (1968) introduced an effective stress approach for soils subjected to undrained loading, enabling resulting pore fluid pressure to be evaluated. Programmes incorporating this alternative are relatively inefficient. Naylor (1973) developed a more elegant approach which allows excess pore pressure to be computed explicitly in terms of material skeleton stiffness parameters and an independently specified pore fluid stiffness. However, Naylor only considers soils that are two-phase system - solids and water.

Due to the presence of bitumen, free and dissolved gas in oil sand, the above mentioned approaches are inadequate to describe the undrained behaviour of oil sand. Not until 1977, Harris and Sobkowicz developed an analytical expression incorporating a linear constitutive relationship for the oil sand, to relate the change in pore pressure to the change in total stress. Dusseault (1979) extended Skempton's one dimensional B equation to model the equilibrium behaviour of oil sand.

Byrne et al (1980) studied the behaviour of oil sand by using finite element method. They extended Harris and Sobkowicz's model and incorporated it into Christian's finite element formulation.

As there are shortcomings of the approaches developed by Harris and Sobkowicz, Dusseault and Byrne et al, a more sophisticated numerical model is required. Vaziri adopted Naylor's approach and extended it to model the undrained behaviour of oil sand using finite

elements.

The stress-strain model for oil sand behaviour is based on the following assumptions.

1) Volumetric change of soil skeleton is governed by the effective stress.
2) Liquids and gas in the voids are at the same pressure, i.e. effect of surface tension between the pore fluid phases are neglected.
3) Free gas in the pores behaves in accordance with classic gas laws with respect to pressure. Gas comes out from solution in accordance with Henry's law. Henry solubility constants are constant.
4) The compressibility of soil grains is negligible, and has no contribution to the volume changes.
5) The gas is in the form of occluded bubbles inside the pore fluid.

The total stress constitutive law may be written as:

$$(\Delta\sigma) = [D]\ (\Delta\varepsilon) \qquad 3.1$$

where $(\Delta\sigma)$, $(\Delta\varepsilon)$ are the incremental total stress vectors and strain vectors respectively, and $[D]$ is the material property matrix (total stress). Computation of element stiffness matrix, assembly and solutions for displacements proceeds along the standard lines. The analysis yields a total stress field.

Since the soil skeleton and the pore fluids deform together when conditions are undrained, strains - in a macroscopic sense - are the same in each phase. Thus in addition to Equation 3.1

$$(\Delta\sigma') = [D'] (\Delta\varepsilon) \qquad 3.2$$

$$(\Delta u) = K_a (\Delta\varepsilon_{11} + \Delta\varepsilon_{22} + \Delta\varepsilon_{33}) \qquad 3.3a$$

$$= K_a (\Delta\varepsilon_v) \qquad 3.3b$$

in which prime means effective, $[D']$ is the material property matrix (effective stress), K_a is the apparent pore fluid bulk modulus and (Δu) is the pore pressure change vector.

The actual pore fluid modulus, K_f, is related to the apparent one as

$$K_a = \frac{K_f}{n} \qquad 3.4$$

where n is the soil porosity.

Derivations of equations 3.3 and 3.4 are presented in Appendix B.

Equation 3.3 may be expressed in a form compatible with equation 3.1 and 3.2 as:

$$(\Delta\sigma_f) = [D_f] (\Delta\varepsilon) \qquad 3.5$$

where $(\Delta\sigma_f) = [\Delta u \quad \Delta u \quad \Delta u \quad 0 \quad 0 \quad 0]^T$

Since the pore fluid cannot transmit shear, $[D_f]$ can be expressed in terms of apparent bulk modulus,

$$[D_f] = K_a \begin{bmatrix} I_3 & O_3 \\ O_3 & O_3 \end{bmatrix} \qquad 3.6$$

where I_3 is as 3 x 3 matrix with all the elements equal to 1, whereas O_3 are 3 x 3 null matrices.

The principle of effective stress may be used to relate the changes in effective stress and pore presusre caused by the applied loads to the corresponding change in total stress

$$(\Delta\sigma) = (\Delta\sigma') + (\Delta\sigma_f) \qquad 3.7$$

Substituting from Equations 3.1, 3.2, and 3.3 into 3.7, yields:

$$[D] = [D'] + [D_f] \qquad 3.8$$

The elastic material is now considered to be two phase, with the stiffness defined by effective stress moduli, E, B and pore fluid apparent builk modulus K_a.

The material properties of $[D']$ and K_a are read in separately. They are combined in the programme automatically using equations 3.6 and 3.8. Thereafter, computation of element stiffness, assembly and solution of displacements and hence strains proceed along the standard lines. The effective stress and pore pressure are obtained by Equations 3.2 and 3.5 respectively.

This approach allows stresses, porepressure and deformation in soil mass, with nearly incompressible to highly compressible pore fluids, to be evaluated by finite elements for undrained conditions. Naylor studied the response of undrained triaxial test on clay using this model. The end platens were rigid and rough. But the computed excess pore pressures near the centre of the sample were in good agreement with the theoretical solutions (Cam-Clay). In the case of drained analysis, Equations 2.7 to 2.10 are used instead, assuming all the pore fluid pressures are known.

3.3 CONSTITUTIVE RELATIONS

3.3.1 Incremental Non-linear Elastic Soil Skeleton

An incremental non-linear elastic-plastic and isotropic stress-strain soil model as described by Duncan et al (1970) is employed in this thesis. In this approach, two independent elastic parameters are required to represent non-linear stress-strain and volume change behaviour. These are usually the Young's modulus, E, and the Poisson's ratio, ν. The shear modulus, G, and the bulk modulus B, are the more fundamental parameters because they separate shear or distortion and volume components of strain and would be the most desirable ones to use. However, the shear modulus is difficult to obtain directly in laboratory testings and for this reason Duncan et al (1980) used the Young's modulus and the bulk modulus as their two parameters. The Young's modulus is very similar in character to the shear modulus as both are a measure of distortional response. Therefore, E and B are used in this thesis.

The stress-dependent E and B are usually obtained from laboratory tests. A typical example for sand is shown in Figure 3.1. The distortional response can be reasonably approximated by modified hyperbolas (Konder) and the volumetric response in exponential form. They are expressed as follows:

The tangent Young's modulus

$$E_t = \left[1 - \frac{R_f(1-\sin\phi)\ (\sigma_1'-\sigma_3')}{2\sigma_3'\ \sin\phi}\right]^2 E_i \qquad 3.9$$

where $$E_i = K_E\ P_a\ \left(\frac{\sigma_3'}{P_a}\right)^n \qquad 3.10$$

and

$$\phi = \phi_1 - \Delta\phi\ \log\ \left(\frac{\sigma_3'}{P_a}\right) \qquad 3.11$$

The tangent bulk modulus

$$B_t = K_B\ P_a\ \left(\frac{\sigma_3'}{P_a}\right)^m \qquad 3.12$$

where E_i = initial Young's modulus

K_E = Young's modulus number

n = Young's modulus exponent

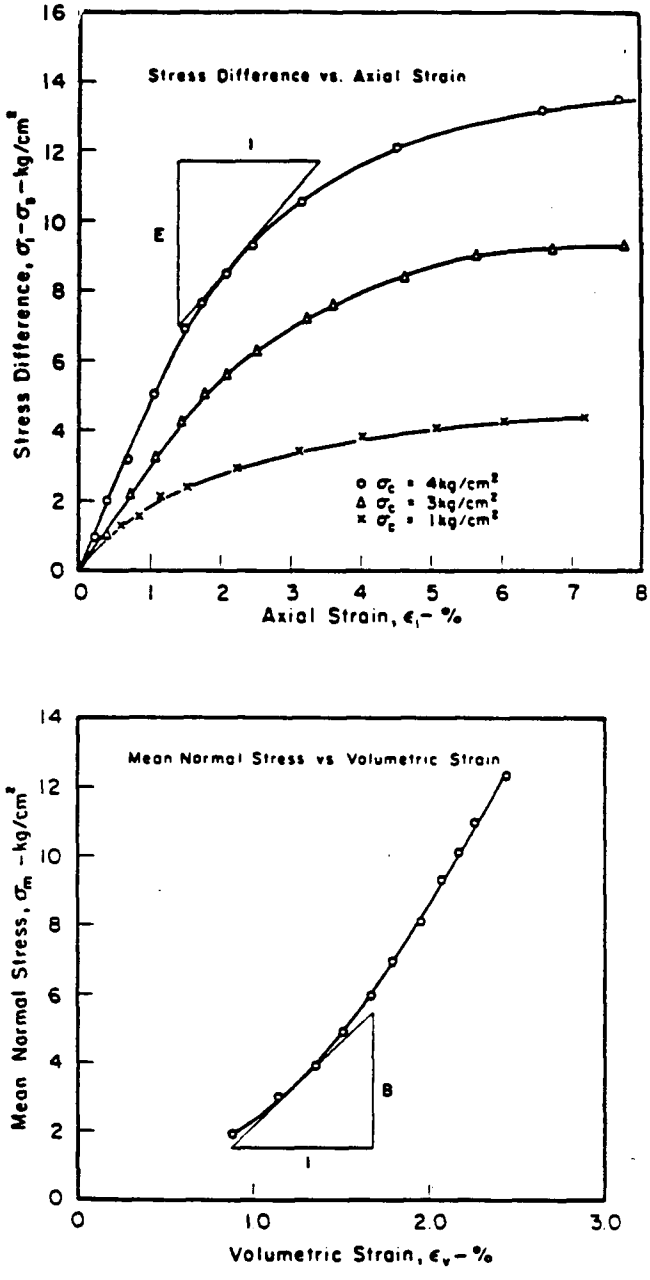

Fig.3.1 - Stress-Strain curves for drained triaxial tests on loose sand
(After Byrne and Eldridge, 1982)

K_B = bulk modulus number

m = bulk modulus exponent

P_a = atmospheric pressure

σ_1', σ_3' = major and minor principal effective stress

R_f = failure ratio

ϕ_1 = friction angle at confining stress of 1 atm

$\Delta\phi$ = decrease in friction angle for a tenfold increase in confining stress

The procedures for evaluating these parameters from laboratory tests are described in detail by Duncan et al (1980) and Byrne and Eldridge (1982).

3.3.2 Incremental Non-linear Fluid Modulus

3.3.2.1 General

An incremental non-linear elastic and isotropic stress-strain fluid model is employed here. Since the fluid cannot transmit shear, the stress-strain relations are defined only by one elastic parameter, the bulk fluid modulus, K_f, which is a measure of volumetric response. Before the derivation of K_f, Henry's law and Boyle's law must be mentioned because these laws govern the derivations.

Pore fluids may be immiscible, miscible, or a combination of the two. Examples of both miscible and immiscible fluids will be considered in this thesis. That is, water undersaturated with air and carbon dioxide, water and bitumen saturated with gas (methane, CO_2). The first combination is to describe the pore fluids of the gassy soils which Sobkowicz (1982) used in his laboratory testings. The second combination is to similate oil sand pore fluids.

If both free gas and liquids are present in the pore fluids, and the gas is soluble in the pore liquid in a certain extent, the pore fluid compressibility will be both pressure dependent and influenced by the solubility relationship. Hence, Boyle's and Henry's laws are appropriate for describing these volume and pressure relationships.

1) Boyle's law (Laidler et al): The volume of a free gas is inversely proportional to the pressure applied to it when the temperature is kept constant. Mathematically,

$$V \propto \frac{1}{P} \qquad 3.13$$

where V is the volume, P is the absolute pressure

2) Henry's law (Laidler et al): The mass of gas m dissolved by a given volume of solvent at constant temperature, is proportional to the pressure of the gas in equilibrium with the solution. Mathematically,

$$m \text{ (dissolved gas)} = H * P \qquad 3.14$$

where H is Henry's solubility constant, P is the absolute pressure.

In other words, the volume of dissolved gas is constant in a fixed volume of solvent at constant temperature when the volume is measured at P

$$V_{dg}\ (\text{dissolved gas}) = H * V\ (\text{solvent}) \qquad 3.15$$

Most gases obey Henry's law when the temperature is not too low and the pressure is moderate. If several gases from a mixture of gases dissolve in a solution, Henry's law applied to each gas independently, regardless of the pressure of the other gases present in the mixture. H is both temperature and pressure dependent, particularly for natural gases in hydrocarbons (Burcik, 1956). Since the variation of H on pressure is not very significant, it is assumed that H is independent of pressure in this thesis.

3.3.2.2 Partly Miscible Gas/Liquid Mixture

Definitions:

1) Pore fluids compressibility, β_f

$$\beta_f = -\frac{1}{V_f} * \frac{dV_f}{dP_f} \qquad 3.16a$$

where V_f is the volume of pore fluids, P is the absolute pressure, assuming surface tension effects are neglected,

$$\beta_f = \frac{-1}{v_f} * \frac{dV_f}{dP} \qquad 3.16b$$

2) Compressibility of a gas β_g

$$\beta_g = - \frac{1}{V_g} * \frac{dV_g}{dP} \qquad 3.17$$

where V_g is the volume of gas.

a) Air/water Mixture

Let the initial volume of free gas and water in a soil element be:

$$V_{fg}^i \text{ and } V_w$$

Thus the total volume of free and dissolved gas

$$V_{Tg}^i = V_{fg}^i + H\ V_w \qquad 3.18$$

For a change in pressure, the volume of water is assumed constant as the compressibility of water is insignificant compared with the pore gas. Applying Boyle's law to the total volume of gas (Fredlung 1973, Sobkowicz 1982) in the element,

$$V_{Tg}^f = V_{Tg}^i * \frac{P_i}{P_f} \qquad 3.19$$

Then the new volume of free gas after change in pressure

$$V_{fg}^f = V_{Tg}^f - V_{dg}^f$$

$$= V_{Tg}^{i} * \frac{P_i}{P_f} - V_{dg}^{f}$$

$$= (V_{fg}^{i} + V_{dg}^{i}) * \frac{P_i}{P_f} - V_{dg}^{f} \qquad 3.20$$

Change of free gas in the soil element

$$\Delta V_{fg} = V_{fg}^{f} - V_{fg}^{i}$$

$$= (V_{fg}^{i} + V_{dg}^{i}) * \frac{P_i}{P_f} - V_{dg}^{f} - V_{fg}^{i}$$

$$= (V_{fg}^{i} + V_{dg}^{i}) * \frac{-\Delta P}{P_i + \Delta P} \qquad 3.21$$

By definition

$$\beta_g = - \frac{1}{V_{fg}^{i}} * \frac{\Delta V_{fg}}{\Delta P}$$

$$= - \frac{(V_{fg}^{i} + V_{dg}^{i})}{V_{fg}^{i}} * \frac{1}{P_i + \Delta P} \qquad 3.22$$

Also, by definition

$$\beta_f = - \frac{1}{V_f} * \frac{dV_f}{dP}$$

$$= - \frac{1}{V_f} \left[\frac{dV_{fg}}{dP} + \frac{dV_w}{dP} \right]$$

$$= - \frac{1}{V_f} \left[- \frac{(V^i_{fg} + V^i_{dg})}{P_i + \Delta P} - V_w \beta_w \right]$$

$$= \frac{1 - S + SH}{P_i + \Delta P} + S \beta_w \qquad 3.23a$$

As ΔP approaches zero,

$$\beta_f = \frac{1 - S + SH}{P} + S\beta_w \qquad 3.23B$$

and

$$K_f = \frac{1}{\beta_f}$$

b) <u>Carbon Dioxide, Air/water Mixture</u>

By definition, the compressibility of pore fluids, β_f,

$$\beta_f = - \frac{1}{V_f} * \frac{dV_f}{dP}$$

$$= - \frac{1}{V_f} \left[\frac{dV_{fg}}{dP} + \frac{dV_w}{dP} \right]$$

$$= -\frac{1}{V_f}\left[-\frac{(V_{fg}^i + V_{dg}^i)}{P_i + \Delta P} - V_w\beta_w\right] \qquad 3.24a$$

in which there may have air and carbon dioxide as free gas, V_{fg}^i.

Consider the phase diagram in Figure 3.2, the volume of solids is assumed to be 1 unit, the volume of void is e units according to definition of void ratios

Therefore

$$\frac{V_{fg}^i}{V_f} = \frac{e - e_w}{e} \qquad 3.25a$$

$$\frac{V_{dg}^i}{V_f} = \frac{H_a\, e_w + H_{co2}\, e_w}{e} \qquad 3.25a$$

Substituting equations 3.25 into 3.24a, yields

$$\beta_f = \frac{1}{e}\left[\frac{(e - e_w) + H_a\, e_w + H_{co2}\, e_w}{P + \Delta P} + \beta_w e_w\right] \qquad 3.24b$$

As ΔP approaches zero,

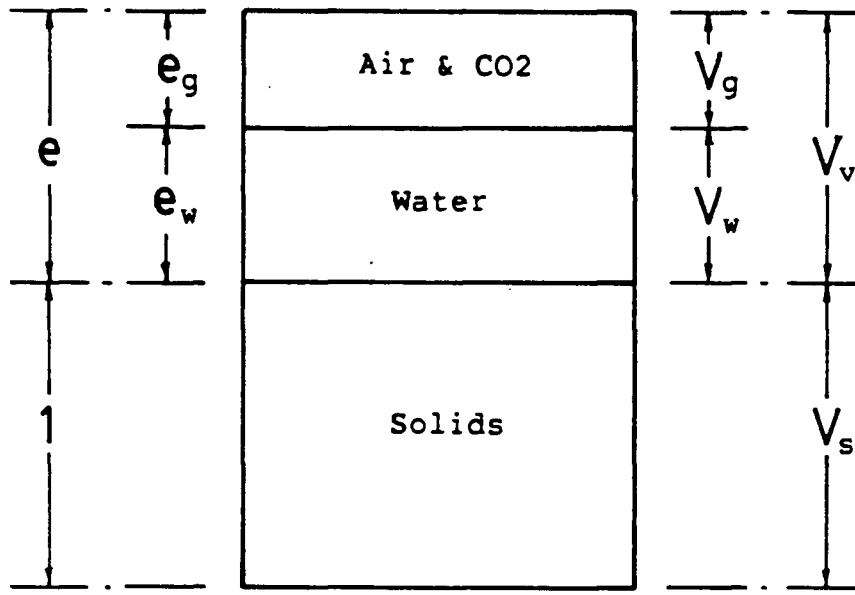

Fig.3.2 - Phase diagram for gassy soil

$$\beta_f = \frac{1}{e}\left[\frac{(e - e_w) + H_a\, e_w + H_{co2}\, e_w}{P} + \beta_w e_w\right] \qquad 3.24c$$

and

$$K_f = \frac{1}{\beta_f}$$

c) Gas (Methane)/Bitumen and Water Mixture

Again, by definition the compressibility of pore fluids

$$\beta_f = -\frac{1}{V_f} * \frac{dV_f}{dP}$$

$$= -\frac{1}{V_f}\left[\frac{dV_{fg}}{dP} + \frac{dV_L}{dP}\right]$$

$$= -\frac{1}{V_f}\left[-\frac{(V^i_{fg} + V^i_{dg})}{P_i + \Delta P} - V_w\beta_w - V_b\,\beta_b\right] \qquad 3.26a$$

Consider the phase diagrams in Figure 3.3, the volume of solids is assumed to be 1 unit, the volume of voids is e units according to definition of void ratios

Therefore

$$\frac{V^i_{fg}}{V_f} = \frac{(e - e_w - e_b)}{e} \qquad 3.27a$$

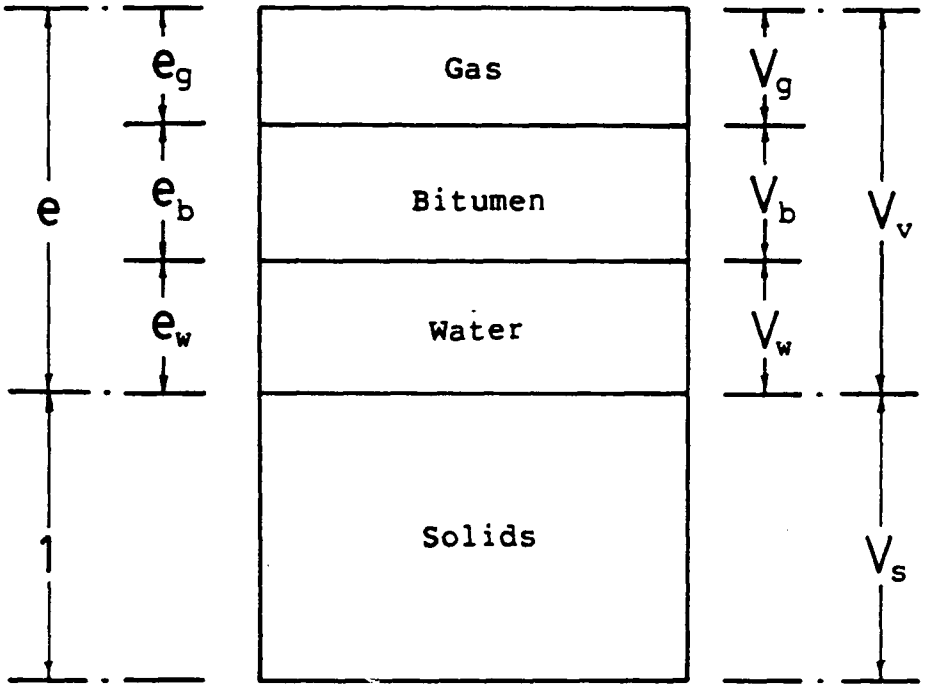

Fig.3.3 - Phase diagram for oil sand

$$\frac{V_{dg}^{i}}{V_f} = \frac{H_{g/w} e_w + H_{g/b}\, e_b}{e} \qquad 3.27b$$

where $H_{g/w}$, $H_{g/b}$ are Henry's solubility constants of gas in water and bitumen respectively.

Substituting Equations 3.27 into 3.26a, and ΔP approaches zero, yields,

$$\beta_f = \frac{1}{e} \left[\frac{(e - e_w - e_b) + H_{g/w}\, e_w + H_{g/b}\, e_b}{P} + \beta_w e_w + \beta_b e_b\right] \qquad 3.26b$$

and

$$K_f = \frac{1}{\beta_f}$$

CHAPTER 4 : FINITE ELEMENT FORMULATIONS

4.1 INTRODUCTION

Two types of formulations are presented herein which are suitable for modelling a variety of problems encountered in practice. Depending on the nature of the problems, they will fall into one of the following categories:

1) Plane strain - 2 Dimensional, e.g. tunnels, shaft, etc.
2) Axisymmetric - 3 Dimensional, e.g. triaxial test, wellbore, etc.

The soil is modelled by isoparametric quadrilateral or triangular elements.

Stress distribution formulations are added to cope with problems where plastic zones are developed during loading or unloading.

4.2. THE PLANE SRAIN FORMULATIONS

4.2.1 The Constitutive Matrix [D]

Plane strain problems are characterized by the following two properties:

1) no deflection in z direction
2) first derivative of the x and y deflections with respect to z are zero.

Therefore

$$w = 0 \qquad 4.1a$$

$$\Delta\varepsilon_{33} = \Delta\varepsilon_{13} = \Delta\varepsilon_{23} = 0 \qquad 4.1b$$

where u, v, w are the displacements in x, y and z directions respectively with corresponding subscripts, 1, 2 and 3 respectively.

From the generalized Hooke's law for incremental elasticity

$$\Delta\varepsilon_{11} = [\Delta\sigma_{11} - \nu\,(\Delta\sigma_{22} + \Delta\sigma_{33})]/E \qquad 4.2a$$

$$\Delta\varepsilon_{22} = [\Delta\sigma_{22} - \nu\,(\Delta\sigma_{11} + \Delta\sigma_{33})]/E \qquad 4.2b$$

$$\Delta\varepsilon_{33} = [\Delta\sigma_{33} - \nu\,(\Delta\sigma_{11} + \Delta\sigma_{22})]/E \qquad 4.2c$$

$$\Delta\varepsilon_{12} = \Delta\sigma_{12}/G \qquad 4.2d$$

$$\Delta\varepsilon_{23} = \Delta\sigma_{23}/G \qquad 4.2e$$

$$\Delta\varepsilon_{31} = \Delta\sigma_{31}/G \qquad 4.2f$$

After substituting the conditions from equation 4.1b into equations 4.2, it follows that:

$$\Delta\sigma_{13} = \Delta\sigma_{31} = 0 \qquad 4.3a$$

$$\Delta\sigma_{23} = \Delta\sigma_{32} = 0 \qquad 4.3b$$

where $\Delta\sigma_{ij}$ is the incremental shear stress with the direction indicated by the subscripts.

With the above eliminations, the incremental stress and strain vectors become

$$(\Delta\sigma) = [\Delta\sigma_{11} \quad \Delta\sigma_{22} \quad \Delta\sigma_{12}]^T \qquad 4.4a$$

$$(\Delta\varepsilon) = [\Delta\varepsilon_{11} \quad \Delta\varepsilon_{22} \quad \Delta\varepsilon_{12}]^T \qquad 4.4b$$

The constitutive relations for a plane strain problem in total stress analysis are written (Naylor, 1973) as:

$$\begin{bmatrix} \Delta\sigma_{11} \\ \Delta\sigma_{22} \\ \Delta\sigma_{12} \end{bmatrix} = \left\{ \frac{E}{(1+\nu)(1-2\nu)} \begin{bmatrix} 1-\nu & \nu & 0 \\ \nu & 1-\nu & 0 \\ 0 & 0 & \frac{(1-2\nu)}{2} \end{bmatrix} + K_a \begin{bmatrix} 1 & 1 & 0 \\ 1 & 1 & 0 \\ 0 & 0 & 0 \end{bmatrix} \right\} \begin{bmatrix} \Delta\varepsilon_{11} \\ \Delta\varepsilon_{22} \\ \Delta\varepsilon_{12} \end{bmatrix} \qquad 4.5a$$

or

$$(\Delta\sigma) = ([D'] + [D_f]) \quad (\Delta\varepsilon) \qquad 4.5b$$

where

E = tangent Young's modulus

ν = tangent Poisson's ratio

K_a = apparent tangent bulk fluid modulus

The constitutive relations can also be written in another equivalent form which is adopted in INCOIL.

$$\begin{bmatrix} \Delta\sigma_{11} \\ \Delta\sigma_{22} \\ \Delta\sigma_{12} \end{bmatrix} = \left\{ \begin{bmatrix} B' + G' & B' - G' & 0 \\ B' - G & B' - G' & 0 \\ 0 & 0 & G' \end{bmatrix} + K_a \begin{bmatrix} 1 & 1 & 0 \\ 1 & 1 & 0 \\ 0 & 0 & 0 \end{bmatrix} \right\} \begin{bmatrix} \Delta\varepsilon_{11} \\ \Delta\varepsilon_{22} \\ \Delta\varepsilon_{12} \end{bmatrix} \qquad 4.6a$$

or

$$(\Delta\sigma) = ([D']) + [D_f]) \ (\Delta\varepsilon) \qquad 4.6b$$

Where

$$B' = \frac{3B}{2(1+\nu)}$$

$$G' = \frac{E}{2(1+\nu)}$$

B = tangent bulk modulus

E = tangent Young's modulus

ν = tangent Poisson's ratio

K_a = apparent tangent bulk fluid modulus

Equation 4.6 can also be written as

$$(\Delta\sigma) = [D] \ (\Delta\varepsilon) \qquad 4.7$$

where

$[D]$ is the constitutive matrix

4.2.2 The Strain Displacement Matrix [B]

For isoparametric elements, the geometry (x,y) and displacement (u,v) are both expressed by te same shape functions and are approximated as:

$$\begin{pmatrix} x \\ y \end{pmatrix} = [N] \{\delta\} \tag{4.10}$$

and

$$\begin{pmatrix} u \\ v \end{pmatrix} = [N] \{\delta'\} \tag{4.11}$$

where

$$[N] = \begin{bmatrix} N_1 & 0 & N_2 & 0 & N_3 & 0 & N_4 & 0 \\ 0 & N_1 & 0 & N_2 & 0 & N_3 & 0 & N_4 \end{bmatrix}$$

$$\{\delta\} = [x_1 \quad y_1 \quad x_2 \quad y_2 \quad x_3 \quad y_3 \quad x_4 \quad y_4]^T$$

$$\{\delta'\} = [u_1 \quad v_1 \quad u_2 \quad v_3 \quad u_3 \quad v_3 \quad u_4 \quad v_4]^T$$

in which $\{\delta\}$ is the nodal coordinate vector and $\{\delta'\}$ is the incremental

nodal displacement vector

and

$N_1 = (1-s)(1-t)/4$

$N_2 = (1-s)(1+t)/4$

$N_3 = (1+s)(1+t)/4$

$N_4 = (1+s)(1-t)/4$

x_i, y_i = nodal coordinates in x and y directions respectively

u_j, v_j = incremental nodal displacement in x and y directions respectively.

s,t are local coordinates

The incremental strain vector can be expressed in terms of displacement as follows:

$$\begin{Bmatrix} \Delta\varepsilon_{11} \\ \Delta\varepsilon_{12} \\ \Delta\varepsilon_{13} \end{Bmatrix} = \begin{Bmatrix} \partial u/\partial x \\ \partial v/\partial y \\ \partial u/\partial y + \partial v/\partial x \end{Bmatrix} \qquad 4.12$$

Substitution of u and v from equation 4.11 into equation 4.12 yields

$$\begin{Bmatrix} \Delta\varepsilon_{11} \\ \Delta\varepsilon_{22} \\ \Delta\varepsilon_{13} \end{Bmatrix} = \begin{bmatrix} \frac{\partial N_1}{\partial x} & 0 & \frac{\partial N_2}{\partial x} & 0 & \frac{\partial N_3}{\partial x} & 0 & \frac{\partial N_4}{\partial x} & 0 \\ 0 & \frac{\partial N_1}{\partial y} & 0 & \frac{\partial N_2}{\partial y} & 0 & \frac{\partial N_3}{\partial y} & 0 & \frac{\partial N_4}{\partial y} \\ \frac{\partial N_1}{\partial y} & \frac{\partial N_1}{\partial x} & \frac{\partial N_2}{\partial y} & \frac{\partial N_2}{\partial x} & \frac{\partial N_3}{\partial y} & \frac{\partial N_3}{\partial x} & \frac{\partial N_4}{\partial y} & \frac{\partial N_4}{\partial x} \end{bmatrix} \begin{Bmatrix} u_1 \\ v_1 \\ u_2 \\ v_2 \\ u_3 \\ v_3 \\ u_4 \\ v_4 \end{Bmatrix} \qquad 4.10$$

Equation 4.10 can also be written in matrix notation as

$$(\Delta\varepsilon) = [B]\ (\delta) \qquad 4.13$$

where

$[B]$ is the strain displacement matrix

However, the shape functions N_i for isoparametric elements are defined with respect to the local coordinates s and t and therefore cannot be differentiated directly with respect to the global x, y axes.

In order to overcome this difficulty it is necessary to obtain

the derivatives of the two sets of coordinates and this can be achieved through the chain rule of partial differentiation.

For plain strain problems, the derivatives are related as

$$\begin{bmatrix} \frac{\partial}{\partial s} \\ \\ \frac{\partial}{\partial t} \end{bmatrix} = [J] \begin{bmatrix} \frac{\partial}{\partial x} \\ \\ \frac{\partial}{\partial y} \end{bmatrix} \qquad 4.14$$

where

$$[J] = \begin{bmatrix} \frac{\partial x}{\partial s} & \frac{\partial y}{\partial s} \\ \\ \frac{\partial x}{\partial t} & \frac{\partial y}{\partial t} \end{bmatrix}$$ is called the Jacobian matrix

Hence the derivatives w•r•t• x and y can be expressed as derivatives w•r•t s and t as follows

$$\begin{bmatrix} \frac{\partial}{\partial x} \\ \\ \frac{\partial}{\partial y} \end{bmatrix} = [J]^{-1} \begin{bmatrix} \frac{\partial}{\partial s} \\ \\ \frac{\partial}{\partial t} \end{bmatrix} \qquad 4.15$$

The strain displacement matrix in Equation 4.13 are evaluated numerically, using Gaussian quadrature over quadrilateral regions. The quadrature rules are all of the form

$$\int\int f(s,t)\, ds\, dt \simeq \sum_{i=1}^{n} \sum_{j=1}^{n} K_i K_j f(s_i, t_j)$$

where K_i, K_i are weighting functions and s_i, t_j are coordinate position within the element.

A 2 x 2 Gauss quadrature is used to evaluate the strain displacement.

4.2.3 The Stiffness Matrix [K]

The stiffness matrix for the force displacement relationship is obtained by the principle of virtual work. For a virtual nodal displacement vector $(\bar{\delta})_e$, the external work done, W(ext), by the external force vector (f) caused by virtual displacements is written as

$$W(ext) = (\bar{\delta})_e^T \ (f) \qquad 4.16$$

The virtual strain vector caused by the virtual displacements vector is written as

$$(\Delta\bar{\varepsilon}) = [B] \ (\bar{\delta})_e \qquad 4.17$$

Hence the internal work done, W(ext), caused by the virtual strain is written as

$$W(int) = \int_A \ (\Delta\bar{\varepsilon})^T \ (\Delta\sigma) \ t \ dA \qquad 4.18a$$

where

t = thickness of the element

A = area of the element

Substituting equation 4.17 into 4.18a yields

$$W(int) = \int_A [\bar{\delta}]_e^T [B]^T [D] [B] [\delta] \, t \, dA \qquad 4.18b$$

Applying principle of virtual work

$$W(ext) = W(int) \qquad 4.19$$

Therefore

$$(f) = \int_A [B]^T [D] [B] [\delta] \, t \, dA \qquad 4.20$$

$$(f) = [K] (\delta) \qquad 4.21$$

where $[K] = \int_A [B]^T [D] [B] \, t \, dA$ is called the stiffness matrix for the element.

The global stiffness matrix, $[K_g]$, is obtained by assembling all the element stiffness matrices together. The procedure of assembling the element matrix is based on the requirement of 'compatibility' at the element nodes. This means that at the nodes where elements are connected, the values of the unknown nodal degrees of freedom are the same for all the elements joining at that node. The global force

vector, $[F]$, is assembled by adding nodal loads of each of the elements sharing the node. Displacements are calculated using standard procedure (e.g. Gaussian elimination) to solve the simultaneous equations, $[K_g]\ [\delta] = [F]$, represented by the global stiffness matrix and the force vector. Strains can be computed from equation 4.13 or 4.36 after knowing the elements nodal displacements. After solving for ~~displacements and~~ strains, the effective stress and pore pressure can be computed from

$$(\Delta\sigma') = [D']\ (\Delta\varepsilon)$$

and

$$(\Delta u) = [D_f]\ (\Delta\varepsilon)$$

4.3 THE AXISYMMETRIC FORMULATIONS

4.3.1 The Constitutive Matrix [D]

Axisymmetric problems are characterized by the following properties:

1) Symmetry of both geometry and loading
2) Stress components are independent of the angular (θ) coordinates.

Hence

$$v = 0 \qquad 4.22a$$

$$\Delta\varepsilon_{13} = \Delta\varepsilon_{31} = 0 \qquad 4.22b$$

$$\Delta\varepsilon_{23} = \Delta\varepsilon_{32} = 0 \qquad 4.22c$$

where u, v, w are displacements in the r, z and θ directions with corresponding cubscripts, 1, 2 and 3 respectively.

From the generalized Hooke's law for incremental elasticity

$$\Delta\varepsilon_{11} = [\Delta\sigma_{11} - \nu\,(\Delta\sigma_{22} + \Delta\sigma_{33})]/E \qquad 4.23a$$

$$\Delta\varepsilon_{22} = [\Delta\sigma_{22} - \nu\,(\Delta\sigma_{33} + \Delta\sigma_{11})]/E \qquad 4.23b$$

$$\Delta\varepsilon_{33} = [\Delta\sigma_{33} - \nu\,(\Delta\sigma_{11} + \Delta\sigma_{22})]/E \qquad 4.23c$$

$$\Delta\varepsilon_{13} = \Delta\sigma_{13}/G \qquad 4.23d$$

$$\Delta\varepsilon_{12} = \Delta\sigma_{12}/G \qquad 4.23e$$

$$\Delta\varepsilon_{23} = \Delta\sigma_{23}/G \qquad 4.23f$$

After substituting the conditions from Equations 4.22b and 4.22c into Equations 4.23, it follows that

$$\Delta\sigma_{13} = \Delta\sigma_{31} = 0 \qquad 4.14a$$

$$\Delta\sigma_{23} = \Delta\sigma_{32} = 0 \qquad 4.15a$$

where $\Delta\sigma_{ij}$ is the incremental shear stress with the direction indicated by the subscripts.

With the above eliminations, the incremental stress and strain vectors become

$$(\Delta\sigma) = [\Delta\sigma_{11} \quad \Delta\sigma_{22} \quad \Delta\sigma_{33} \quad \Delta\sigma_{12}]^T \qquad 4.25$$

$$(\Delta\varepsilon) = [\Delta\varepsilon_{11} \quad \Delta\varepsilon_{22} \quad \Delta\varepsilon_{33} \quad \Delta\varepsilon_{12}]^T \tag{4.26}$$

The constitutive relations for an axisymmetric problem in total stress analysis are written (Naylor, 1973) as

$$\begin{bmatrix} \Delta\sigma_{11} \\ \Delta\sigma_{22} \\ \Delta\sigma_{33} \\ \Delta\sigma_{12} \end{bmatrix} = \left\{ \frac{E}{(1+\nu)(1-2\nu)} \begin{bmatrix} 1-\nu & \nu & \nu & 0 \\ \nu & 1-\nu & \nu & 0 \\ \nu & \nu & 1-\nu & 0 \\ 0 & 0 & 0 & \frac{1-2\nu}{2} \end{bmatrix} + K_a \begin{bmatrix} 1 & 1 & 1 & 0 \\ 1 & 1 & 1 & 0 \\ 1 & 1 & 1 & 0 \\ 0 & 0 & 0 & 0 \end{bmatrix} \right\} \begin{bmatrix} \Delta\varepsilon_{11} \\ \Delta\varepsilon_{22} \\ \Delta\varepsilon_{33} \\ \Delta\varepsilon_{12} \end{bmatrix} \tag{4.27a}$$

Also

$$(\Delta\bar{\sigma}) = \left[[D'] + [D_f] \right] (\Delta\varepsilon) \tag{4.27b}$$

where

E = tangent Young's modulus

ν = tangent Poisson's ratio

K_a = apparent tangent bulk modulus

The constitutive relations can also be written in another equivalent form which is adopted in INCOIL.

$$\begin{bmatrix} \Delta\sigma_{11} \\ \Delta\sigma_{22} \\ \Delta\sigma_{33} \\ \Delta\sigma_{12} \end{bmatrix} = \left\{ \begin{bmatrix} B'+G' & B'-G' & B'-G' & 0 \\ B'-G' & B'+G' & B'-G' & 0 \\ B'-G' & B'-G' & B'+G' & 0 \\ 0 & 0 & 0 & G' \end{bmatrix} + K_a \begin{bmatrix} 1 & 1 & 1 & 1 & 0 \\ 1 & 1 & 1 & 1 & 0 \\ 1 & 1 & 1 & 1 & 0 \\ 0 & 0 & 0 & 0 & 0 \end{bmatrix} \right\} \begin{bmatrix} \Delta\varepsilon_{11} \\ \Delta\varepsilon_{22} \\ \Delta\varepsilon_{33} \\ \Delta\varepsilon_{12} \end{bmatrix} \qquad 4.28a$$

or

$$[\Delta\sigma] = ([D'] + [D_f])\ [\Delta\varepsilon] \qquad 4.28b$$

where

$$B' = \frac{3B}{2(1+\nu)}$$

$$G' = \frac{E}{2(1+\nu)}$$

B = tangent bulk modulus

E = tangent Young's modulus

ν = tangent Poisson's ratio

K_a = apparent tangent bulk fluid modulus

Equation 4.28 may be written in matrix notation as

$$(\Delta\sigma) = [D]\ (\Delta\varepsilon) \qquad 4.29$$

where $[D]$ is the constitutive matrix.

4.3.2 The Strain Displacement Matrix $[B]$

The isoparametric elements, the geometry (r, z) and displacements (u, v) are both expressed by the same shape functions and are approximated as:

$$\begin{Bmatrix} r \\ z \end{Bmatrix} = [N]\ (\delta) \qquad 4.32$$

$$\begin{Bmatrix} u \\ v \end{Bmatrix} = [N]\ (\delta') \qquad 4.33$$

$$[N] = \begin{bmatrix} N_1 & 0 & N_2 & 0 & N_3 & 0 & N_4 & 0 \\ 0 & N_1 & 0 & N_2 & 0 & N_3 & 0 & N_4 \end{bmatrix}$$

$$(\delta) = [r_1 \quad z_1 \quad r_2 \quad z_2 \quad r_3 \quad z_3 \quad r_4 \quad z_4]$$

$$(\delta') = [u_1 \quad v_1 \quad u_2 \quad v_2 \quad u_3 \quad v_3 \quad u_4 \quad v_4]$$

in which (δ) is the nodal coordinate vector, (δ') is the incremental

nodal displacement vector and the shape functions N_i are the same as given in Section 4.2.2.

and

r_i, z_i = nodal coordinates in x and y directions respectively,

u_j, v_j = incremental nodal displacements in x and y directions respectively.

The incremental strain vector can be expressed in terms of displacements as follows:

$$\begin{Bmatrix} \Delta\varepsilon_{11} \\ \Delta\varepsilon_{22} \\ \Delta\varepsilon_{33} \\ \Delta\varepsilon_{12} \end{Bmatrix} = \begin{Bmatrix} \frac{\partial u}{\partial r} \\ \frac{\partial v}{\partial r} \\ \frac{u}{r} \\ \frac{\partial v}{\partial r} + \frac{\partial u}{\partial z} \end{Bmatrix} \qquad 4.34$$

Substitution of u and v from Equation 4.33 into Equation 4.30 yields

$$\begin{Bmatrix} \Delta\varepsilon_{11} \\ \Delta\varepsilon_{22} \\ \Delta\varepsilon_{33} \\ \Delta\varepsilon_{12} \end{Bmatrix} = \begin{bmatrix} \frac{\partial N_1}{\partial r} & 0 & \frac{\partial N_2}{\partial r} & 0 & \frac{\partial N_3}{\partial r} & 0 \\ 0 & \frac{\partial N_1}{\partial z} & 0 & \frac{\partial N_2}{\partial z} & 0 & \frac{\partial N_3}{\partial z} \\ \frac{N_1}{r} & 0 & \frac{N_2}{r} & 0 & \frac{N_3}{r} & 0 \\ \frac{\partial N_1}{\partial z} & \frac{\partial N_1}{\partial r} & \frac{\partial N_2}{\partial z} & \frac{\partial N_3}{\partial r} & \frac{\partial N_3}{\partial z} & \frac{\partial N_3}{\partial r} \end{bmatrix}$$

$$\begin{bmatrix} \frac{\partial N_4}{\partial r} & 0 \\ 0 & \frac{\partial N_4}{\partial z} \\ \frac{N_4}{r} & 0 \\ \frac{\partial N_4}{\partial z} & \frac{\partial N_4}{\partial r} \end{bmatrix} \begin{Bmatrix} u_1 \\ v_1 \\ u_2 \\ v_2 \\ u_3 \\ v_3 \\ u_4 \\ v_4 \end{Bmatrix} \qquad 4.35$$

Equation 4.35 can also be written in matrix notation as

$$(\Delta\varepsilon) = [B]\,(\delta) \qquad 4.36$$

where

$[B]$ is the strain displacement matrix

However, the shape functions N_i for isoparametric elements are defined with respect to the local coordinates s and t therefore cannot be differentiated directly with respect to the global x, y axes.

In order to overcome this difficulty it is necessary to obtain a relationship between the derivatives of the two sets of coordinates and this can be achieved through the chain rule of partial differentiation.

$$\begin{Bmatrix} \frac{\partial}{\partial s} \\ \frac{\partial}{\partial t} \end{Bmatrix} = [J] \begin{Bmatrix} \frac{\partial}{\partial r} \\ \frac{\partial}{\partial z} \end{Bmatrix} \qquad 4.37$$

where

$$[J] = \begin{bmatrix} \frac{\partial r}{\partial s} & \frac{\partial z}{\partial s} \\ \frac{\partial r}{\partial t} & \frac{\partial z}{\partial t} \end{bmatrix}$$ is called the Jacobian matrix

Hence the derivatives w•r•t x and y can be expressed as derivatives w•r•t s and t as follows

$$\begin{bmatrix} \frac{\partial}{\partial r} \\ \frac{\partial}{\partial z} \end{bmatrix} = [J]^{-1} \begin{bmatrix} \frac{\partial}{\partial s} \\ \frac{\partial}{\partial t} \end{bmatrix} \qquad 4.38$$

A similar Gauss quadrature mentioned in Section 4.2.2. is employed to evaluate the above $[B]$ matrix numerically.

4.3.3 The Stiffness Matrix [K]

The stiffness matrix for the force displacement relatinship is obtained by the principle of virtual work. For a virtual nodal displacement vector $(\bar{\delta})_e$, the external work done, W(ext), by the external force vector (F) caused by the virtual displacements is written as

$$W(ext) = (\bar{\delta})_e^T \ (f) \qquad 4.39$$

The virtual strain vector caused by the virtual displacements vector is

written as

$$(\Delta\bar{\varepsilon}) = [B]\ (\bar{\delta})_e \qquad 4.40$$

Hence the internal work done, W(int), caused by the virtual strain is written as

$$W(int) = \int_V\ (\Delta\bar{\varepsilon})^T\ (\Delta\sigma)\ dV \qquad 4.41a$$

where V = volume of the element

Substituting Equation 4.40 into 4.41a yields

$$W(int) = \int_V\ (\bar{\delta})_e^T\ [B]^T\ [D]\ [B]\ [\delta]\ dV \qquad 4.41b$$

Applying the principle of virtual work

$$Wext = Wint \qquad 4.42$$

Therefore

$$(f) = \int_V\ [B]^T\ [D]\ [B]\ [\delta]\ dV \qquad 4.43$$

$$(f) = [K]\ (\delta) \qquad 4.44$$

where $\int_V [B]^T [D] [B] \, dV$ is called the stiffness matrix for the element.

The procedure of obtaining element stresses and strains is the same as described in Section 6.2.3.

4.4 LOAD SHEDDING (PLAIN STRAIN) (Byrne 1983)

Problems arise when any element within the solution domain violates the failure criteria (Mohr Coulomb). That is, for unloading of a shaft or tunnel, a plastic zone usually developes adjacent to the shaft. The extent of plastic zone and hence volume changes are only approximated since the stress redistribution has not been considered during the formation of the zone.

The analysis predicts the stress path ABC instead of ABD on unloading. But the stress state at C (Figure 4.1) violates the failure criterion (Mohr Coulomb). If load shedding technique is used, the overstress can be distributed to the adjacent elements by applying an appropriate set of nodal forces described herein and brings the stress path BC back to the correct BD.

The overstress, $\Delta\tau$, in the element can be removed by subtracting the computed stresses by $\Delta\sigma_{11}$, $\Delta\sigma_{22}$ and $\Delta\sigma_{12}$ amount as shown in Figure 4.21b.

where $\Delta\sigma_{ij}$ have the same notation as those in Section 4.2 and 4.3

$$(\Delta\sigma) = \begin{bmatrix} \Delta\sigma_{11} \\ \Delta\sigma_{22} \\ \Delta\sigma_{12} \end{bmatrix} = [T] \begin{bmatrix} \Delta\sigma_1 \\ \Delta\sigma_3 \\ \Delta\tau_{13} \end{bmatrix} \qquad 4.45$$

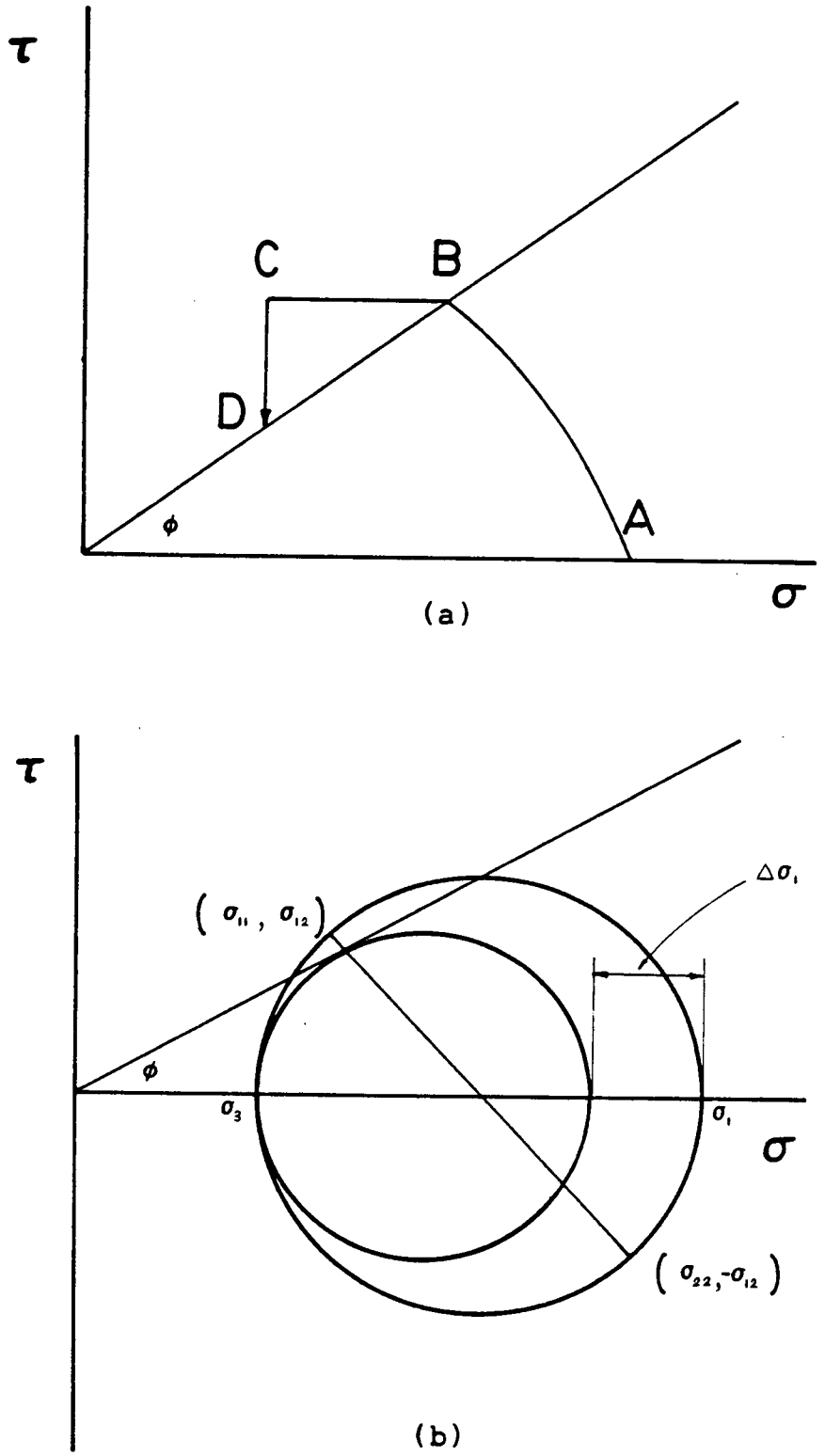

Fig.4.1 - Stresses associated with load shedding

where

$$(T) = \begin{bmatrix} \frac{1}{2} - \frac{\cos 2\theta}{2} & \frac{1}{2} + \frac{\cos 2\theta}{2} & 0 \\ \frac{1}{2} + \frac{\cos 2\theta}{2} & \frac{1}{2} - \frac{\cos 2\theta}{2} & 0 \\ -\frac{\sin 2\theta}{2} & \frac{\sin 2\theta}{2} & 0 \end{bmatrix}$$ is called the transformation matrix

$\Delta\sigma_3$ = minor principal stress = 0

$\Delta\sigma_1$ = major principal stress

$= \sigma_1 - \sigma_3 \tan^2 (45 + \frac{\phi}{2})$

$\Delta\tau_{13}$ = principal shear stress = 0

The derivation of these stresses changes and the transformation matrix is in Appendix E,

The removal of these overstresses can be achieved by applying a set of nodal forces which is obtained by the principle of virtual work. The incremental nodal force vector causes a virtual displacement vector. Hence the external work done, W(ext), can be written as

$$W(ext) = (\bar{\delta})_e^T \ (\Delta f)_e \qquad 4.46$$

The incremental virtual strain vector caused by the virtual displacement vector is

$$(\Delta\bar{\varepsilon})_e = [B] \ (\bar{\delta})_e \qquad 4.47$$

Therefore, the internal work done, W(int), is

$$W(int) = \int_A \left(\Delta\bar{\varepsilon}\right)_e^T \left(\Delta\sigma\right)_e \, t \, dA \qquad 4.48a$$

Substitution of Equation 4.43 to 4.48 yields

$$W(int) = \int_A \left(\bar{\delta}\right)^T [B] \left(\Delta\sigma\right) \, t \, dA \qquad 4.48b$$

Applying the principle of virtual work

$$W(ext) = W(int) \qquad 4.49$$

Hence

$$[\Delta f]_e = t\int_A [B]^T [\Delta\sigma]_e \, dA \qquad 4.50$$

where $[B]$ is the strain displacement matrix in Section 4.2.2.
and $[\Delta\sigma]_e$ is the stress vector shown in Equation 4.41.

The failed element will have a stress change of $\Delta\sigma_{11}$, $\Delta\delta_{22}$ and $\Delta\sigma_{12}$. However, the computed stresses may not lie on the failure envelope due to the application of the nodal forces. Therefore iterations may be required to bring this to the assigned tolerance.

The loading shedding technique presented herein gives the same results compared with INCOIL (σ_m' = constant). However, the number of iterations required to bring the computed stresses back to the failure envelope is less.

With the incorporation of load shedding technique, the sand

skeleton is modelled as a non-linear elastic-plastic porous material. The soil skeleton is coupled with the pore fluids in the undrained model. For undrained conditions, this model allows stresses, pore pressure and deformations of oil sand masses to be evaluated by finite elements.

CHAPTER 5 : COMPARISONS WITH EXISTING SOLUTIONS

5.1 INTRODUCTION

It is important to check the validity of the developed model before any major application. Two types of comparisons are presented herein which are suitable for checking the stress-strain model of the soil skeleton and also the newly developed gas law model.

For the validation of the analytical procedure, the computed results are compared with elastic and elastic-plastic closed form solutions. The gas law model is validated by comparing computed solutions with observed data, such as expansion of oil sand cores and triaxial tests on gassy soils.

5.2 COMPARISONS WITH THEORETICAL RESULTS

5.2.1 Elastic Closed Form Solutions

The theory for elastic closed form solution was first developed by Timoshenko (1941). The plane strain solutions of stresses and displacements in a thick wall cylinder are presented herein:

Stresses

$$\sigma_r = \frac{a^2 P_i - b^2 P_o}{b^2 - a^2} + \frac{(P_i - P_o)\, a^2\, b^2}{(b^2 - a^2)\, r^2} \qquad 5.1a$$

$$\sigma_\theta = \frac{a^2\, P_i - b^2 P_o}{b^2 - a^2} - \frac{(P_i - P_o)\, a^2\, b^2}{(b^2 - a^2)\, r^2} \qquad 5.1b$$

Displacement

$$\delta = \frac{(1-2\nu)\ (1+\nu)}{E}\ \frac{(a^2P_i - b^2\ P_o)r}{b^2 - a^2}$$

$$+ \frac{(1+\nu)}{E}\ \frac{(P_i - P_o)\ a^2b^2}{(b^2 - a^2)\ r} \qquad 5.1c$$

where P_i = Pressure on the inner surface of cylinder

P_o = Pressure on outer surface of cylinder

E = Young's modulus

ν = Poisson's ratio

and a, b, r are defined in Figure 5.1

The response of unloading a thick wall cylinder is being investigated.

The stresses and displacements predicted by the programme are in remarkably good agreement with the closed form solution as shown in Figure 5.2. Hence the analytical procedure is validated

5.2.2 Elastic-Plastic Closed Form Solution

For a tunnel or shaft problem, the initial state of stress will be the same throughout the domain. As the support pressure of the tunnel drops, yielding will occur if the strength of the soil is exceeded. Yielding develops on the inside face first as a plastic annular zone and extends radially outward if the support pressure is reduced further. Hence there exists a plastic and an elastic zone in the domain concentrically. The solutions of stresses and displacements

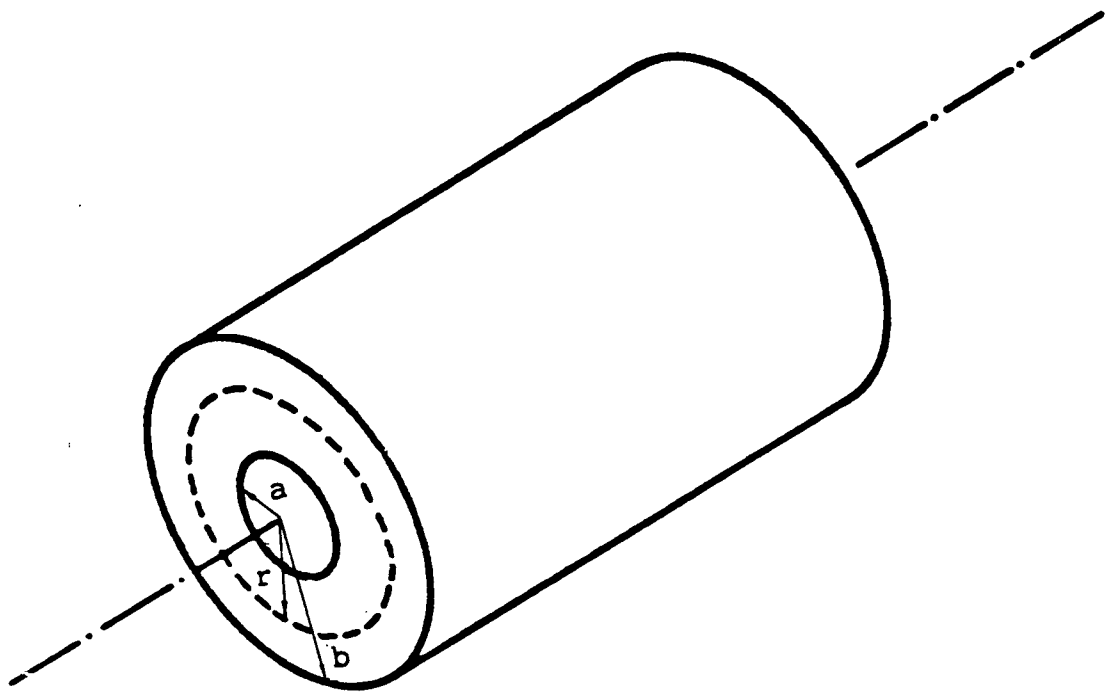

Fig.5.1 - Thick wall cylinder

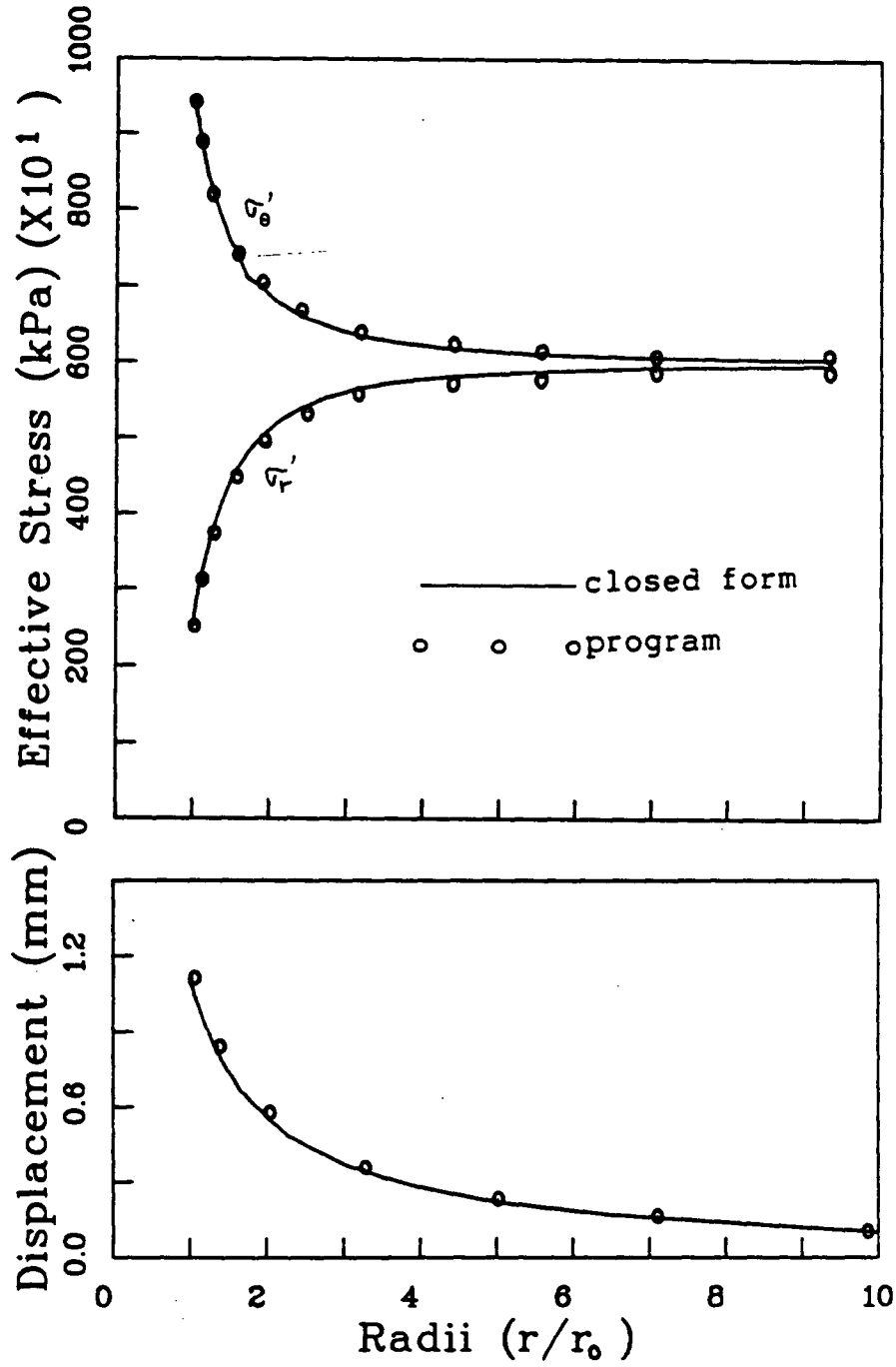

E = 3000 MPa
ν = 1/3
initial stress : $\sigma_r = \sigma_\theta$ = 6000 kPa
final stress : σ_r = 2500 kPa
inside radius : r_o = 1 m

Fig.5.2 - Stresses and displacements around circular opening in an elastic material

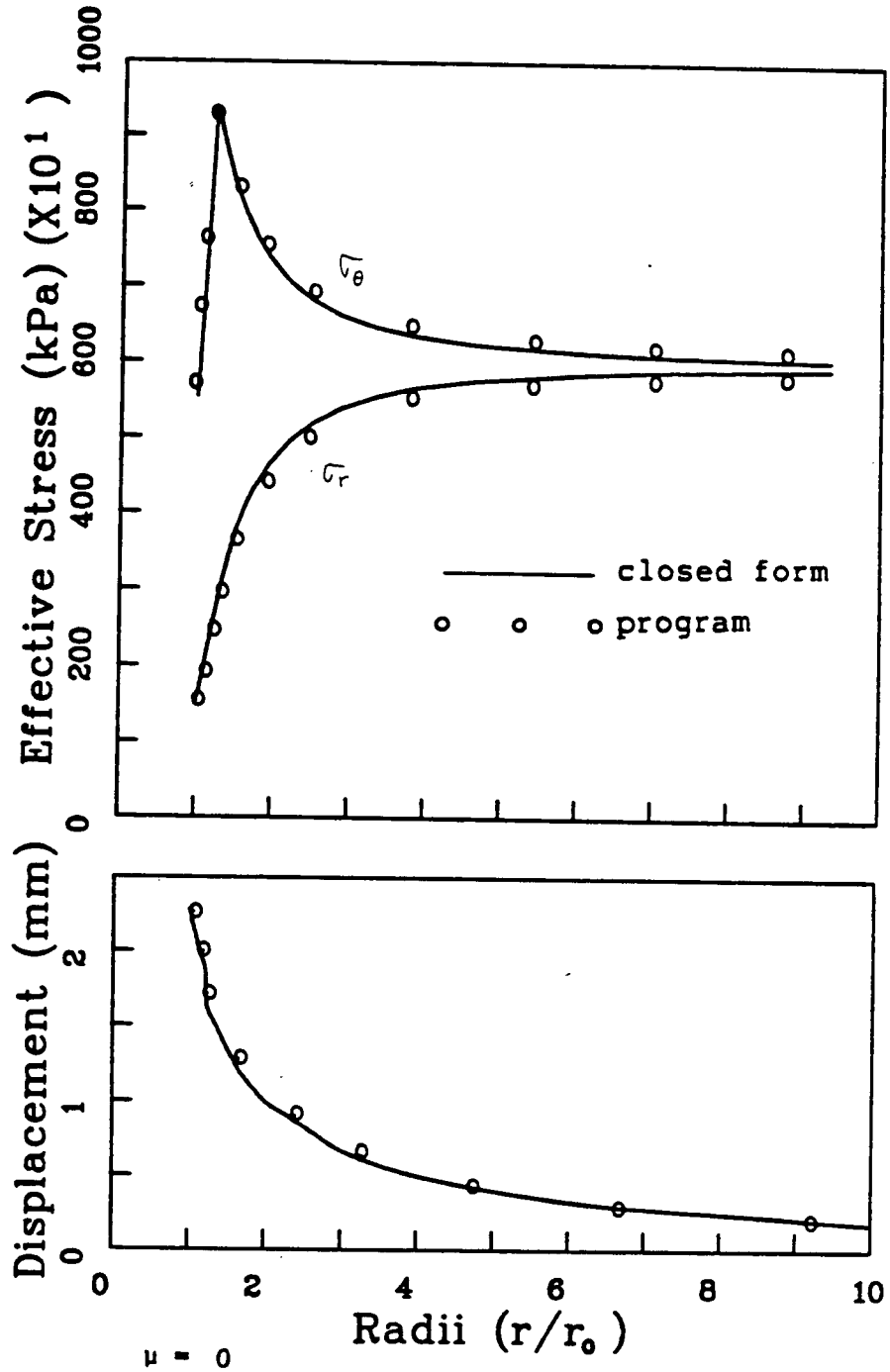

$\mu = 0$
$E = 3000$ kPa
$\nu = 1/3$
$\phi = 40°$
initial stress : $\sigma_r = \sigma_\theta = 6000$ kPa
final stress : $\sigma_r = 1500$ kPa
inside radius : $r_o = 1$m

Fig.5.3 - Stresses and displacements around circular opening in an elastic-plastic material

for the plastic and elastic zone will be quite different.

The stresses and displacements for the elastic zone are just an extension of Equation 5.1 by setting b to infinity. They may be written as

Stresses

$$\sigma_r = P_o + (P_i - P_o) \frac{a^2}{r^2} \qquad 5.2a$$

$$\sigma_\theta = P_o - (P_i - P_o) \frac{a^2}{r^2} \qquad 5.2b$$

Displacement

$$\delta = \frac{1+\nu}{E} \frac{a^2}{r} (P_i - P_o) \qquad 5.2c$$

where P_i = Pressure on inner surface of cylinder

P_o = Pressure on outer surface of cylinder

E = Young's Modulus

ν = Poison's Ratio

Different investigators, Gibson and Anderson (1951), Ladanyi (1963), Vesic (1972) and Hughes et al developed closed form solutions of stresses and displacements for the plastic zone. Hughes et al presented the more elegant solutions which are presented herein:

All the sand is assumed to fail with a constant ratio of principal stresses, so that

$$\frac{\sigma'_\theta}{\sigma'_r} = N = \tan^2 (45 + \frac{\phi}{2}) \qquad 5.3$$

The equilibrium equation that must be satisfied is

$$\frac{d\sigma_r}{dr} + \frac{\sigma'_r - \sigma'_\theta}{r} = 0 \qquad 5.4$$

Substituting for σ'_θ from Equation 5.3, integrating and using outer boundary conditions of $\sigma'_r = \sigma'_R$ at $r = R$.

$$\ell n \ \frac{\sigma'_r}{\sigma'_R} = (1-N) \ \ell n \ (\frac{R}{r}) \qquad 5.5$$

where σ'_r = radial stress at r within the plastic zone

σ'_R = radial stress at the outer boundary, R, of the plastic zone

$$\sigma'_R = P_o \ (1 - \sin\phi) \qquad 5.6$$

$$R = a \ [\frac{P_o}{P_i} \ (1 - \sin\phi)] \ \frac{1-\sin\phi}{2\sin\phi} \qquad 5.7$$

Equation 5.5 governs the distribution of the radial effective stress within the plastic zone.

Continuity of stresses and displacements between the plastic and elastic zone must be maintained. Hence Equation 5.6 is substituted into Equation 5.2c, the displacement, U_R at the elastic-plastic zone contact is

$$U_R = - \frac{1+\nu}{E} R P_o \sin \phi \qquad 5.8$$

Hughes et al also show that the displacements, u, within the plastic zone

$$\frac{u}{r} = (\frac{R}{r})^{n+1} (\frac{U_R}{R}) \qquad 5.9$$

where $n = \tan^2 (45 + \frac{\mu}{2})$

μ = dilation angle

The response of unloading a tunnel is investigated. The comparisons in Figure 5.3 show that the analysis of stresses and displacements in elastic-plastic materials predicted by the programme is in good agreement with the closed form solutions. The minor discrepancies are due to the limit of Poisson's ratio and the coarseness of the mesh. An upper limit of 0.499 is adopted in the programme (MHANS) to maintain numerical stability, whereas the actual value should be 0.5. The agreement in displacements and the extent of the plastic zone also confirm that the load shedding technique in the programme (MHANS) is working properly. This is a satisfactory check of the programme in drained analysis.

Unfortunately, the load shedding technique in INCOIL cannot be successfully tested. The element type in this programme is QM-6. Non-equilibrium of stresses arise in QM-6 elements at high Poisson's ratio ($\nu > 0.4$) if the geometry of the elements is non-rectangular.

Since the elements in a finite element mesh for modelling plane strain shaft problems are not rectangular, non-equilibrium of stresses arise before load shedding is required.

5.3 COMPARISONS WITH OBSERVED DATA

5.3.1 One Dimenional Unloading of Oilsand

This is an opportunity for the new gas law model to be checked with some field data. Since the unloading is 1-D, the validity of the schematic spring analogy model (Figure 1.1) can also be demonstrated.

Unconfined oilsand core taken from drilled holes swells by 5 to 15% of the original volume (Dusseault 1980, Byrne et al 1980). Maximum expansion potential generally cannot be reached because expansion stops when there is adequate intercommunication of gas voids to permit flow of gas out of the sample. This leads to disruption of the soil fabric. This is the equilibrium saturation point in which gas becomes mobile and the maximum gas saturation value is 15% (Amyx et al 1960). However, the total amount of expansion is impossible to predict and can only be measured for individual cores.

The core liners are specifically designed oversized to prevent the jamming of the core within the barrel. Radial expansion is assumed to be completed when the oil sand core is brought up from the drilled hole. The liners and steel containers are assumed to be rigid and frictionless so that only axial expansion of the core is allowed. Therefore, the oilsand core can be modelled as 1-D unloading after recovery.

The initially high stressed core specimen is modelled as shown in Figure 5.4a. Vertical stress is reduced from 750 kPa to zero. The stresses, pore pressure and displacements are shown in Figure 5.4b.

It can be seen that the change in total stress is apportioned between the effective stess and the pore pressure as suggested by the spring analogy model.

Case A: Gas saturation pressure = 100 kPa.

Initially pore pressure is above gas saturation pressure and saturation remains 100%. Therefore loads come off from the pore fluids while effective stress remains fairly constant because pore fluid is the stiffer phase as shown in Figure 5.4b. As pore pressure drops below the gas saturation pressure, gas starts to evolve which causes the pore fluid to become flexible. Stress change will be taken up by the soil skeleton on further unloading until zero effective stress. Further reduction on boundary load at zero effective stress is entirely accommodated by the pore fluids.

Case B: Gas Saturation pressure = 300 kPa.

Because of gas exsolution the pore fluids start as a flexible phase so effective stress drops to zero with no appreciable change of pore pressure on unloading. Reduction of boundary stress beyond this stage is entirely taken by the fluid phases as the soil skeleton essentially has no stiffness at zero effective stress as shown in Figure 5.4b.

It may be seen from figure 5.4b that there are no appreciable displacements when the effective stress is positive. The displacements essentially come from unloading at zero effective stress. The total displacements upon total removal of vertical stress lie within the range of 5 to 15% of the original length.

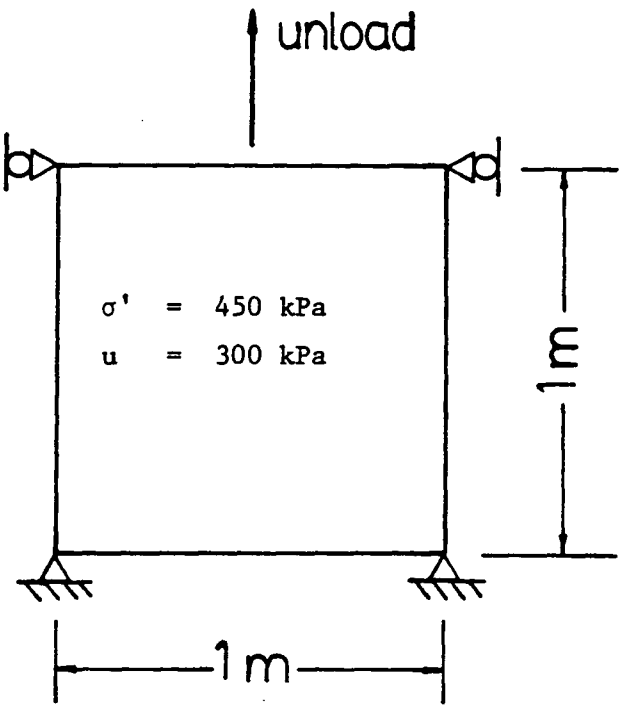

K_E = 1565 , n = 0.5
K_B = 1000 , m = 0.25
ϕ = 65° , $\Delta\phi$ = 22°
R_f = 0.9
n_o = 0.243
n_w = 0.045
H_o = 0.2
H_w = 0.02
S = 100%

5.4 - Model for one dimensional unloading of oil sand

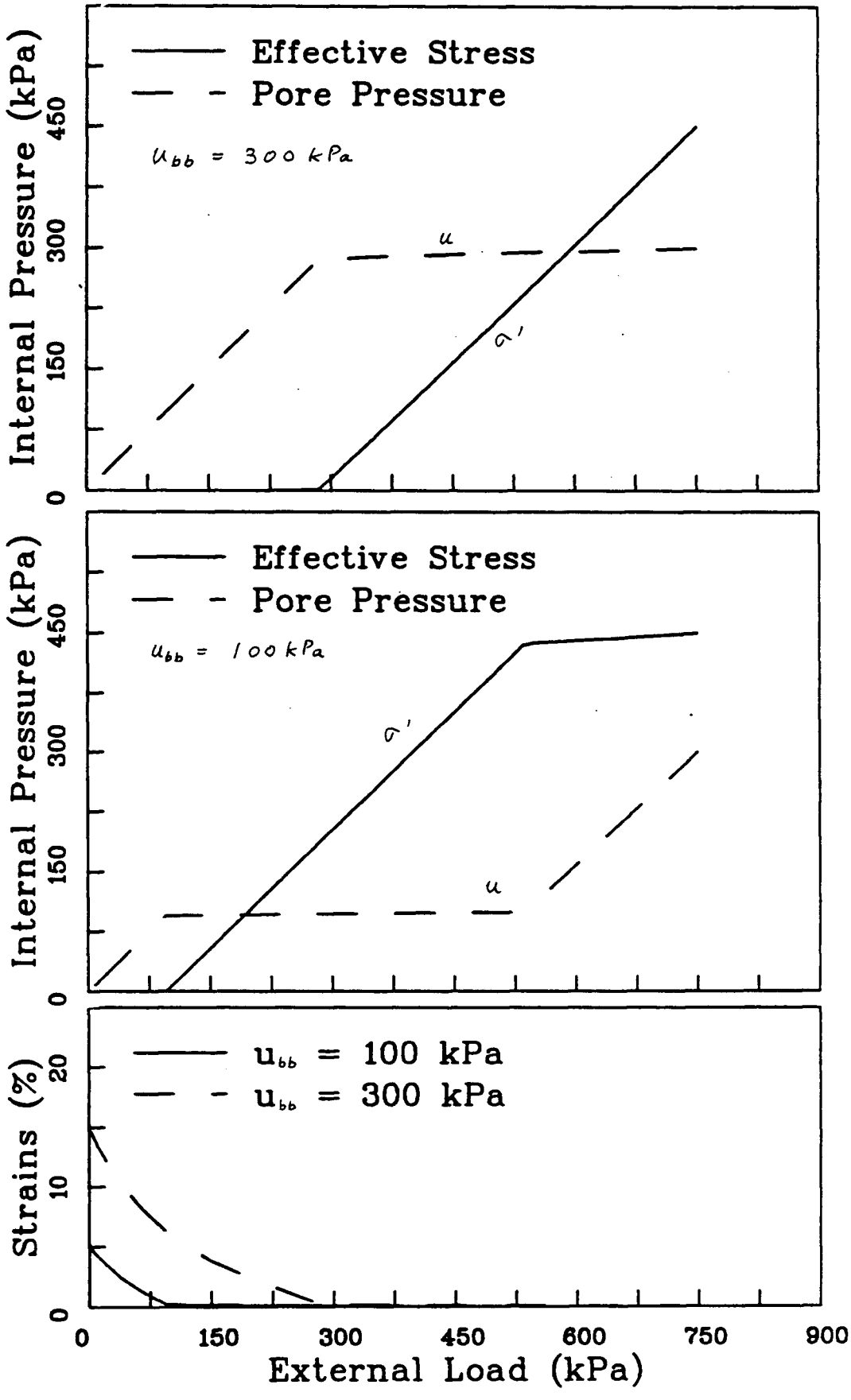

Fig.5.4 - Response of oil sand to one dimensional unloading

The results show that the new stress strain model has the excellent capability of predicting undrained response of oil sand.

5.3.2 Triaxial Tests on Gassy Soils (Sobkowicz 1982)

Performance of gassy soil on laboratory triaxial tests are reported by Sobkowicz (1982). A review of his work shows that the gas law model is generally correct. An appraisal of the predictive capabilities of the gas law model is made by comparing predicted and laboratory observed response of the immediate pore pressure, the immediate (short term) B value, the equilibrium pore presusre, the equilibrium (long term) B value, and value of saturation and displacements.

Since only test 11 in Sobkowicz's thesis is documented in detail, a comparison between predicted and observed response for this test is made to evaluate the validity of the undrained model. Analysis is performed using the same initial condition as test 11: S = 99.75%, n = 32.28%, σ = 1403.3 kPa, u = 652.3 kPa and β_s = 9E-6 kPa^{-1}. The compressibilkity of solid is comparable with that of water (β_w = 5 x 10^{-7} kPa^{-1}) so that the B (short term) value will not equal to one even for full saturation. These components are converted into parameters to be read in by the programme. The conversion and parameters are shown in Appendix F. The unloading sequence is shown in Table 5.1.

During any phase of the isotropic unloading test, pore pressure responses are predicted from the knowledge of soil skeleton and fluid compressibilities which are a function of effective stress,

pore pressure, saturation and porosity. For short term reponse, H is set to zero in Equation 3.26b since there is no time for gas exsolution. $H_{air/water} = 0.02$ and $H_{co2/water} = 0.86$ are used for the equilibrium response when gas exsolution is complete.

The comparisons are summarized in Table 5.1 and are presented graphically in Figures 5.5 and 5.6. They include:

1) predicted undrained response by the present undrained model
2) measured undrained response (Test 11, Sobkowicz 1982)

A careful examination of Table 5.1 and Figures 5.5 and 5.6 show that the predictive capability of the gas law model is remarkably good, especially for the long term undrained response. The minor discrepancies are due to the loss of gas from the sample as the result of gas diffusion and leakage through the membrane.

The observed immediate pore pressure are higher than the predicted values because of the time elapse (15 to 30 seconds) between reducing the total stress and taking the first reading. Thus, the predicted short term B is always higher than the observed ones.

It can be seen that the stress reduction is apportioned between soil skeleton and pore fluids, depending on their compressibilities. The sample in Test 11 was initially saturated with respect to air in water and undersaturated with respect to carbon dioxide in water. On unloading, during the first few phases, as $P_{co2/water} < P < P_{air/water}$, a small amount of gas exsolves for H (air/water) = 0.02. The change of effective stress and pore pressure

TABLE 5.1a

A Comparison of Computed and Measured Results (Test 11, Sobkowicz)

Phase	Total Stress (kPa)	Short Term B		Long Term B		Saturation (%)	
		Predicted	Measured	Predicted	Measured	Predicted	Measured
A	1322.4	0.897	0.694	0.523	0.606	99.65	99.67
B	1220.5	9.843	0.69	0.477	0.433	99.50	99.54
C	1112.1	0.781	0.68	0.378	0.403	99.30	99.38
D	978.2	0.705	0.64	0.021	0.011	98.90	99.11
E	883.6	0.628	0.548	0.022	0.016	98.61	98.93
F	766.4	0.584	0.508	0.024	0.034	98.22	98.93
G	654.9	0.548	0.482	0.026	0.07	97.80	98.27
H	559.0	0.536	0.50	0.031	0.155	97.38	97.90
J_1	457.3	0.569	0.590	0.129	0.21	96.40	
J_2		1	1	1	1	95.15	
J_3		1	1	1	1	94.66	

Predicted: Results predicted by Programme

Measured: Results measured in Test 11 by Sobkowicz

TABLE 5.1b

A Comparison of Computed and Measured Results (Test 11, Sobkowicz)

Phase	Measured Strains (%)		Volumeteric	Porosity (%)	
	Horizontal	Vertical		Predicted	Measured
A	0.112 E-1	0.112 E-1	0.336 E-1	32.30	32.30
B	0.275 E-1	0.275 E-1	0.825 E-1	32.33	32.33
C	0.490 E-1	0.490 E-1	0.147	32.38	32.36
D	0.929 E-1	0.919 E-1	0.2757	32.46	32.42
E	0.124	0.124	0.372	32.53	32.46
F	0.167	0.167	0.501	32.62	32.53
G	0.214	0.214	0.624	32.72	32.61
H	0.261	0.261	0.783	32.80	32.69
J_1	0.376	0.376	1.128		
J_2					
J_3					

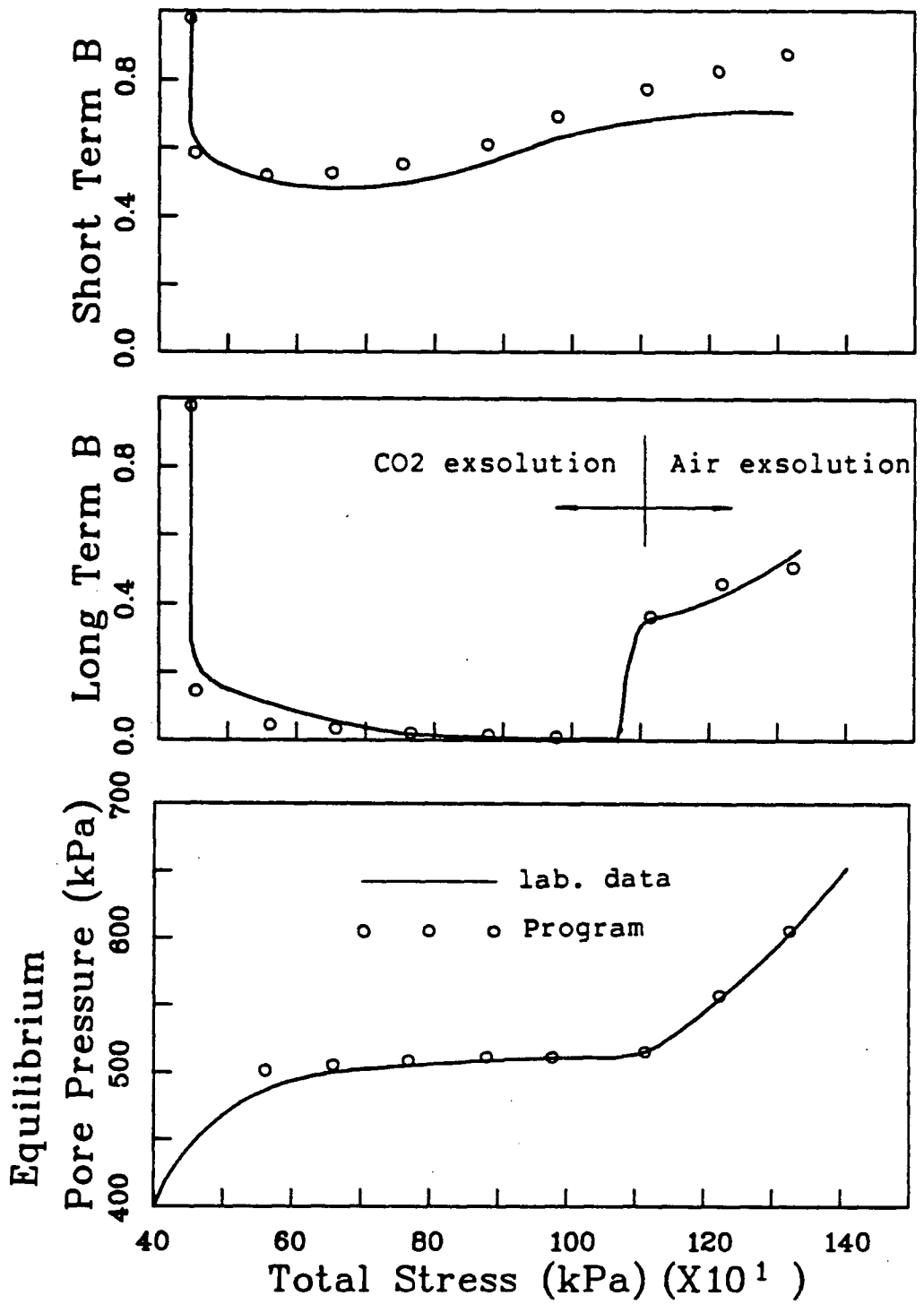

Fig.5.5 - Comparisons of predicted and observed pore pressure

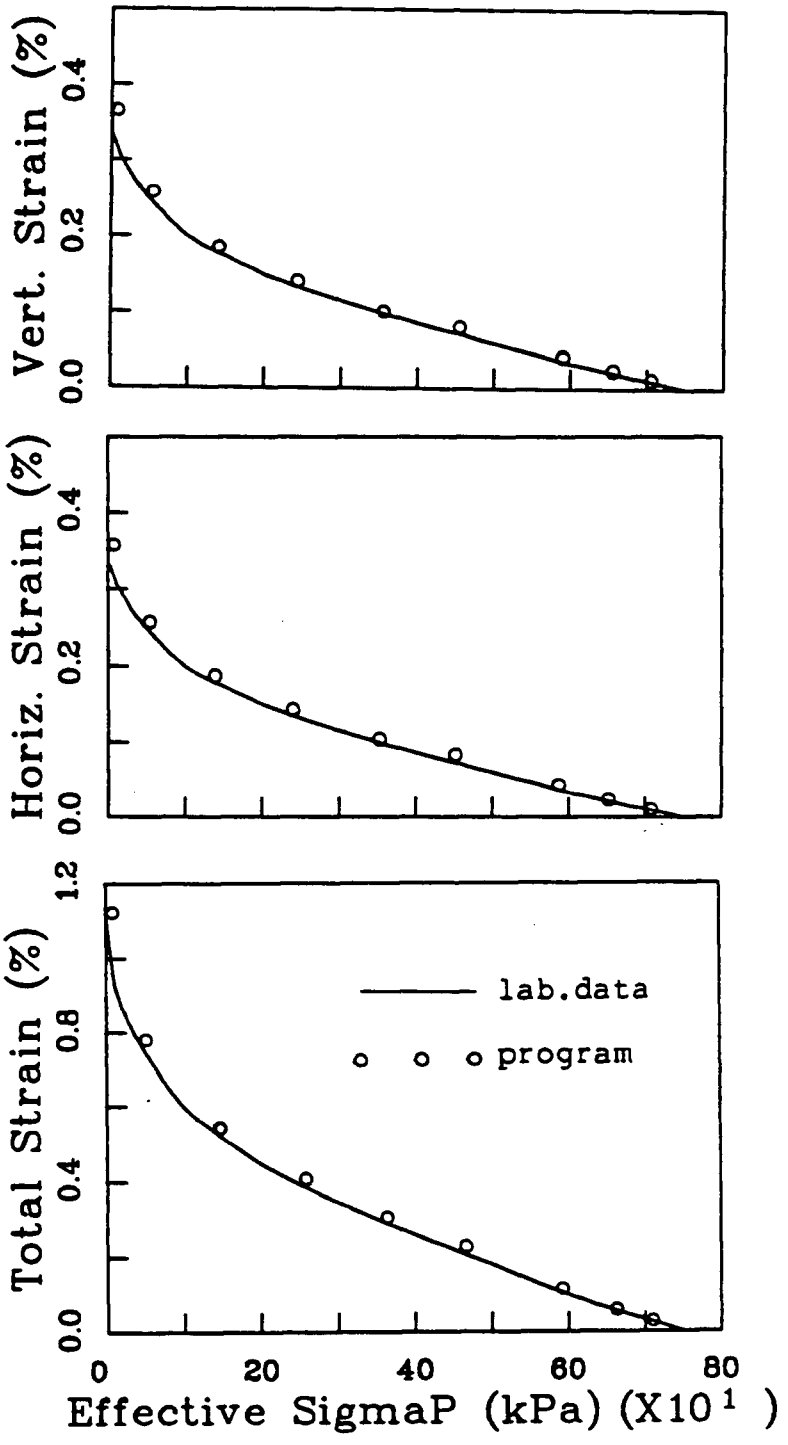

Fig.5.6 - Comparisons of predicted and observed strains

are roughly the same because the compressibilities of both soil skeleton and pore fluids are comparable. This characteristic is similar to those of unsaturated soils. On further unloading, as $P < P_{co2/water}$, a large amount of gas exsolves because the high solubility ($H_{co2} = 0.86$) of carbon dioxide in water. This causes a sudden increase in flexibility of the fluid phase and hence most of the load is transferred to the soil skeleton. When the effective stress in the skeleton approaches zero, the fluid once again becomes the stiffer phase, hence the B value rises to one. This is the typical behaviour of gassy soil on unloading.

The predicted and measured displacements are in remarkably good agreement. This indicates that the input parameters (Appendix f) and the ratio of the parameters, $K_B = 0.6\ K_E$ and $n = 2m = 0.5$ (Byrne and Cheung) are generally correct.

CHAPTER 6 - STRESSES AROUND A WELLBORE OR SHAFT IN OIL SAND

6.1 INTRODUCTION

The response of a wellbore in oil sand upon unloading is considered because it is an important problem in oil recovery in oil sand. In general, knoweldge of the stress solutions around a borehole is of great importance in several situations:

1) borehole stability
2) hydraulic fracturing
3) production or injection

A theoretical solution for stresses around a wellbore was developed by Risnes et al (1982) and the equations are presented herein. Validation of the programme (MHANS) for drained analysis is made by comparing computed response with the closed form solutions developed by Risnes et al. A linear elastic-plastic constitutive relationship is used for the above validation.

Upon validation of the programme, it was used to study the behaviour of a wellbore in oil sand upon unloading. Undrained and drained analyses were performed to obtain the short term and long term response respectively. In the undrained analysis, the gas exsolution is assumed to be very fast relative to the construction of wellbore. In the drained analysis, the pore pressure profile is estimated by using Dupuit's theory (Section 6.3.3).

6.2 GENERAL MODEL DESCRIPTION

The wellbore under consideration is supported by fluid pressure. As a model, a vertical cylindrical hole through a horizontal layer of oil sand is considered. The geometry, finite element mesh, and initial conditions of the problem are shown in Figure 6.1 and 6.2. Loading and geometry are assumed to be symmetrical around the well axis. Only radial displacement after the initial overburden loading are considered. These correspond to the assumption of axisymmetric and plane strain conditions.

The sand formation is assumed permeable, isotropic, homogeneous and initially fully saturated. The material is assumed elastic-perfectly plastic and obeys Mohr Coulomb failure criterion.

Only stress solutions for $\sigma_\theta > \sigma_z$ at the elastic-plastic boundary will be investigated.

6.3 THEORETICAL SOLUTIONS FOR STRESSES AROUND A BOREHOLE

A closed form solution for streses around a well, using a linear elastic-plastic stress-strain relationship, can be obtained from Risnes et al (1982).

The derivations of the stress solutions follow that of Risnes et al (1982) with two additional assumptions.

1) Insitu state of stress is considered to be isotropic initially, i.e. $\sigma_r = \sigma_\theta = \sigma_z$.
2) The Mohr Coulomb failure criterion in a porous material is

$$f = \sigma_1' - 2S \tan\alpha - \sigma_3' \tan^2\alpha = 0 \qquad 6.1$$

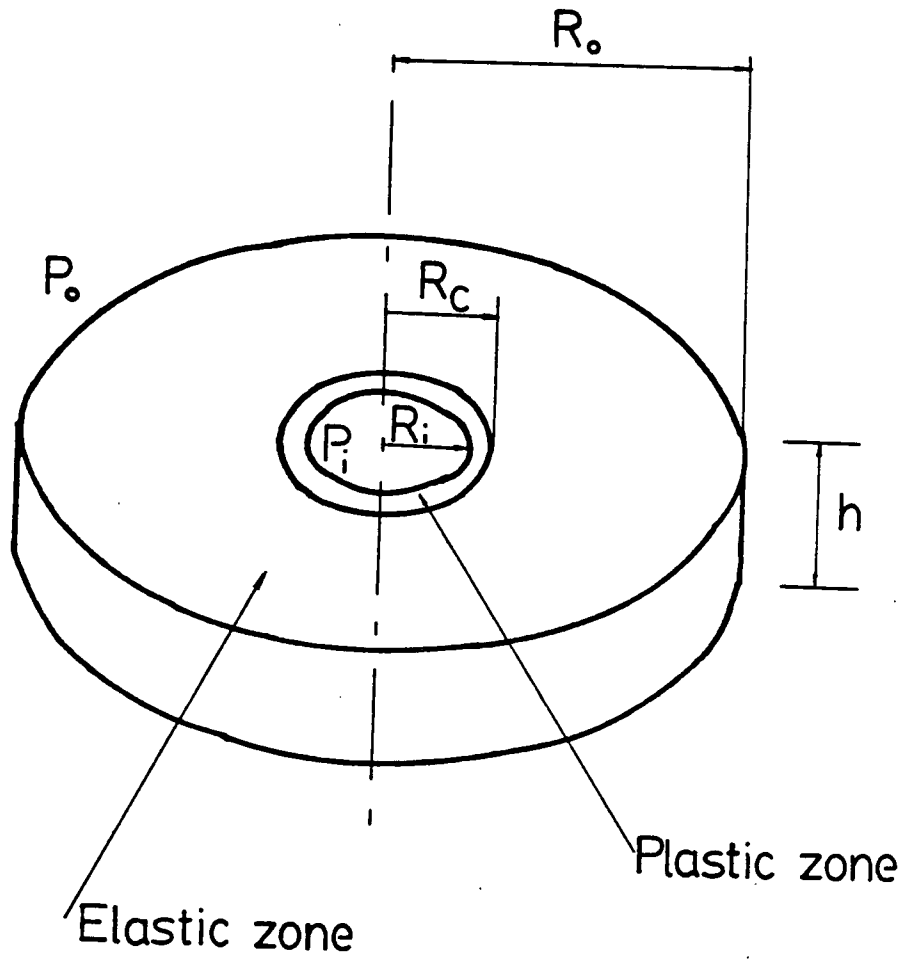

Fig.6.1 - Outline of the problem

Initial Stress: $\sigma_r' = \sigma_\theta' = \sigma_z' = 4000$ kPa

$u_o = 3500$ kPa

Bubble Pressure: 3500 kPa

$K_E = 1565$, $n = 0.5$

$K_B = 1000$, $m = 0.25$

$R_f = 0.8$

$\phi = 35^o$, $\Delta\phi = 0^o$

$e = 0.4286$, $S = 100\%$

$H_o = 0.2$, $H_w = 0.02$

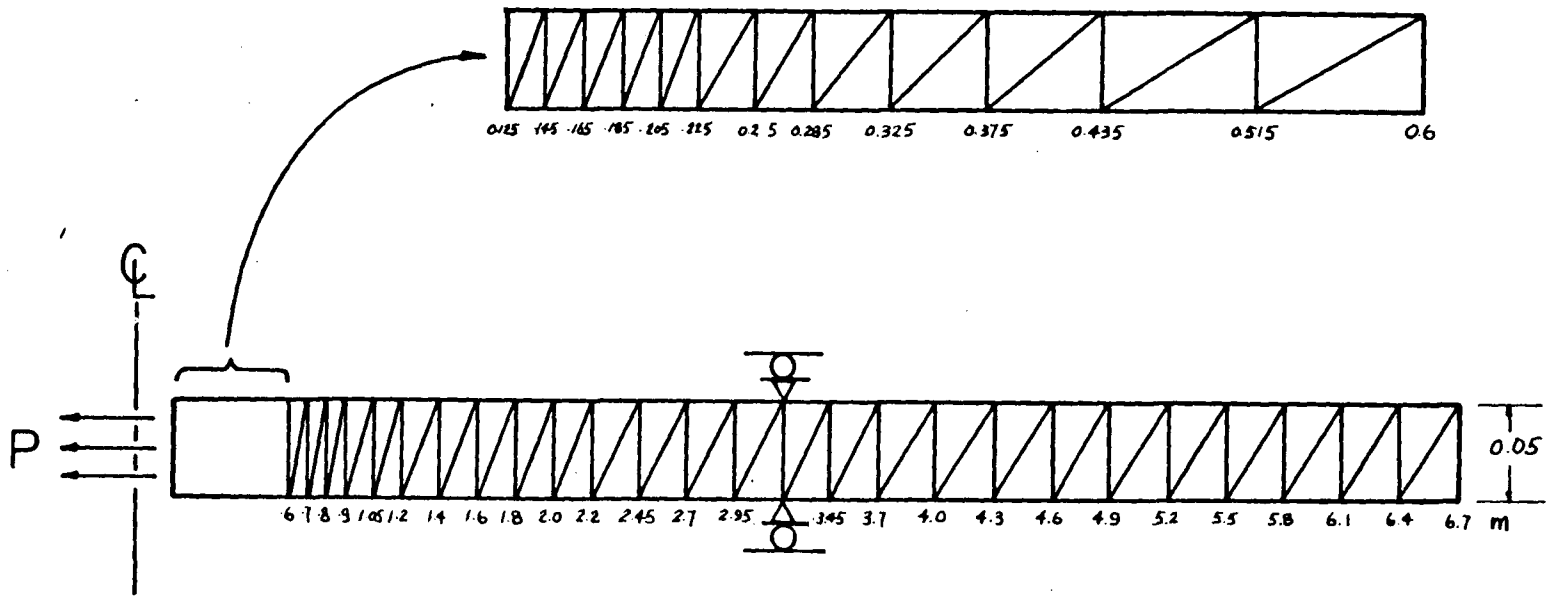

76 elements , 78 nodes

Fig. 6.2 - Finite element mesh for wellbore problem

where S is the cohesion intercept (or apparent cohesion)

α is the failure angle, i.e. $\frac{\pi}{4} + \frac{\phi'}{2}$

ϕ' is the internal friction angle

These symbols are also explained in Figure 6.2b

6.3.1 Stresses

6.3.1.1 Stresses in Elastic Zone

The stresses around a hole in an elastic thick wall cylinder, with porous material saturated with fluid, may be written as follows:

$$\sigma_r = \sigma_{ro} + (\sigma_{ro} - \sigma_{ri}) \frac{R_i^2}{R_o^2 - R_i^2} \left[1 - \left(\frac{R_o}{r}\right)^2\right]$$

$$- (P_o - P_i) \frac{1-2\nu}{2(1-\nu)} \cdot$$

$$\left(\frac{R_i^2}{R_o^2 - R_i^2} \left[1 - \left(\frac{R_o}{r}\right)^2\right] + \frac{\ell n\left(\frac{R_o}{r_o}\right)}{\ell n\,(R_o/R_i)}\right) \qquad 6.2$$

$$\sigma_\theta = \sigma_{ro} + (\sigma_{ro} - \sigma_{ri}) \frac{R_i^2}{R_o^2 - R_i^2} \left[1 + \left(\frac{R_o}{r}\right)^2\right]$$

$$- (P_o - P_i) \frac{1-2\nu}{2(1-\nu)} \cdot$$

$$\left(\frac{R_i^2}{R_o^2 - R_i^2} \cdot \left[1 + \left(\frac{R_o}{r}\right)^2\right] + \frac{1}{\ell n\,(R_o/R_i)}\right.$$

$$\left.\left[\ell n\left(\frac{R_o}{r}\right) - 1\right]\right) \qquad 6.3$$

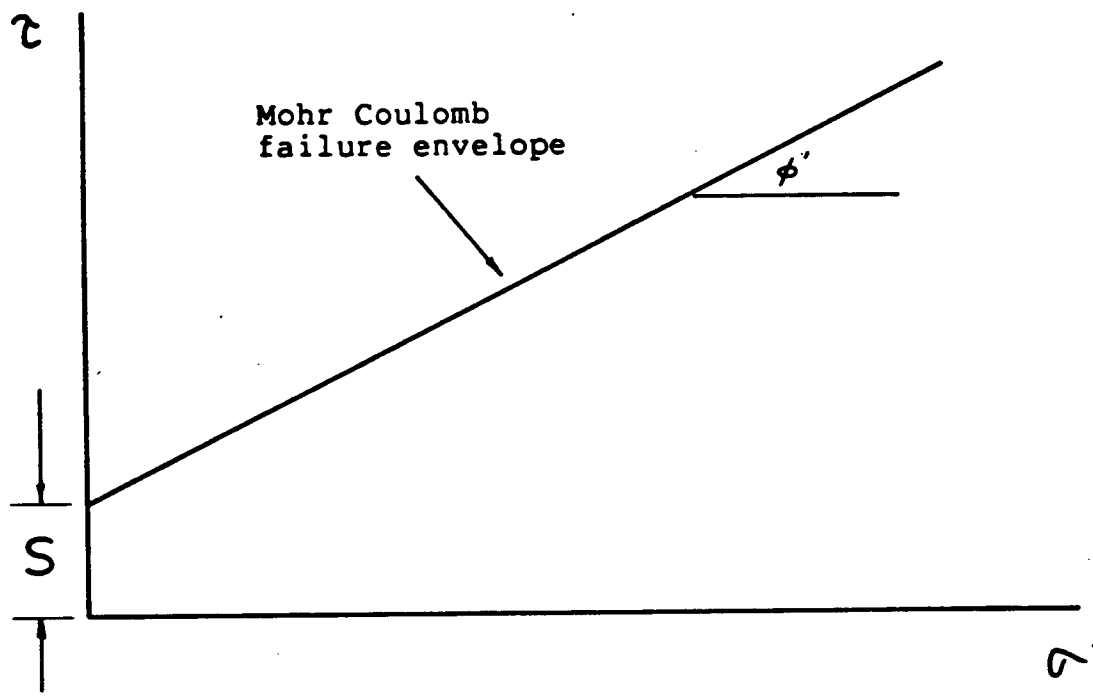

Fig.6.2 b - Mohr Coulomb failure envelope

$$\sigma_z = \sigma_{zo} + 2\nu\,(\sigma_{ro} - \sigma_{ri})\,\frac{R_i^2}{R_o^2 - R_o^2} - (P_o - P_i)$$

$$\frac{1-2\nu}{2(1-\nu)}\left(\nu\,\frac{2R_i^2}{R_o^2 - R_i^2} + \frac{2}{\ell n\,(R_o/R_i)}\left[\ell n\,(\frac{R_o}{r}) - \frac{\nu}{2}\right]\right) \qquad 6.4$$

The procedure for obtaining these stress solutions is given in Appendix G.

6.3.1.2 Stresses in Plastic Zone

As long as f = 0 (Equation 6.1), a plastic zone will start to develop at the borehole wall, and then expanding in size as support pressure is decreased. Equation 6.1 will apply within the plastic zone.

If the stress state at the boundary between the elastic and plastic zone is considered, the elastic stress solutions at this boundary are given by Equation 6.2 to 6.3, with $R_o = r = R_i$, $\sigma_{rc} = \sigma_{ri}$ and $P_c = P_i$. With the assumption of no fluid flow (i.e. $P_c = P_o$) and $R_o >> R_c$, the stress solutions from Equations 6.2, 6.3 and 6.4 may be written as:

$$\sigma_{rc} = \sigma_{rc} \qquad 6.4$$

$$\sigma_{\theta c} = 2\sigma_{ro} - \sigma_{rc} \qquad 6.5$$

$$\sigma_{zc} = \sigma_{zo} \qquad 6.6$$

The elastic solutions (Figure 5.2) show clearly that the radial stress

will be the smallest at the boundary between elastic and plastic zones, and following the assumption (1) of initial isotropic stress, the state of stress at the elastic-plastic boundary will be $\sigma_{rc} < \sigma_{zc} < \sigma_{\theta c}$.

The stress solutions within the plastic zone may be derived by combining Coulomb failure criterion (6.1) and the equation of equilibrium.

$$\frac{d\sigma_r}{dr} + \frac{\sigma_r - \sigma_\theta}{r} = 0 \qquad 6.7$$

The stress solutions for the plastic zone may be written as:

For $R_i < r < R_c$

$$\sigma_r = P_i + \frac{\mu q}{2\pi hk} \ell n \frac{r}{R_i} + \frac{1}{t} \left(2S \tan\alpha - \frac{\mu q}{2\pi hk}\right) \left[\left(\frac{r}{R_i}\right)^t - 1\right] \qquad 6.8$$

For $R_i < r < R_c$

$$\sigma_\theta = P_i + \frac{\mu q}{2\pi hk} \left(1 + \ell n \frac{r}{R_i}\right) + \frac{1}{t} \left(2S \tan\alpha - \frac{\mu q}{2\pi hk}\right) \left[(t+1) \left(\frac{r}{R_i}\right)^t - 1\right] \qquad 6.9$$

For $R_i < r < R_b$

$$\sigma_z = P_i + \frac{\mu q}{2\pi hk}\left(1 + \ell n \frac{r}{R_i}\right) + \frac{1}{t}\left(2S \tan\alpha - \frac{\mu q}{2\pi hk}\right)\left[(t+1)\left(\frac{r}{R_i}\right)^t - 1\right] \qquad 6.10$$

For $R_b < r < R_c$

$$\sigma_z = \left(P_i + \frac{\mu q}{2\pi hk} \ell n \frac{r}{R_i}\right) + \nu \frac{\mu q}{2\pi hk} + \frac{(1-\nu)(1-2\nu)}{1-\nu}$$

$$(\sigma_{zo} - P_o) + \frac{\nu}{t}\left[2S \tan\alpha - \frac{\mu q}{2\pi hk}\right] \left[(t+2)\left(\frac{r}{R}\right)^t - 2\right] \qquad 6.11$$

where $t = \tan^2\alpha - 1$, $\alpha = 45° + \frac{\phi^1}{2}$

μ = fluid viscocity

The procedure to derive Equations 6.7 to 6.11 is given in Appendix H.

6.3.1.3 Radius of the Plastic Zone

Radius of the inner Plastic Zone R_b

At the boundary of inner and outer plastic zones, the tangential stress and vertical stress given by equations 6.9 and 6.11 are equal.

Setting Equations 6.9 equal to 6.11 and $r = R_b$, yields.

$$a_1 \left(\frac{R_b}{R_i}\right)^t + a_2 = 0 \qquad 6.12$$

where

$$a_1 = \frac{1}{t}\left(2S\tan\alpha - \frac{\mu q}{2\pi hk}\right)\left[(t+1) - \nu(t+2)\right]$$

$$a_2 = (1-\nu)\frac{\mu q}{2\pi hk} - \frac{(1+\nu)(1-2\nu)}{1-\nu}(\sigma_{zo} - P_o)$$

$$- \frac{1}{t}\left(2S\tan\alpha - \frac{\mu q}{2\pi hk}\right)(1-2\nu)$$

Radius of the Entire Plastic Zone

There are two requirements that must be satisfied at the boundary of elastic and plastic zones

1) Mohr Coulomb criterion must hold

2) Continuity of radial stress

Inserting radial stress from Equation 6.8 and tangential stress from 6.3 into Mohr Coulomb failure criterion 6.1, the resulting equation for the radius of plastic zone R_c is

$$b_1 R_c^{t+2} \ln\frac{R_o}{R_c} + b_2 R_c^{t} \ln\frac{R_o}{R_c} + b_3 R_c^2 + b_4 R_c^2 \ln\frac{R_c}{R_i} + b_5 R_c^2 \ln\frac{R_o}{R_c}$$

$$+ b_6 \ln\frac{R_o}{R_c} \cdot \ln\frac{R_c}{R_i} + b_7 \ln\frac{R_c}{r_i} + b_8 \ln\frac{R_o}{R_c} + b_9 = 0 \qquad 6.13$$

where

$$b_1 = (2S \tan \alpha - \frac{\mu q}{2\pi hk}) R_i^{-t}$$

$$b_2 = - \frac{t + 2}{t} C_1 R_o^2$$

$$b_3 = - \frac{1 - 2\nu}{2(1-\nu)} (P_o - P_i)$$

$$b_4 = \frac{1 - 2\nu}{2(1-\nu)} \frac{\mu q}{2\pi hk}$$

$$b_5 = \frac{\mu q}{2\pi hk}$$

$$b_6 = - (2 - \frac{1 - 2\nu}{1 - \nu}) C_5 R_o^2$$

$$b_7 = - b_4 R_o^2$$

$$b_8 = [\frac{2\nu}{1-\nu} \sigma_{z0} + \frac{1 - 2\nu}{1 - \nu} (P_o + P_i) - 2P_i + \frac{2}{t} 2S \tan \alpha$$

$$- \frac{t+2}{t} \frac{\mu q}{2\pi hk}]$$

$$b_9 = - C_3 R_o^2$$

6.3.2 Stability

It is noted that the radial stress component in Equation 6.8 consists of two r-dependent terms, one logarithmic and one to the power

of t. The last term will become dominant when the exponent t has a value greater than about two.

Setting $$C = \frac{1}{t}\left(2S \tan \alpha - \frac{\mu q}{2\pi hk}\right) R_i^{-t} \qquad 6.14$$

If C is positive, radial stress in the plastic zone will increase with r, and combined plastic-elastic solutions are possible. But when the flow rate q is large enough to cause C to become negative, radial stress will decrease with increasing distance r, and combined solutions are not possible. Hence, there exists a stability criterion.

$$C > 0 \qquad 6.15$$

with the limit

$$\frac{\mu q}{2\pi hk} = 2S \tan \alpha \qquad 6.16$$

This study concentrates on oil sand which has $S \simeq 0$. If the wellbore is supported only by fluid pressure, equation 6.16 indicates that instability arises when flow into the wellbore occurs.

6.3.3 Pore Pressure Profile

When steady-state conditions around the wellbore have been reached, the pore pressure in the soil elements may be estimated if the piezometric surface is known. Dupuit developed a theory which enables the quantity of steady-state seepage and the piezometric surface around a well to be evaluated. His theory is based on three assumptions:

1) the hydraulic gradient is equal to the slope of the free surface and is constant with depth,
2) for small inclinations of the line of seepage the streamlines may be taken as horizontal.
3) The permeability of the soil is constant

With the terminology in Figure 6.2a the flow when steady state conditions exist is given by:

$$Q = \pi k (h_2^2 - h_1^2) \frac{1}{\ell n(R/r_w)} \qquad 6.17$$

and the location of the free surface is

$$h^2 = h_1^2 + \frac{h_2^2 - h_1^2}{\ell n(R/r_w)} \ell n \left(\frac{r}{r_w}\right) \qquad 6.18$$

There is a controversy about the location of the piezometric surface predicted by Dupuit's theory, especially in the vicinity of the well. This is because the surface of seepage is omitted in Dupuit's prediction. But the problem is modelled as a disk of sand below the seepage surface (Figure 6.3b). Only radial flow is assumed in the sand disk. Hence equation 6.16 is accurate enough to estimate the pore pressure profile.

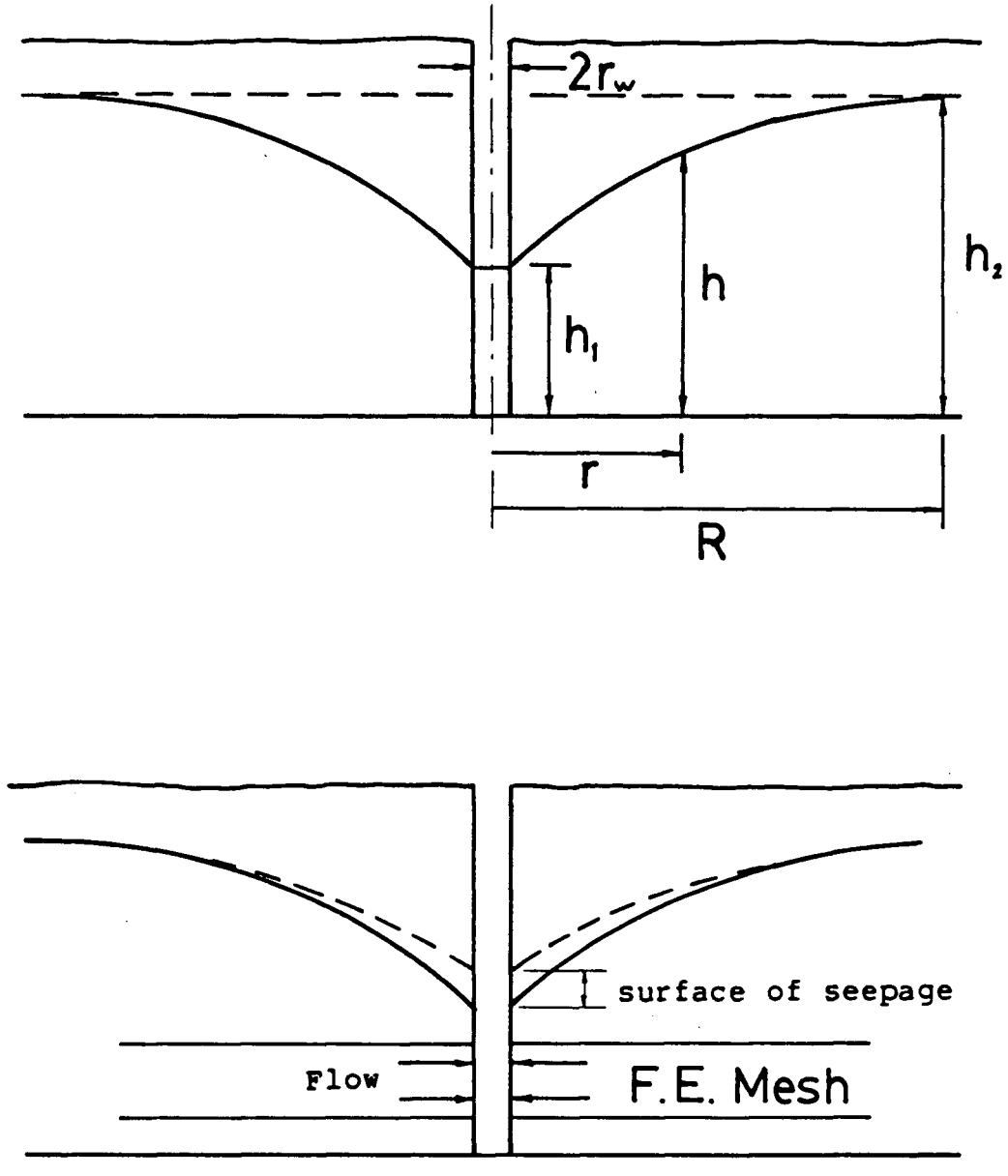

Fig.6.3 - Idealised flow to a wellbore

6.4. Comparisons of Predicted Response and Closed Form Solution

The response of unloading a borehole, with linear elastic-plastic porous material, is investigated. A drained analysis was performed. The initial and final conditions of the problem are shown in Figure 6.4(a). When the fluid support pressure is higher than the initial pore pressure, no flow from the borehole into the sand formation is assumed. Since the final fluid support (4100 kPa) is higher than the initial pore pressure, flow into the borehole is not considered herein.

The stress solutions computed by the programme are in good agreement with the closed form solutions mentioned in Section 6.3, and shown in Figure 6.4. The radius of the entire plastic zone is small which shows that the borehole is stable at the final fluid support pressure of 4100 kPa.

6.5.1 Undrained Response

The undrained non-linear elastic-plastic model will now be used to study the response of a wellbore on unloading. The finite element mesh and initial conditions are shown in Figure 6.1b. Only the long term undrained response will be investigated in this thesis because this condition is felt to be more realistic ($t \neq 0$) and it was also shown that the long term undrained condition is more critical than the immediate response (Sobkowicz, 1982) in terms of stability.

The wellbore is unloaded by decreasing the total stress at the wellbore wall, and the stress solutions and displacements are shown graphically in Figures 6.5. A careful examination of these figures indicates some interesting results:

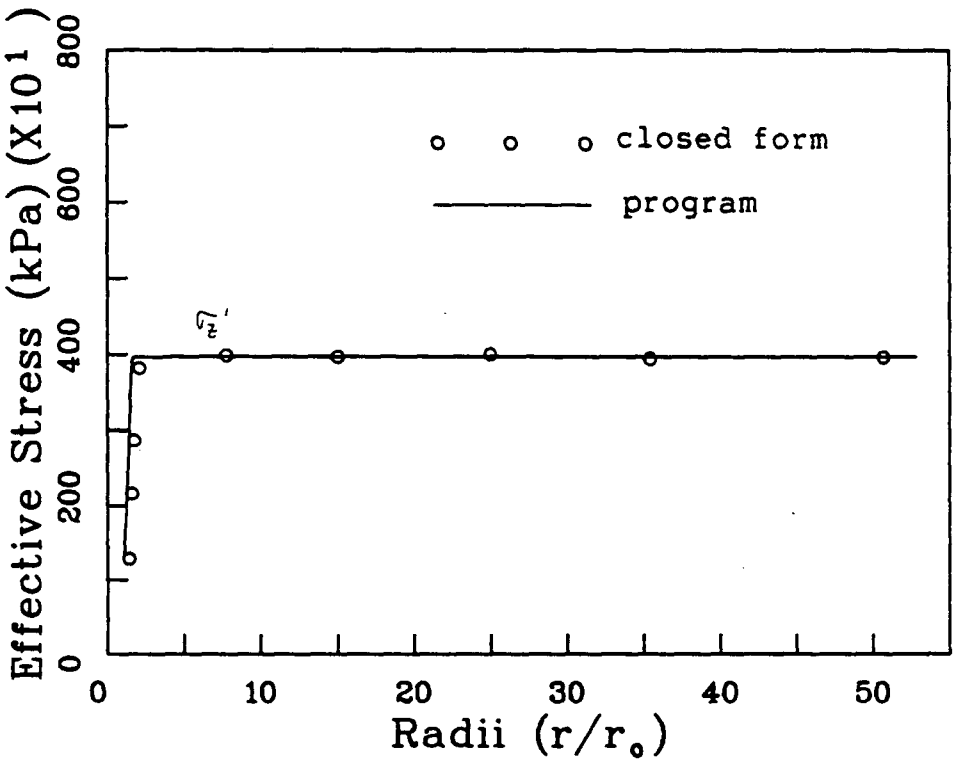

E = 60 MPa
ν = 0.45
ϕ = 35°
initial stress : $\sigma_r = \sigma_\theta = \sigma_z$ = 4000 kPa
final stress : σ_r = 600 kPa
inside radius : r_0 = 0.125 m
outside radius : R = 6.7 m

(a)

Fig.6.4 - Stresses around a wellbore in an elastic-plastic material

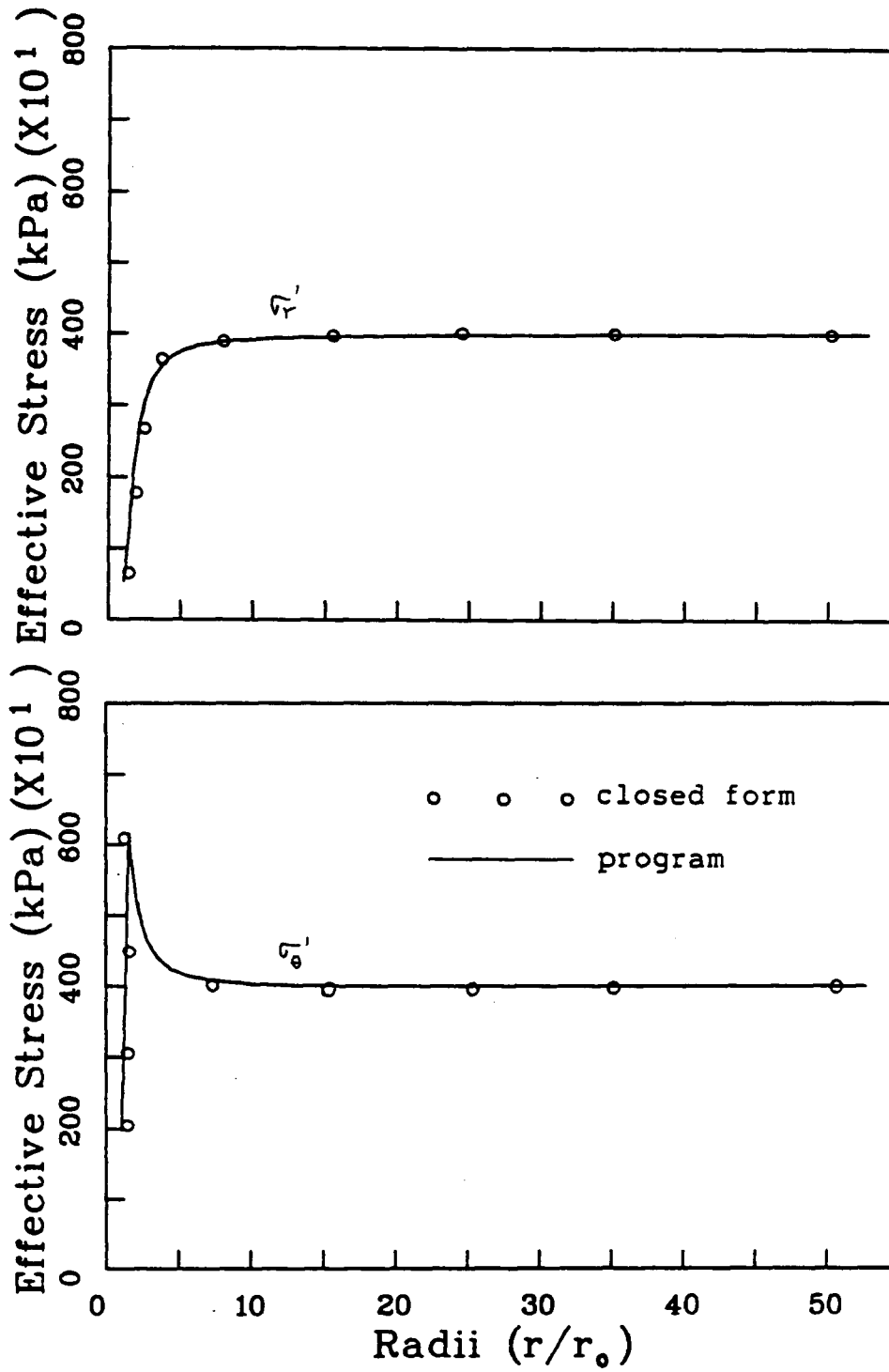

(b)

Fig.6.4 - Stresses around a wellbore in an elastic-plastic material

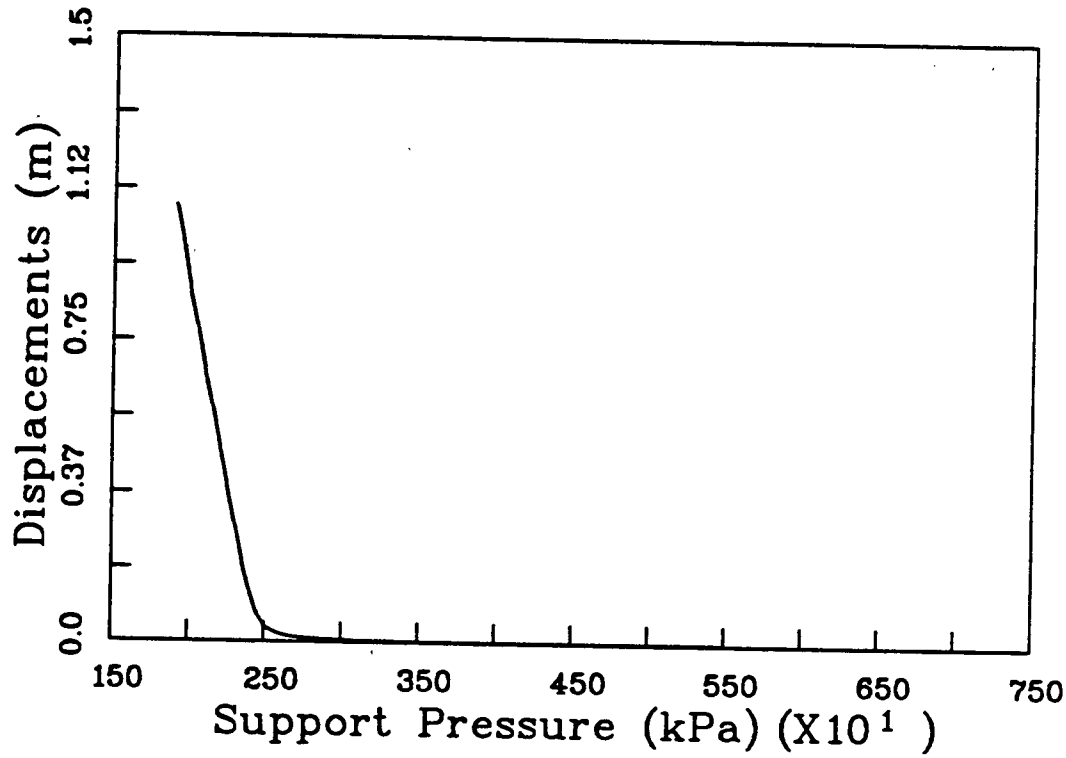

(a)

Fig.6.5 - Undrained response of a wellbore in oil sand on unloading

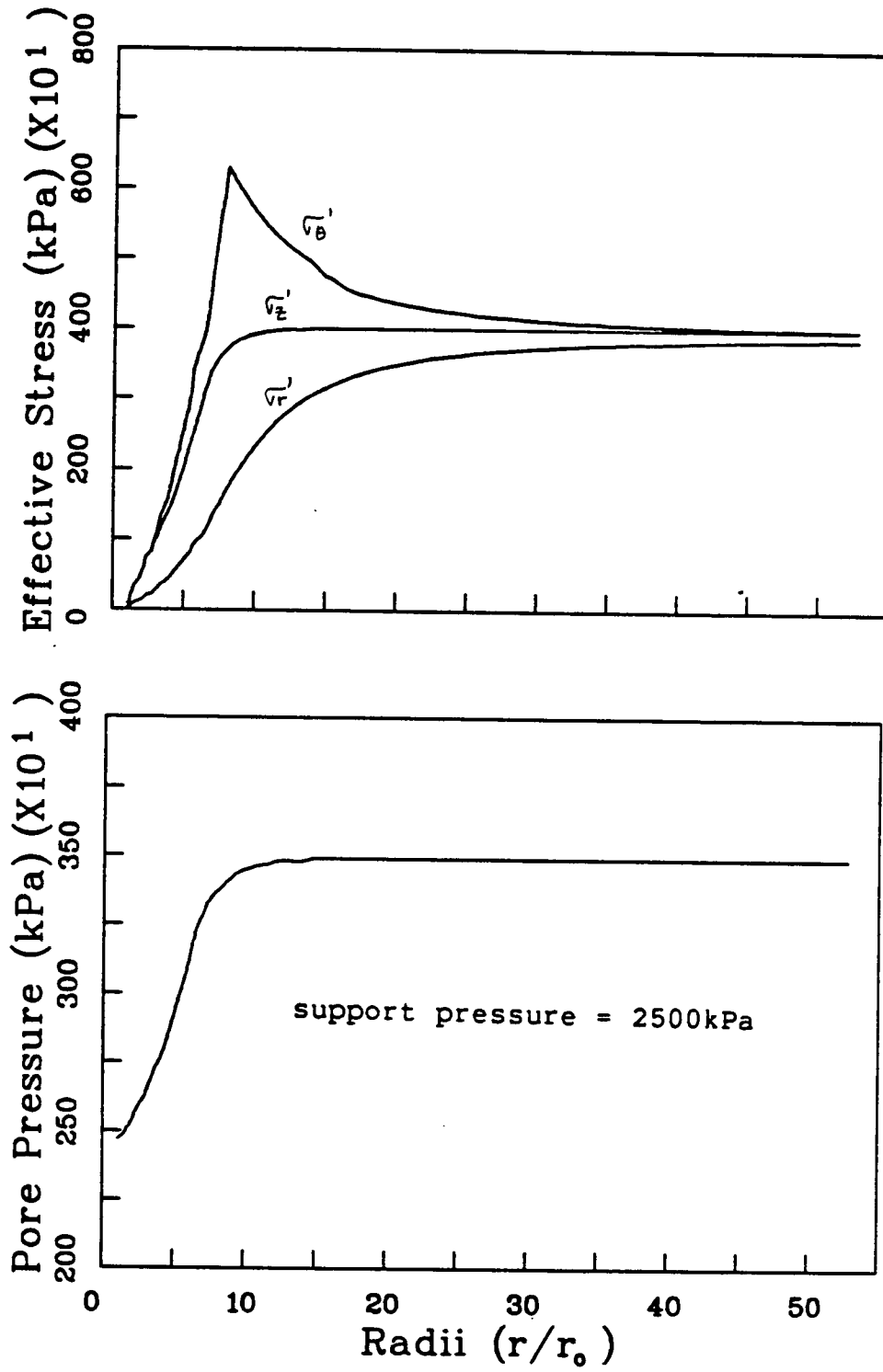

(b)

Fig.6.5 - Undrained response of a wellbore in oil sand on unloading

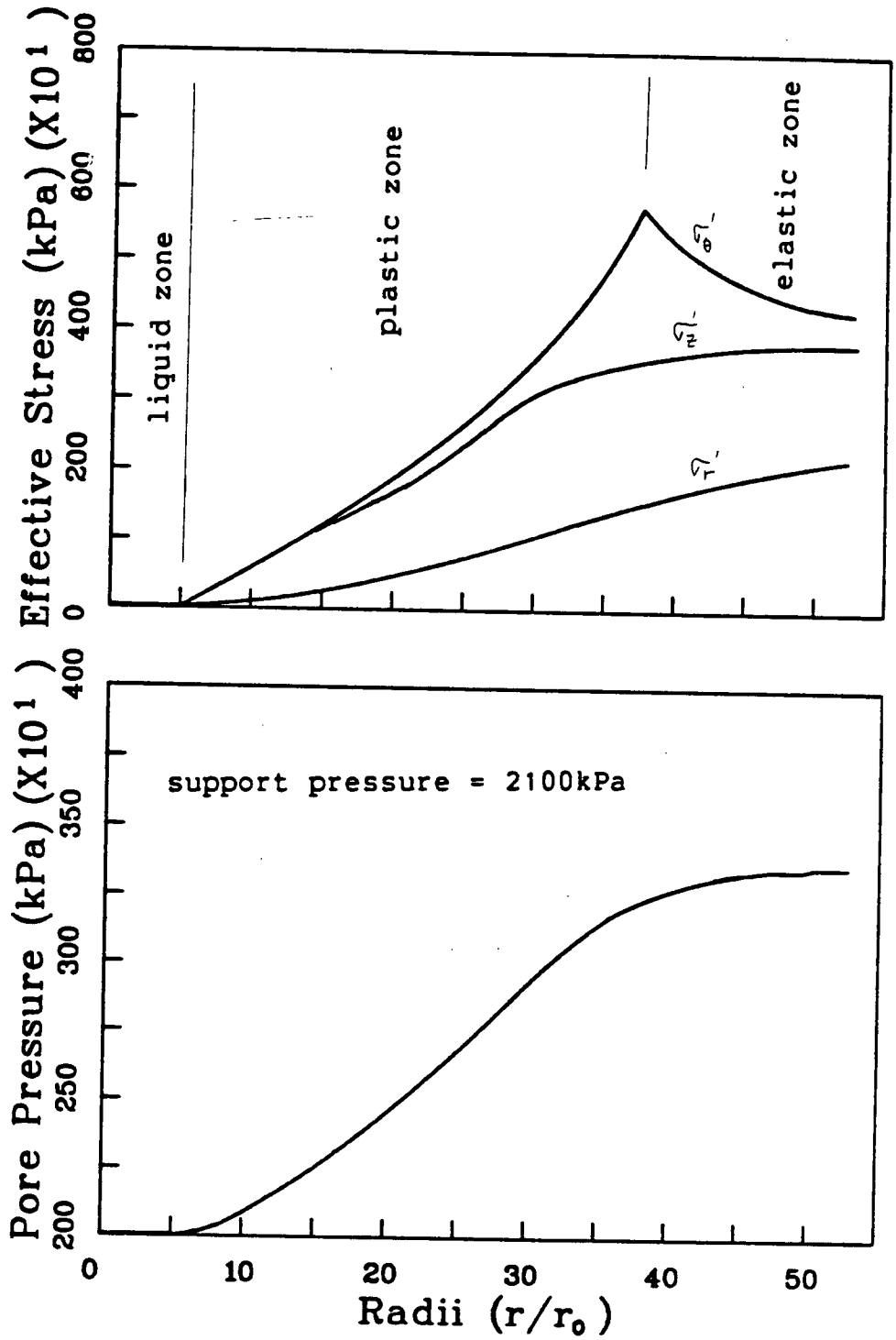

(c)

Fig.6.5 - Undrained response of a wellbore in oil sand on unloading

1) The support pressure can be reduced below the initial pore fluid pressure and the wellbore is still stable; instability is defined when large displacements start to occur at the wellbore wall.

2) Instability occurs at a support pressure of approximately 2500 kPa.

3) The size of the plastic zone remains small as long as the support pressure is higher than 2500 kPa (Figure 6.5 b). Once the support pressure drops below 2500 kPa, the size of the plastic zone increases rapidly (Figure 6.5 c).

4) Pore fluid pressure changes only occur in the plastic zone. The evaluation of the fluid pressure response depends on volumetric strain $\Delta\varepsilon_v = \Delta\varepsilon_v^e + \Delta\varepsilon_v^P$. But in the elastic zone, $\Delta\varepsilon_r^e = -\Delta\varepsilon_\theta^e$ and $\Delta\varepsilon_z^e \simeq 0$ so that $\Delta\varepsilon_v^e = 0$, and hence no change in pore fluid pressure is predicted.

5) Once instability has been reached, a liquid zone with zero effective stress associated with a large plastic zone will form adjacent to the wellbore. These zones will extend into the sand formation rapidly upon further reduction of support pressure, leading to large displacements.

6.5.2 Drained Response

For the drained condition, the pore fluid pressure is assumed to be known. Dupuit's theory described in Section 6.4.3 is adopted to estimate the pore pressure profile around the borehole in this study. Two typical pore pressure profiles are shown in Figure 6.7 with R = 100 and 150 m with the fluid support pressure fluid at 3200 kPa. There are some intermediate pore pressure profiles between support pressure of 3500 kPa to 3200 kPa, depending on the number of increments on unloading, but they are not shown here. When the fluid support pressure is above 3500 kPa, no flow from the wellbore into the sand formation is assumed.

The wellbore is unloaded in the same manner as for the undrained analysis. The results of the stress solutons are shown in Figure 6.7. A careful examination of these results indicate some interesting points:

1) To maintain borehole stability, the support pressure cannot be reduced to less than the initial pore pressure; instability is defined as large displacements start to occur at the wellbore wall.
2) The stress solutions only differ by a few percent when the input pore pressure profiles are generated by using R = 100 and 150 m. Therefore, only one set of stress solutons is presented here in Figure 6.7.
3) Once stability has been reached, a liquid zone with zero effective stress associated with a large plastic zone will extend into the sand formation rapidly upon further

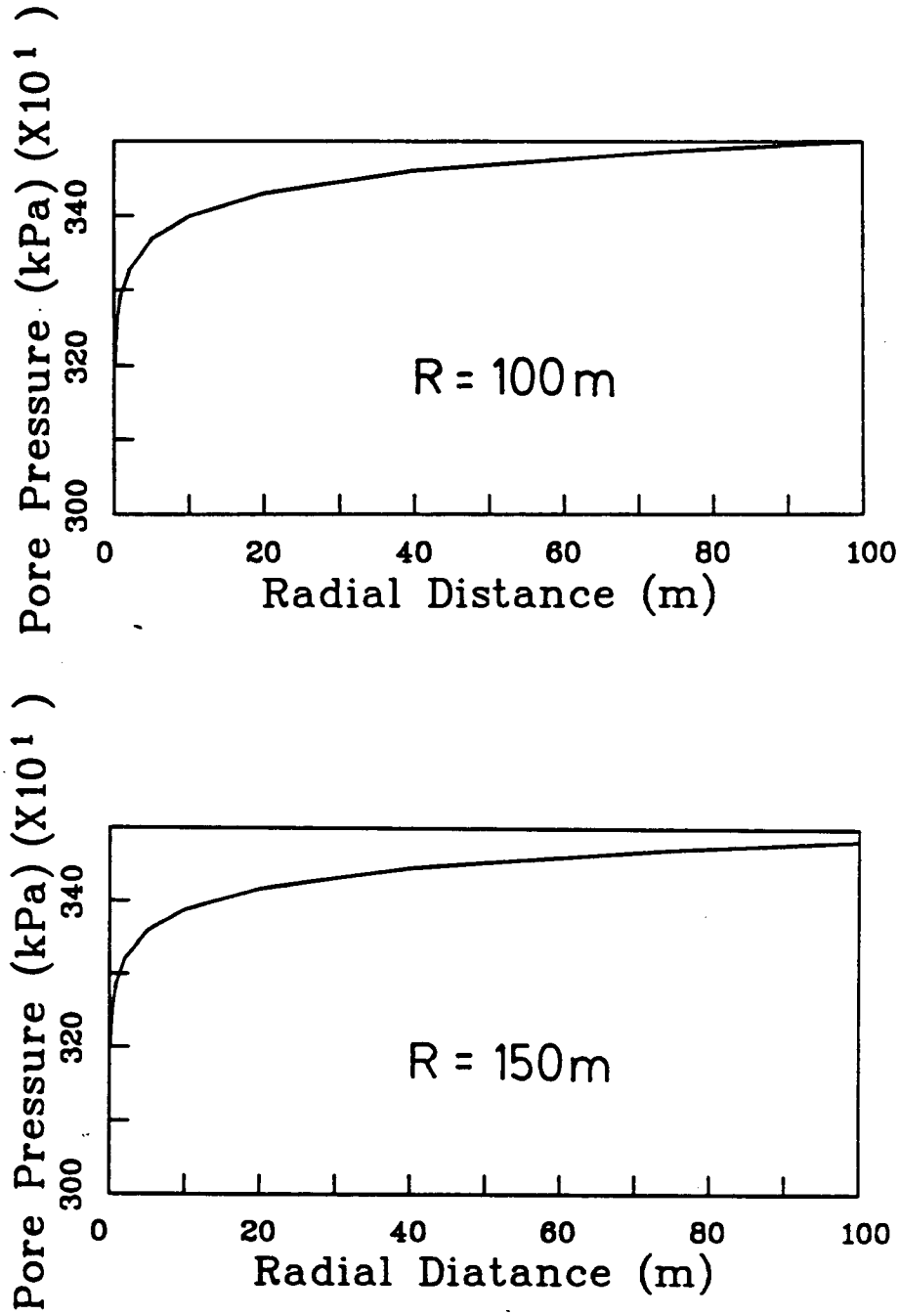

Fig.6.6 - Pore pressure profile around a borehole

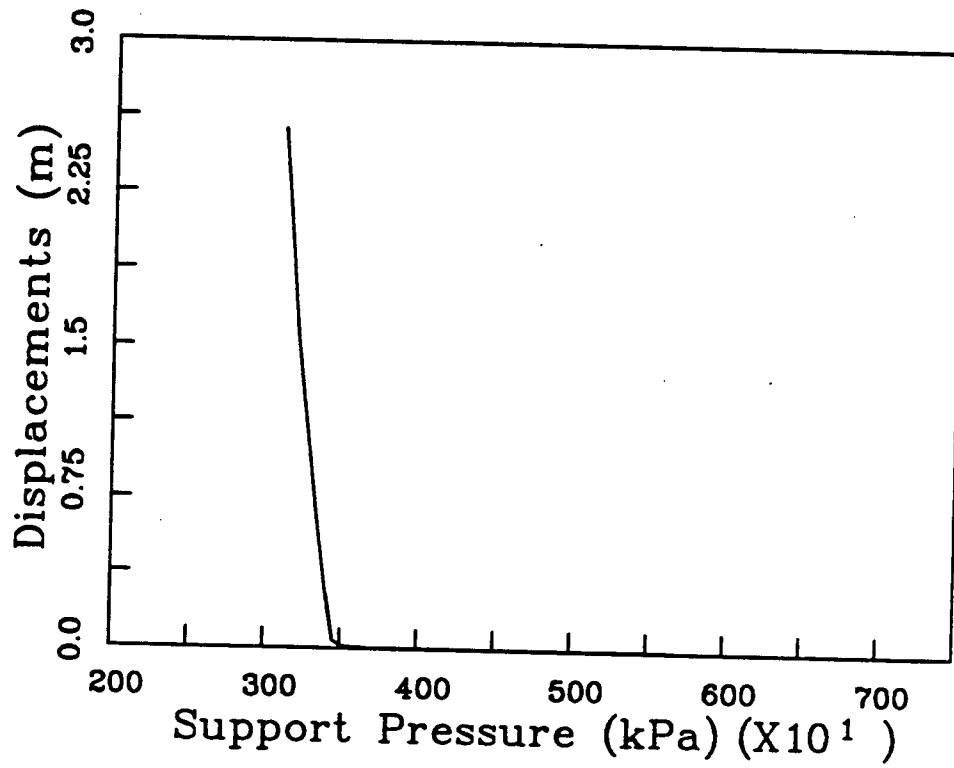

(a)

Fig.6.7 - Drained response of a wellbore in oil sand on unloading

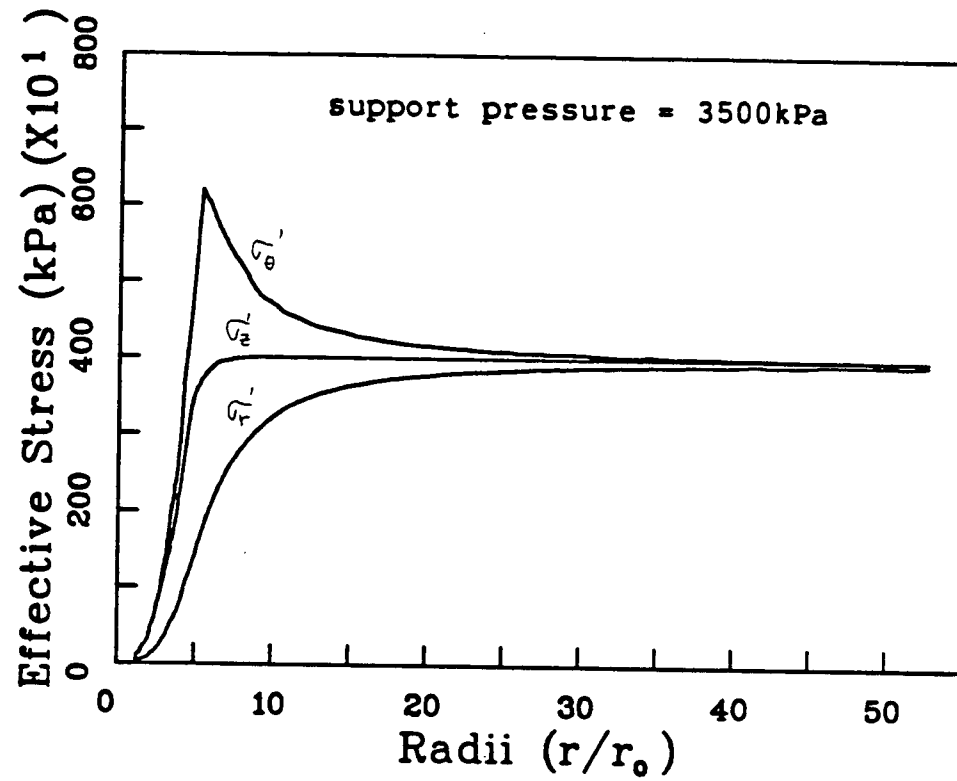

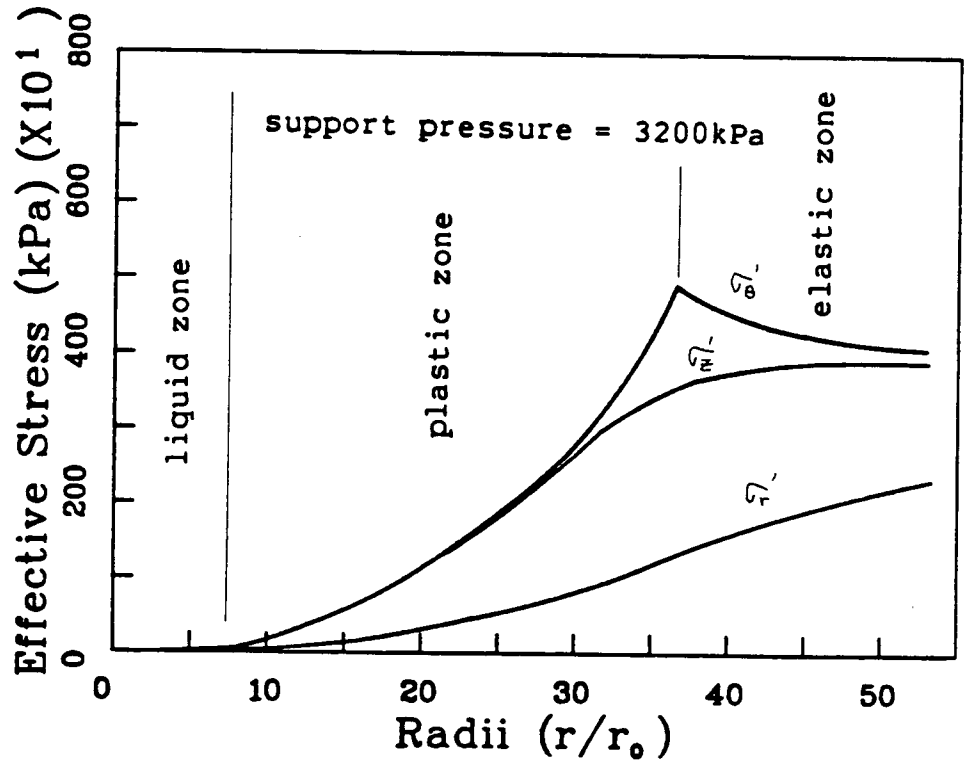

(b)

Fig.6.7 - Drained response of a wellbore in oil sand on unloading

reduction of support pressure, leading to large displacements.

6.5.3 Implications of Undrained and Drained Analyses

The analyses show that there are limits on the fluid support pressure reduction in order to maintain borehole stability.

Comparisons of both analysis are made at support pressure of 3500 kPa and 3200 kPa. 3500 kPa is the critical pressure below which instability occurs in drained condition. It is noted that in Figure 6.9 the plastic zone in the undrained analysis is much smaller than the one in drained analysis. At a support pressure of 3200 kPa, the borehole is obviously unstable under drained conditions (Figure 6.9), showing a large plastic zone and consequently large displacements. But the borehole only exhibits a small plastic zone at this support pressure (3200 kPa) under undrained conditions (Figure 6.9). This is because the pore pressure around the wellbore is lower in the undrained case, which results in a higher effective stress.

Consolidation is the process which bridges the fully undrained and drained conditions. An interesting point is that the pore pressure will increase around the borehole during consolidation, leading to lower effective stress. Hence, the long term drained condition is less stable than the undrained condition.

6.6 Application to Oil Recovery

For oil production, the final support pressure must be reduced below the in-situ pore fluid pressure. Based on the undrained analyses with the wellbore supported only by fluid pressure, the support

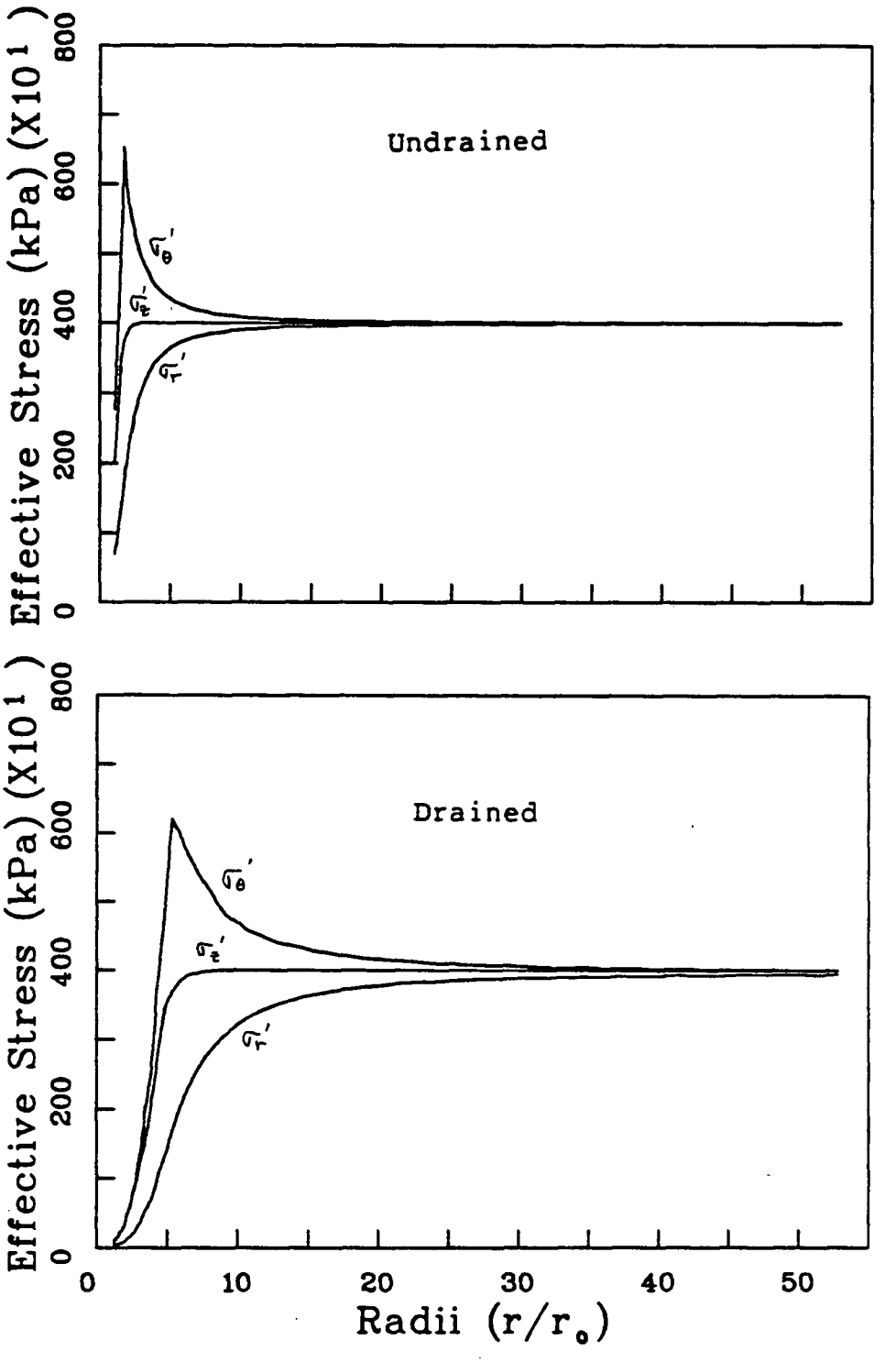

Fig.6.8 - Comparisons of undrained and drained response of a wellbore in oil sand at a support pressure of 3500kPa

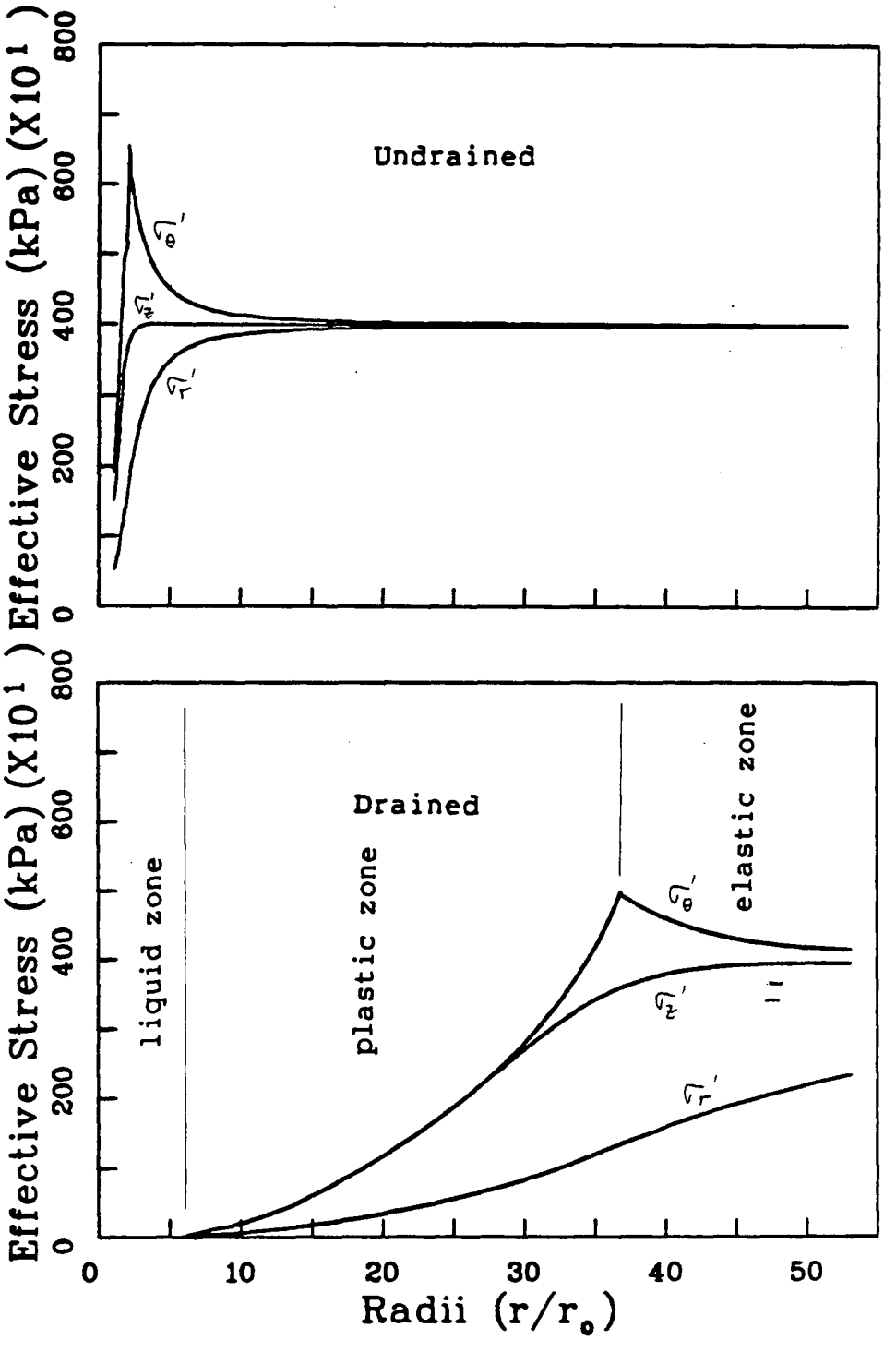

Fig.6.9 - Comparisons of undrained and drained response of a wellbore in oil sand at a support pressure of 3200kPa

pressure can be reduced below the in-situ pore fluid pressure and the wellbore is still stable. This allows the construction of the wellbore and initial reduction of fluid support pressure below in-situ pore fluid pressure. However, for the drained condition, the wellbore becomes unstable which causes collapse of the well and hence no oil production.

Instability results in the formation of large liquid and plastic zones (Figure 6.9) around the wellbore. Since the permeability in the liquid and plastic zones are higher due to the expansion of sand skeleton, it is desirable to have these zones around the oil production well. This effectively increases the diameter of the well.

To enhance oil production and maintain wellbore stability, a screen may be installed to provide effective support pressure after the liquid and plastic zones have formed.

The three dimensional and viscous effects have not been considered in the analysis, however they may help in stabilizing the wellbore.

CHAPTER 7 : SUMMARY AND CONCLUSIONS

A new stress-stress relationship for modelling the undrained response of oil sand has been presented. An analysis which couples the soil skeleton and pore fluids is used. The pore pressure changes are computed from the constraint of volume compatibility.

Separate stress-strain models are required for both soil skeleton and pore fluids in this analysis. The conventional hyperbolic stress-strain model described by Duncan et al is adopted for the soil skeleton. The pore fluids stress-strain relationships are formulated on the basis of ideal gas laws.

The developed model is incorporated into a finite element programme for analysing the deformation behaviour of gassy soils (e.g. oil sand). Upon validation in Chapter 5, it is shown that the undrained model is capable of predicting the response of unsaturated to gassy soils. Naylor has shown that this model can be used to predict the response of saturated soils.

For non-rectangular QM-6 elements, equilibrium cannot be achieved for Poisson's ratio values greater than 0.4, but higher order element can remedy this.

In the study of the response of wellbore in oil sand upon unloading, the fluid support pressure can be reduced below in-situ pore fluid pressure under undrained condition and the wellbore is still stable. However, for the drained conditin, the fluid support pressure cannot be reduced below the in-situ pore fluid pressure in order to maintain wellbore stability.

For oil production, the fluid support must be reduced below in-situ pore pressure which results in formation of large liquid and

plastic zones. It is desirable to have these zones around the wellbore because the diameter of the well is effectively larger.

To enhance oil production and maintain wellbore stability, a screen may be installed to provide effective support pressure after the liquid and plastic zones have formed.

BIBLIOGRAPHY

Atukorala, U.D. Finite Element Analysis of Fluid Induced Fracture Behaviour in Oilsand. M.A.Sc. Thesis, U.B.C. 1983.

Biot, M.A. General Theory of Three-Dimensional Consodilation. Journal of Applied Physics, Vol. 12, February 1941.

Bishop, A.W. The Influence of an Undrained Change in Stress on the Pore Pressure in Porous media of Low Compressibility. Geotechnique, V.23, N.3. 1973.

Bishop, A.W. The Influence of System Compressibility on the Observed Pore Pressure Response to an Undrained Change in Stress in Saturated Rock. Geotechnique, V.26, 1976.

Brooker, E.W. Tar Sand Mechanics and Slopes Evaluation. 10th Canadian Rock Mechanics Symposium, Department of Mining Engineering, Queen's University, 1975.

Byrne, P.M. and Cheung, H. Soil Parameters for Deformation Analysis of Sand Masses. Soil Mechanics Series No. 81, Department of Civil Engineering, U.B.C. 1984.

Byrne, P.M. and Eldridge, T. A Three parameter Dilatant Elastic Stress-Strain Model for Sand. Soil Mechanics Series No. 57, Department of Civil Engineering, U.B.C. 1982.

Byrne, P.M. and Janzen. W. Soilstress. Soil Mechanics Series No. 52, Department of Civil Engineering, U.B.C. 1981.

Byrne, P.M. and Janzen, W. INCOIL. Soil Mechanics Series No. 80, Department of Civil Engineering, U.B.C. 1984.

Chatterji, P.K., Smith, L.B., Insley, A.E. and Sharma, L. Construction of Saline Creek Tunnel in Athabasca Oil Sand. Canadian Geotechnical Journal, 1, 1979.

Christian, J.T. Undrained Stress Distribution by Numerical Methods. J.S.M.F.D., A.S.C.E., S.M.6, 1968.

Cook, R.D. Concepts and Applications of Finite Element Analysis. 2nd Edition, John Wiley & Sons, 1981.

Duncan, J.M. and Chang, C.Y. Nonlinear Analysis of Stress and Strain in Soils. J.S.M.F.D., A.S.C.E., S.M.5, 1970.

Duncan, J.M., Byrne, P.M., Wong, K.S. and Mabry, P. Strength, Stress-Strain and Bulk Modulus Parameters for Finite Element Analysis of STresses and Movements in Soil Masses. Report No. UCB/GT/80-01, August 1980.

Dusseault, M.B. Sample Disturbance in Athabasca Oil Sand. Journal of Canadian Petroleum Technology, V.19, N.2, .

Dusseault, M.B. Undrained Volume and Stress Change Behaviour of Unsaturated Very Dense Sands. Canadian Geotechnical Journal, Volume 16, 1979.

Dusseault, M.B. and Morgenstern, N.R. Shear Strength of Athabasca Oil Sands. Canadian Geotechnical Journal, V.15, N.2, 1978.

Dusseault, M.B. and Morgenstern, N.R. Characteristics of Natural Slopes in the Athabasca Oil Sands, V.15, N.2, 1978.

Florence, A.L. and Schwer, L.E. Axisymmetric Compression of a Mohr-Coulomb Medium Around or Circular Hole. International Journal for Numerical and Analytical Methods in Geomechanics, Vol. 2, 1978.

Fredlund, D.G. Density and Compressibility of Air-water Mixture. Canadian Geotechnical Journal, V.3, 1976.

Geertsma, J. Some Rock-Mechanical Aspects of Oil and Gas Well Completions. Paper EUR 38 presented at the 1978 SPE European Offshore Petroleum Conference and Exhibition, London, October 24-26.

Hardy, R.M. and Hemstock, R.A. Shear Strength Characteristics of Athabasca Oil Sands. K.A. Clark Volume, Alberta Research Council, Information Series No. 45, 1963.

Harr, Groundwater and Seepage. McGraw-Hill

Harris, M.C., Poppen, S. and Morgenstern N.R. Tunnels in Oil Sand. Journal of Canadian Petroleum Technology, 1979.

Harris, M.C. and Sobkowicz, J.C. Engineering Behaviour of Oil Sand. The Oil Sands of Canada-Venezuela, 1977. CIM Special Volume 17.

Hughes, J.M.O., Wroth, C.P. and Windle, D. Pressuremeter Tests in Sands. Geotechnique 27, 1977.

Naylor, D.J. Discussion. Proceedings of the Symposium on the Role of Plasticity in Soil Mechanics, Cambridge, 13-15, p. 291-294. September 1973.

Pasley, P.R. and Cheatham, J.B. Rock Stresses Induced by Flow of Fluids Into Boreholes. Soc. Pet. Eng., J., p. 85-94, March 1963.

Risnes, R., Bratli, R.K. and Horsrud, P. Sand Stresses Around a Wellbore. Society of Petroleum Engineering Journal, Col. 22, No. 6, 1982.

Smith, L.B. and Burn, P.M. Convergence-Confinement Method of Design for Shafts and Tunnels in Oilsands. Conference on Applied Oilsands Geoscience, Edmonton, Alberta, 1980.

Sobkowicz, J.C. The Mechanics of Gassy Sediments. Ph.D. Thesis, University of Alberta, Civil Engineering Department, 1982.

Timoshenki, S. Strength of Materials. Vol. 2, 1941, Van Nostrand, New Yord.

Todd, . Ground Water Hydrology. John Wiley and Sons, Inc.

Vaziri, H. Forthcoming Ph.D. Thesis, Department of Civil Engineering, U.B.C. 1985.

APPENDIX A

The constitutive relationship may be written:

$$(\Delta\sigma') = [D'] (\Delta\varepsilon) \qquad \text{A.1}$$

in which $(\Delta\sigma')$ is the incremental stress vector, $(\Delta\varepsilon)$ is the incremental strain vector and $[D']$ is the incrmental effective stress strain matrix.

The incremental strain vector is related to the nodal displacements by:

$$(\Delta\varepsilon) = [B] (\delta) \qquad \text{A.2}$$

in which $[B]$ is a matrix that depends on element geometry.

By the principle of virtual work, the external work done by the virtual displacement is equal to the internal work done by the increment of virtual strains:

$$(\bar{\delta})^T (f) - \int_A (\Delta\bar{\varepsilon})^T (\Delta\sigma') \, dA + \int_A (\Delta\bar{\varepsilon})^T \begin{pmatrix} 1 \\ 0 \end{pmatrix} \Delta u \, dA \qquad \text{A.3}$$

in which (f) = the element force vector

$(\Delta\sigma')$ = the element incremental effective stress vector

(Δu) = the element incremental pore pressure vector

Substituting for $(\Delta\bar{\epsilon})$ and $(\Delta\sigma')$ from Equations A.1 and A.2,

$$(\bar{\delta})\ (f) = (\bar{\delta})^T\ [B]^T\ [D']\ [B]\ (\delta)\ A_e + (\bar{\delta})^T\ [B]^T \begin{pmatrix} 1 \\ o \end{pmatrix}$$

$$\Delta u\ A_e \qquad \text{A.4}$$

in which A_e is the area of the element with unit thickness.

Rearrangement of Equation A.4 yields

$$[K]\ (\delta) = (f) - (K_w)\ (\Delta u) \qquad \text{A.5}$$

in which $[K] = [B]^T\ [D]\ [B]\ A_e$

$$[K_w] = [B]^T \begin{pmatrix} 1 \\ o \end{pmatrix} A_e$$

where $[K]$ is the element stiffness matrix and (K_w) is a load vector associated with the pore pressure.

APPENDIX B

Assumptions:

1) the volume of solids is 1 unit, then the volume of voids is e units by the definition of void ratio,
2) the solids are incompressible.

The undrained response of the element under a change on external pressure will be

$$\text{Skeleton} \quad (\Delta\varepsilon_v)_{SK} = \frac{\Delta\sigma_m'}{B_{SK}} \qquad \text{B.1}$$

$$\text{Fluid} \quad (\Delta\varepsilon_v)_f = \frac{\Delta u}{K_f} \qquad \text{B.2}$$

in which $(\Delta\varepsilon_v)_{SK}$, $(\Delta\varepsilon_v)_f$ = volumetric strain: Skeleton, Fluid

B_{SK}, K_f = bulk modulus: Skeleton, fluid

$\Delta\sigma_m'$ = mean effective stress change

Δu = pore pressure change

Since the soil skeleton and the pore fluids deform together when the conditions are undrained, in additions to Equations B.1 and B.2:

Compatibility $e\,(\Delta\varepsilon_v)_f = (1 + e)\,(\Delta\varepsilon_v)_{SK}$ B.3a

or $(\Delta\varepsilon_v)_f = \frac{1}{n}\,(\Delta\varepsilon_v)_{SK}$ B.3b

in which e is the void ratio and n is the porosity.

Substituting B.3b into B.1, the pore pressure change, Δu, may be written as:

$$\Delta u = K_a\,(\Delta\varepsilon_v)_{SK} \qquad \text{B.4}$$

in which $K_a = \frac{K_f}{n}$, the apparent bulk fluid modulus

In finite element analysis

$$\Delta u = K_a\,(\Delta\varepsilon_v)$$

$$= K_a\,(\Delta\varepsilon_{11} + \Delta\varepsilon_{22} + \Delta\varepsilon_{33})$$

APENDIX C

Poisson's ratio is equal to 0.5 in undrained analysis theoretically. This means that bulk modulus is infinite and numerical instability will arise (this sentence does not sound right). Therefore the default of Poisson's ratio, ν, is always less than 0.5 (e.g. 0.495) to maiontain stability and accuracy. In the total stress model developed in Section 3.2, it is the combined Poisson's ratio, ν_{cb} for matrix $[D]$ that controls the overall numerical stability, not just ν.

The elastic moduli in matrix $[D']$ are related as

$$G = \frac{E}{2(1+\nu)} \qquad \text{C.1}$$

$$B = \frac{E}{3(1-2\nu)} \qquad \text{C.2}$$

Assuming the elastic moduli in matrix $[D] = [D'] + [D_f]$ are related as

$$G_{cb} = \frac{E_{cb}}{2(1+\nu_{cb})} \qquad \text{C.3}$$

$$B_{cb} = \frac{E_{cb}}{3(1-2\nu_{cb})} \qquad \text{C.4}$$

in which suffic cb means combined, $G = G_{cb}$ as pore fluid does not transmit shear.

Just consider the direct stress terms in the constitutive relationship

$$\begin{bmatrix} \Delta\sigma_{11} \\ \Delta\sigma_{12} \\ \Delta\sigma_{33} \end{bmatrix} = \begin{bmatrix} L + K_a & L*M+K_a & L*M+K_a \\ L*M+K_a & L+K_a & L*M+K_a \\ L*M+K_a & L*M+K_a & L +K_a \end{bmatrix} \begin{bmatrix} \Delta\varepsilon_{11} \\ \Delta\varepsilon_{22} \\ \Delta\varepsilon_{33} \end{bmatrix} \qquad \text{C.5}$$

in which $$L = \frac{E(1-\nu)}{(1+\nu)(1-2\nu)}$$

$$M = \frac{\nu}{1-\nu}$$

Substituting C.2 into C.5, yields,

$$\begin{bmatrix} \Delta\sigma_{11} \\ \Delta\sigma_{22} \\ \Delta\sigma_{33} \end{bmatrix} = \begin{bmatrix} P+K_a & Q+K_a & Q+K_a \\ Q+K_a & P+K_a & Q+K_a \\ Q+K_a & Q+K_a & P+K_a \end{bmatrix} \begin{bmatrix} \Delta\varepsilon_{11} \\ \Delta\varepsilon_{22} \\ \Delta\varepsilon_{33} \end{bmatrix} \qquad \text{C.6}$$

in which $P = \frac{3B(1-\nu)}{(1+\nu)}$

$$Q = \frac{3B\nu}{1+\nu}$$

Adding the direct stress in Equation C.6 and rearranging

$$\frac{\frac{1}{3}(\Delta\sigma_{11} + \Delta\sigma_{22} + \Delta\sigma_{33})}{(\Delta\varepsilon_{11} + \Delta\varepsilon_{22} + \Delta\varepsilon_{33})} = \frac{B(1-\nu)}{1-\nu} + \frac{2B\nu}{1+\nu} + K_a$$

$$= B_{cb} \qquad \text{C.7}$$

Eliminating E_{cb} from Equations C.3 and C.4, yields

$$\nu_{cb} = \frac{3B_{cb} - 2G}{6B_{cb} + 2G} \qquad \text{C.8}$$

Substituting C.7 into C.8, rearranging

$$\nu_{cb} = \frac{3(B + K_a) - \frac{E}{1+\nu}}{6(B + K_a) + \frac{E}{1+\nu}} \qquad \text{C.9}$$

APPENDIX D

In the incremental elastic method, two iterations are performed to obtain the tangent moduli of the soil skeleton. Hence two iterations are also employed to evaluate the tangent bulk fluid modulus in order to make the procedure compatible. The parameters at the end of previous increment will be used in the analysis of the present increment, and then updated at the end of this increment.

The tangent bulk fluid modulus and the procedure to update the parameters are shown herein:

Equation 3.24e and 3.26b are programmed as:

$$\beta_{f1} = \frac{1}{e}\left[\frac{e-n_w(1+e) + H_w n_w (1+e) + H_{co2} n_w (1+e)}{P} + \beta_w N_w (1+e)\right] \qquad D.1$$

$$\beta_{f2} = \frac{1}{e}\left[\frac{e-n_o(1+e) - n_w(1+e) + H_b n_b(1+e) + H_w n_w(1+e)}{P} + \beta_b n_b(1+e) + \beta_w n_w (1+e)\right] \qquad D.2$$

The parameters in Equation D.1 and D.2 may be updated according to the following formulae based on the assumptions:

1) volume of solids is 1 unit

2) bitumen, water and soil solids are incompressible

$$\Delta e = (1+e)\,\Delta\varepsilon_v \qquad \text{D.3}$$

$$e_f = e_i + \Delta e \qquad \text{D.4}$$

$$S_f e_f = S_i e_i \qquad \text{D.5}$$

$$n'_g = \frac{n_g(1+e) + \Delta e}{1+e+\Delta e} \qquad \text{D.6}$$

$$n'_b = \frac{n_b(1+e)}{1+e+\Delta e} \qquad \text{D.7}$$

$$n'_w = \frac{n_w(1+e)}{1+e+\Delta e} \qquad \text{D.8}$$

$$P = u + \Delta u \qquad \text{D.9}$$

APPENDIX E

Refer to Figure 4.1b

$$\sigma_1 = \frac{\sigma_{11} + \sigma_{22}}{2} + \sigma_{12} \text{ cosec } 2\theta \qquad \text{E.1}$$

$$\sigma_3 = \frac{\sigma_{11} + \sigma_{22}}{2} - \sigma_{12} \text{ cosec } 2\theta \qquad \text{E.2}$$

$$\tau_{13} = 0 \qquad \text{E.3}$$

The overstress in the element is removed by reducing $\Delta\sigma_1$, $\Delta\sigma_3$, $\Delta\tau_{12}$ as follows

$$\Delta\sigma_1 = \sigma_1 - \sigma_3 \tan^2 (45° + \frac{\phi}{2}) \qquad \text{E.4}$$

$$\Delta\sigma_3 = 0 \qquad \text{E.5}$$

$$\Delta\tau_{12} = 0 \qquad \text{E.6}$$

These change in principal stresses can be expressed in terms of stresses in x-y space:

$$\Delta\sigma_{11} = \frac{\Delta\sigma_1 + \Delta\sigma_3}{2} + \frac{\Delta\sigma_1 - \Delta\sigma_3}{2} \cos 2\theta \qquad \text{E.7}$$

$$\Delta\sigma_{22} = \frac{\Delta\sigma_1 + \Delta\sigma_3}{2} - \frac{\Delta\sigma_1 - \Delta\sigma_3}{2} \cos 2\theta \qquad \text{E.8}$$

$$\Delta\sigma_{12} = \frac{\Delta\sigma_1 - \Delta\sigma_3}{2} \cos 2\theta \qquad \text{E.9}$$

Equations E.7, E.8 and E.9 may be expressed in matrix form

$$\begin{bmatrix} \Delta\sigma_{11} \\ \Delta\sigma_{22} \\ \Delta\sigma_{12} \end{bmatrix} = [T] \begin{bmatrix} \Delta\sigma_1 \\ \Delta\sigma_3 \\ \Delta\tau_{13} \end{bmatrix} \qquad \text{E.10}$$

$[T]$ is the transformation matrix

$$[T] = \begin{bmatrix} \frac{1}{2} - \frac{\cos 2\theta}{2} & \frac{1}{2} + \frac{\cos 2\theta}{2} & 0 \\ \frac{1}{2} + \frac{\cos 2\theta}{2} & \frac{1}{2} - \frac{\cos 2\theta}{2} & 0 \\ -\frac{\sin 2\theta}{2} & \frac{\sin 2\theta}{2} & 0 \end{bmatrix}$$

APPENDIX F

Back Calculation of Soil Parameters

Given the compressibility of soil β_s = 9 E-b kPa^{-1} and the effective stress σ_3' = 751 kPa, the bulk modulus K_B number can be backcalculated by assuming a value of m.

From Equation 3.12

$$B = K_B \, P_a \, (\frac{\sigma_3'}{P_a})^m \qquad \text{F.1}$$

i.e.

$$\frac{1}{\beta_s} = K_B \, P_a \, (\frac{\sigma_3'}{P_a})^m \qquad \text{F.2}$$

Substituting β_s, σ_3' and P_a and assuming m = 0.25 (Byrne and Cheung) in F.2,

$$K_B = 665$$

Adopting the relationship $K_B = 0.6 \, K_E$ (Byrne and Cheung)

$$K_E = 1108$$

Other parameters are depicted from Byrne and Eldridge on Byrne and Cheung reports. A complete set of soil parameters for Test 11 may be written as:

K_E = 1108

n = 0.5

K_B = 665

m = 0.25

R_f = 0.8

ϕ' = 42°

$\Delta\phi'$ = 8°

n = 0.3228 (e = 0.4767)

S = 0.9975

APPENDIX G

Elastic Stress Solution

If the fluid pressure is included, the displacement u of an elastic material may be written as

$$(\lambda + 2G)\,\frac{d}{dr}\left(\frac{du}{dr} + \frac{u}{r}\right) + \beta\,\frac{dp}{dr} = 0 \qquad \text{G.1}$$

where $\lambda = \dfrac{E\,\nu}{(1+\nu)\,(1-2\nu)}$

$G = \dfrac{E}{2(1+\nu)}$

$\beta = 1 - \dfrac{C_r}{C_b}$ which is assumed equal to 1

C_r = sand matrix compressibility

C_b = sand bulk compressibility

The pressure may be expressed by Darcy's law in radial form

$$\frac{dp}{dr} = \frac{\mu q}{2\pi h K r} \qquad \text{G.2}$$

The stresses are written as

$$\sigma_r = \lambda\,\varepsilon_v^e + 2G\,\varepsilon_r^e + P \qquad \text{G.3}$$

$$\sigma_\theta = \lambda \varepsilon_v^e + 2G \varepsilon_\theta^e + P \qquad G.4$$

$$\sigma_z = \lambda \varepsilon_v^e + 2G \varepsilon_z^e + P \qquad G.5$$

Where ε_r^e, ε_θ^e and ε_z^e are the elastic strain components and $\varepsilon_v^e = \varepsilon_r^e + \varepsilon_\theta^e + \varepsilon_z^e$ G.6

Assuming the initial loading cause a deformation only in the vertrical direction, but no displacement in the horizontal directions ($\varepsilon_r = \varepsilon_\theta = 0$), the initial vertical strain ε_{zo}, is given by G.5 as

$$\varepsilon_{zo} = \frac{\sigma_{zo} - P_o}{\lambda + 2G} \qquad G.7$$

Assuming only radial displacement after initial loading, the strains are

$$\varepsilon_r^e = \frac{du}{dr} \qquad G.8$$

$$\varepsilon_\theta^e = \frac{u}{r} \qquad G.9$$

$$\varepsilon_z^e = \varepsilon_{zo} \qquad G.10$$

By solving Equation G.1 with the boundary conditions

$$\sigma_r = \sigma_{ri} \text{ when } r = R_i$$

$$\sigma_r = \sigma_{ro} \text{ when } r = R_i$$

and combining the results with Equations G.8, G.9 and G.10, the stress solutions (Equations 6.2, 6.3, 6.4) can be found by inserting the result in Equations G.3 through G.5

APPENDIX H

Plastic Stress Solutions ($\sigma_r < \sigma_z < \sigma_\theta$)

The conditions must be satisfied within the plastic zone

1) Equilibrium

$$\frac{d\sigma_r}{dr} + \frac{\sigma_r - \sigma_\theta}{r} = 0 \qquad \text{H.1}$$

2) Mohr Coulomb failure criteria

$$f = \sigma_\theta - \sigma_r \tan^2 \alpha + (\tan^2 \alpha - 1) P - 2S \tan \alpha = 0 \qquad \text{H.2}$$

The flow rule associated with yield condition is

$$\varepsilon_r^p = \lambda \frac{\partial f}{\partial \sigma_r} = - \lambda \tan^2 \alpha \qquad \text{H.3a}$$

$$\varepsilon_\theta^p = \lambda \frac{\partial f}{\partial \sigma_\theta} = \lambda \qquad \text{H.3b}$$

$$\varepsilon_z^p = \lambda \frac{\partial f}{\partial \sigma_z} = 0 \qquad \text{H.3c}$$

From Equations H.3a and H.3b, it follows that

$$\varepsilon_r^p + \varepsilon_\theta^p \tan^2 \alpha = 0 \qquad \text{H.4}$$

The total strain components may be written as

$$\varepsilon_r = \varepsilon_r^e + \varepsilon_r^p \qquad \text{H.5a}$$

$$\varepsilon_\theta = \varepsilon_\theta^e + \varepsilon_\theta^p \qquad \text{H.5b}$$

$$\varepsilon_z = \varepsilon_z^e + \varepsilon_z^p = \varepsilon_{zo} \qquad \text{H.5c}$$

$\varepsilon_z^p = 0$ because it is assumed that there is only radial displacement after initial loading.

Combining Equations H.5a and H.5b, inserting into H.4, gives

$$\varepsilon_r + \varepsilon_\theta \tan^2 \alpha = \varepsilon_r^e + \varepsilon_\theta^e \tan^2 \alpha \qquad \text{H.6}$$

Applying Hooke's law of elasticity for porous material, yields

$$E\varepsilon_r^e = \sigma_r - \nu (\sigma_\theta + \sigma_z) - (1-2\nu)P \qquad \text{H.7a}$$

$$E\varepsilon_\theta^e = \sigma_\theta - \nu (\sigma_r + \sigma_z) - (1-2\nu)P \qquad \text{H.7b}$$

$$E\varepsilon_z^e = \sigma_z - \nu (\sigma_r + \sigma_\theta) - (1-2\nu)P \qquad \text{H.7c}$$

Substituting Equation H.5c into H.7c yields

$$\sigma_z = E\varepsilon_{zo} + \nu\,(\sigma_r + \sigma_\theta) + (1-2\nu)P \qquad \text{H.8}$$

Combining Equations H.7 and H.8, inserting into the yield criterion Equation H.2 with the strain relation in H.6, it gives

$$\begin{aligned}\left[\tan^4\alpha + 1 - \nu\,(\tan^2\alpha + 1)^2\right]\sigma_r &= 2G\,\varepsilon_r + 2G\,\varepsilon_\theta \tan^2\alpha \\ &+ \left[\tan^2\alpha\,(\tan^2\alpha - 1) - \nu\,(\tan^4\alpha - 1)\right. \\ &+ \left.(\tan^2\alpha + 1)\,(1 - 2\nu)\right]P - \left[\tan^2\alpha\,(1-\nu) - \nu\right] 2\,S\tan\alpha \\ &+ \nu\,(\tan^2\alpha + 1)\,2G\,\varepsilon_{zo} \qquad \text{H.9}\end{aligned}$$

and

$$\begin{aligned}\left[\tan^4\alpha + 1 - \nu\,(\tan^2\alpha + 1)^2\right]\sigma_\theta &= 2G\varepsilon_r \tan^2\alpha + 2G\varepsilon_\theta \tan^4\alpha \\ &+ \left[\nu\,(\tan^4\alpha - 1) - (\tan^2\alpha - 1)\right. \\ &+ \left.\tan^2\alpha\,(\tan^2\alpha + 1)\,(1-2\nu)\right]P - \left[\nu\,(\tan^2\alpha + 1) - 1\right] 2S\tan\alpha \\ &+ \nu\tan^2\alpha\,(\tan^2\alpha + 1)\,2G\varepsilon_{zo} \qquad \text{H.10}\end{aligned}$$

Substituting Equations H.9 and H.10 into equilibrium Equation H.1, together with the strain-displacement relations G.8 and G.9, the displacement equation may be written as

$$r^2 \frac{d^2u}{dr^2} + r \frac{du}{dr} - u\tan^2\alpha = \frac{r}{2G}\left(-\left[\tan^2\alpha\,(\tan^2\alpha - 1) - \nu(\tan^4 - 1)\right.\right.$$

$$\left. + (\tan^2\alpha + 1)\,(1-2\nu)\right]\frac{\mu q}{2\pi hk} + (\tan^2\alpha + 1)\,(1-2\nu)\,2\,S\tan\alpha$$

$$\left. + \nu\,(\tan^2\alpha - 1)\,2G\,\varepsilon_{zo}\right) \qquad \text{H.11}$$

The displacement solution of Equation H.11 is

$$2Gu = A_1 r^{\tan^2\alpha} + A_2 r^{-\tan^2\alpha} + Br \qquad \text{H.12}$$

and the corresponding strains are

$$2G\varepsilon_r = \tan^2\alpha\, A_1 r^{\tan^2\alpha - 1} - \tan^2\alpha\, A_2\, r^{-\tan^2\alpha} + B \qquad \text{H.13}$$

$$2G\varepsilon_\theta = A_1 r^{\tan^2\alpha} + A_2\, r^{-\tan^2\alpha} + B \qquad \text{H.14}$$

Where A_1 and A_2 are constants of integrations which depend on initial conditions.

$$B = \left[\frac{\tan^2\alpha}{\tan^2\alpha+1} + \frac{1-2\nu}{\tan^2\alpha-1}\right] \frac{\mu q}{2\pi hk} - \frac{1-2\nu}{\tan^2\alpha-1} 2\ S\tan\alpha$$

$$- \nu\ 2G\ \varepsilon_{zo} \qquad \text{H.15}$$

Substituting Equations H.13 and H.14 into Equations H.9 and H.10 together with Darcy's law for radial flow,

$$P = P_i + \frac{\mu q}{2\pi hk} \ell n \frac{r}{R_i} \qquad \text{H.16}$$

gives

$$\sigma_r = P_i + \frac{\mu q}{2\pi hk} \ell n \frac{r}{R_i} - \frac{1}{t} \left(2S\tan\alpha - \frac{\mu q}{2\pi hk}\right)$$

$$+ 2\tan^2 \alpha \frac{A_1}{T} r^t \qquad \text{H.17}$$

$$\sigma_\theta = P_i + \frac{\mu q}{2\pi hk} \ell n \frac{r}{R_i} - \frac{1}{t} \left(2S\tan\alpha - \tan^2 \alpha \frac{\mu q}{2\pi hk}\right)$$

$$+ 2\tan^4\alpha \frac{A_1}{T} r^t \qquad \text{H.18}$$

$$\sigma_z = P_i + \frac{\mu q}{2\pi hk} \ell n \frac{r}{R_i} - \frac{\nu}{t} \left[4\text{Stan } \alpha - (\tan^2 \alpha + 1). \right.$$

$$\left. \frac{\mu q}{2\pi hk}\right] + \frac{(1-\nu)(1-2\nu)}{1-\nu} (\sigma_{zo} - P_o) + \nu (\tan^2\alpha + 1).$$

$$2\tan^2 \alpha \frac{A_1}{T} r^t \qquad \text{H.19}$$

where $t = \tan^2 \alpha - 1$

$T = \tan^4 \alpha + 1 - \nu (\tan^2 \alpha + 1)^2$

The constant of integration A_1 can be found by inserting the boundary condition, $\sigma_r = P_i$ when $r = R_i$, into H.17.

APPENDIX J

The quantity of steady-state seepage at any distance r from the centre of the well is

$$Q = k\ 2\pi rh \frac{dh}{dr} \qquad \text{J.1}$$

on setting the limit of integration, yields

$$\frac{Q}{2\pi k} \int_{r_w}^{R} \frac{dr}{r} = \int_{h_1}^{h_2} h\ dh$$

and

$$Q = \pi\ k\ (h_2^2 - h_1^2) \frac{1}{\ell n\ (R/r_w)} \qquad \text{J.2}$$

Equating J.1 and J.2, yields

$$2rh \frac{dh}{dr} = (h_2^2 - h_1^2) \frac{1}{\ell n\ R/r_w} = C \qquad \text{J.3}$$

integrating J.3

$$h^2 = C\ \ell n\ r + D \qquad \text{J.4}$$

where D is the constant of integration

Substituting the boundary conditions $r = r_w$ and $h = h_1$ in J.4, yields,

$$D = h_1^2 - C \ln r_w \qquad \text{J.5}$$

Substituting J.5 into J.4, yields

$$h^2 = h_1^2 + \frac{h_2^2 - h_1^2}{\ln R/r_w} \ln \frac{r}{r_w} \qquad \text{J.6}$$